

Optimal Design under Interference, Homophily, and Robustness Trade-offs

Vydhourie Thiyageswaran* Alex Kokot* Jennifer Brennan†
 Marina Meila‡ Christina Lee Yu§ Maryam Fazel*

Abstract

To minimize the mean squared error (MSE) in global average treatment effect (GATE) estimation under network interference, a popular approach is to use a cluster-randomized design. However, in the presence of homophily, which is common in social networks, cluster randomization can instead increase the MSE. We develop a novel potential outcomes model that accounts for interference, homophily, and heterogeneous variation. In this setting, we establish a framework for optimizing designs for worst-case MSE under the Horvitz-Thompson estimator. This leads to an optimization problem over the covariance matrices of the treatment assignment, trading off interference, homophily, and robustness. We frame and solve this problem using two complementary approaches. The first involves formulating a semidefinite program (SDP) and employing Gaussian rounding, in the spirit of the Goemans-Williamson approximation algorithm for MAXCUT. The second is an adaptation of the Gram-Schmidt Walk, a vector-balancing algorithm which has recently received much attention. Finally, we evaluate the performance of our designs through various experiments on simulated network data and a real village network dataset.

Keywords: network interference, causal inference, optimization

*University of Washington

†Google Research

‡University of Waterloo

§Cornell University

1 Introduction

Network interference models settings in which the outcome of one unit depends on the treatment assignment of its neighbors in a network. The presence of network interference complicates the estimation of global average treatment effects (GATE), the difference between the average outcome when all units are treated and the average outcome when all units are assigned to control, as it violates the Stable Unit Treatment Value Assumption (SUTVA). In particular, in an experiment with partial treatment assignments where there is a mixture of treated units and control units, the difference in treatment assignments between neighboring units can bias each unit’s outcome relative to the all-treated and all-control outcomes. Therefore, basic experimental designs such as unit-level Bernoulli randomization lead to biased GATE estimation under standard estimators.

Cluster randomization approaches [Ugander et al., 2013, Ugander and Yin, 2023, Brennan et al., 2022, Viviano et al., 2023] are considered to be a useful way to reduce this bias. All of these methods stem from the same principle. Since bias is introduced by the conflicting treatment assignments between neighboring units, if we were to cluster together units that are strongly connected before assigning treatment at the cluster level, we would successfully reduce the bias. Consider a social network in which the outcome of interest is each individual’s likelihood of joining a premium social media platform. If treatment consists of offering a free trial, an individual’s outcome may depend not only on their own assignment, but also on whether their friends receive free trials and subsequently join the platform. Consequently, the outcomes from when all people in the social network are treated and from when all people are assigned to control will be different from when there is an experiment run where people are uniformly randomly assigned to treatment and control, due to the interference between friends who have different treatment assignments. Assigning tightly connected friends to the same treatment group, whether treatment or control, reduces this discrepancy between the outcomes in the experimental setting and in the full treatment and control settings.

However, networks are often homophilous: individuals tend to form connections with others who are similar to themselves, a phenomenon first noted by Lazarsfeld et al. [1954] and commonly summarized as “birds of a feather flock together” [McPherson et al., 2001].

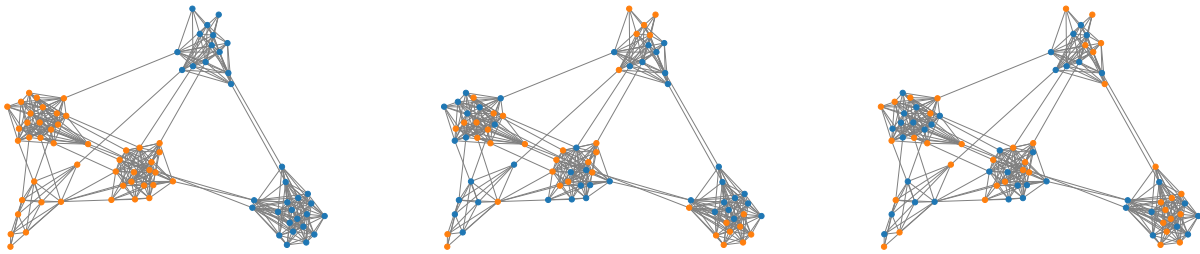


Figure 1.1: Optimized treatment assignments under interference-homophily tradeoffs on a synthetic network as homophily levels increase from left to right. See Appendix A for more details.

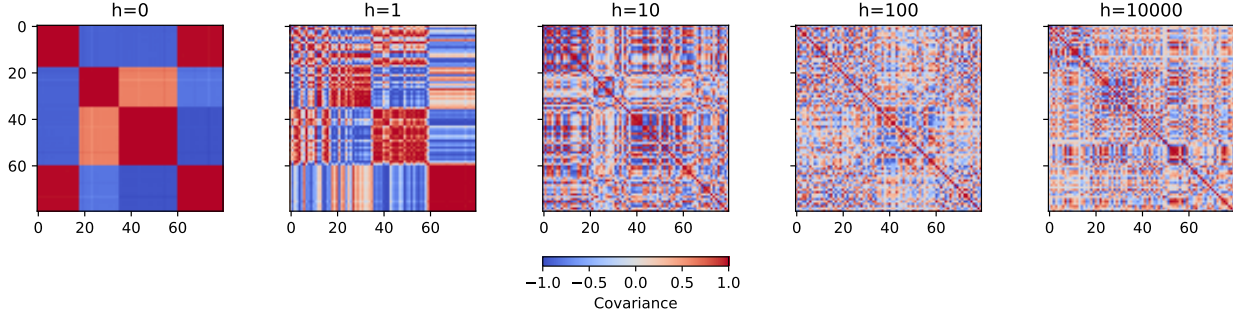


Figure 1.2: Optimal design covariance matrices under interference-homophily tradeoffs as homophily increases from left to right. See Appendix A for more details.

Similarities along socioeconomic, demographic, or behavioral dimensions [Jackson et al., 2023] increase the likelihood of social connection, and these same dimensions may also drive heterogeneous treatment responses. For example, younger and older individuals may respond differently to incentives for adopting new technologies. When cluster-randomized designs align with such homophilous groupings, covariate distributions can vary substantially across clusters, leading to unrepresentative treatment or control samples. Some covariate groups may be rarely or never exposed to treatment, inflating the imprecision of the estimator. In the presence of homophily, one would perhaps, now contradictorily, be incentivized to spread treatments across the network, to more effectively sample across different social groups. This reflects the typical goal of covariate balancing, where estimation accuracy is improved by enforcing similarity between treatment and control groups [Efron, 1971]. Finally, an effective design is one that is robust to heterogeneous variation, i.e., differences in potential outcomes poorly explained by the network structure. In Appendix L.2, we simulate experiments using network data from villages in Karnataka, India, collected by Banerjee et al. [2013b], which exhibit caste-based homophily. We observe that for large ranges of interference and heterogeneous variation levels, our designs, in the worst-case, perform better than existing unit-level and cluster-level randomization designs.

1.1 Our Contributions and Overview of Results

We formalize the trade-off between network interference and homophily, recovering well-studied designs in limiting regimes, and show how this trade-off interacts with randomization to yield a unifying three-way framework generalizing various results in the literature [Harshaw et al., 2024, Viviano et al., 2023]. We focus on the Horvitz-Thompson estimator which is commonly used in practice, and operate under the potential outcomes framework. We provide methods to solve for mean squared error (MSE)-optimal designs under the worst case potential outcomes within the subclass $\chi(\eta, \gamma, \kappa)$ (made precise in Section 4.1), where homophily, interference, and heterogeneous variation conditions are separately satisfied with parameters η , γ , and κ , respectively.

We consider the GATE, $\tau = \frac{1}{n} \langle \mathbf{1}, Y(\mathbf{1}) - Y(\mathbf{0}) \rangle = \frac{1}{n} \langle \mathbf{1}, \phi \rangle$, where $Y(z)$ is the outcome vector

observed under the treatment assignment vector $z \in \{0, 1\}^n$. We focus on the vanilla Horvitz-Thompson estimator $\hat{\tau} = \left\langle Y, \frac{z}{pn} - \frac{\mathbf{1}-z}{(1-p)n} \right\rangle$ with uniform treatment probability p across nodes, $p = \mathbb{P}(z_i = 1) = \mathbb{P}(z_j = 1)$ for all $i, j \in [n]$. Let L be the graph Laplacian* underlying the interference structure, and L^\dagger its pseudo-inverse. We can then characterize the homophily, interference, and robustness trade-offs with parameters η , γ , and κ , respectively.

Theorem 1 (Informal version of Theorem 2). *Let $x \in \{-1, 1\}^n$ by defining $x := 2z - 1$. Define $X := \mathbb{E}[xx^T]$. Then, for $q \geq 1$,*

$$\sup_{X(\eta, \gamma, \kappa)} \mathbb{E}[(\hat{\tau} - \tau)^2] \leq \frac{C}{n^2} \{ \text{Tr}(\mathbf{1}\mathbf{1}^T X) + C_1 \eta \text{Tr}(L^\dagger X) + C_2 \kappa \|X\|_q + C_3 \gamma \text{Tr}(LX) \},$$

for known constants C, C_1, C_2, C_3 that depend on p .

We propose two complementary approaches. The first approach involves formulating a semidefinite program (SDP) and employing Gaussian rounding, in the spirit of the Goemans-Williamson approximation algorithm [Goemans and Williamson, 1995] for MAXCUT. In particular, we cast the optimal design problem as an optimization problem over X , the covariance matrix of the design. Reparameterizing with $\tilde{\gamma}, \tilde{\eta}$, and $\tilde{\kappa}$, so that $\tilde{\gamma} := C_3 \gamma$, $\tilde{\eta} := C_1 \gamma$, and $\tilde{\kappa} := C_2 \kappa$, we can write an SDP more explicitly in terms of the new trade-off parameters:

$$\begin{aligned} \min_{X \in \mathbb{R}^{n \times n}} \quad & \tilde{\eta} \text{Tr}(L^\dagger X) + \tilde{\gamma} \text{Tr}(LX) + \tilde{\kappa} \|X\|_q + \text{Tr}(\mathbf{1}\mathbf{1}^T X) \\ \text{s.t.} \quad & X \succeq 0, \quad \text{diag}(X) = \mathbf{1}. \end{aligned} \tag{1.1}$$

To generate treatment assignments, we proceed with a Gaussian rounding procedure. As a second approach, we adapt the Gram-Schmidt Walk [Harshaw et al., 2024], a vector-balancing algorithm which has recently received much attention. In doing so, we uncover a natural interpretation of the spectra of the graph Laplacian and its inverse, associated with interference and homophily, respectively, and link them to the covariate balancing literature. Specifically, these eigenvalue-scaled eigenvectors can be interpreted as covariates associated with each unit, thereby connecting the covariate-balancing and interference literatures. In Appendix F, we present our framework for general similarity kernels beyond the graph Laplacian. We demonstrate improvements over existing designs through various experiments on simulated network data and a real village network dataset.

1.2 Related Work

Harshaw et al. [2024] propose the Gram-Schmidt Walk design that navigates trade-offs between covariate balancing and robustness under a potential outcomes model. Our paper is of a similar flavor as we study designs that trade off homophily, interference, and robustness

*Here $L := D - W$, where D is the diagonal degree matrix and W is the edge-weight matrix; see Sections 1.3 and 2 for details.

to heterogeneous variation. We adapt the Gram-Schmidt Walk algorithm to our setting as one approach, and contrast its performance with an alternative method of solving an SDP followed by Gaussian rounding.

Optimization-based designs for causal estimation are well studied. [Viviano et al. \[2023\]](#) propose an SDP to construct clusters for cluster-randomized designs by minimizing the MSE of a difference-in-means estimator under network interference, but do not consider the effects of homophily. The work most closely related to ours is [Chen et al. \[2024\]](#), who also minimize an MSE objective over the treatment assignment covariance matrix. Their focus, however, is restricted to cluster randomization and does not address homophily. They consider a non-convex formulation arising from Grothendieck's identity and propose a projected gradient method to find stationary points. In contrast, we adopt a convex SDP formulation and apply a Gaussian rounding procedure that generalizes the MAXCUT approximation of [Goemans and Williamson \[1995\]](#) via Grothendieck's identity.

In Appendix E, we discuss other related works.

1.3 Notation

We consider undirected weighted graphs $G = (V, E)$ with vertices (or nodes) $V = [n]$ and edges $E \subseteq V \times V$, representing a finite population of size n . An edge $(i, j) \in E$ represents the presence of dependence between the treatment of unit i and the outcome of unit j and vice versa. We consider undirected graphs with edge weights $W_{ij} \in [0, 1]$ for each edge $(i, j) \in E$, and degrees $d_i = \sum_{j \in N(i)} W_{ij}$ for each $i \in V$, $N(i) := \{j : W_{ij} > 0\}$ the neighborhood of vertex i . We take $D := \text{diag}(d)$, the diagonal matrix of node degrees, $L := D - W$, the graph Laplacian, and L^\dagger its Moore–Penrose pseudo-inverse.

2 Homophily and Heterogeneous Variation

Network interference models how the outcome of units depend on the treatment assignments of neighboring units in the network. With regards to the GATE, the bias arising from network interference can be written as the component of the potential outcome model accounting for disparate treatments among units. As such, the bias notably vanishes in a graph where all units are treated (respectively controlled). In this section, we focus on the terms that are left over, the baseline α , and treatment effect ϕ . We discuss the interference terms in full detail in Section 3. Denote the outcomes by $Y := Y(z)$, with treatment assignment $z \in \{0, 1\}^n$. We consider outcomes associated with $\mathbf{0}$ and $\mathbf{1}$, the treatment assignment vectors of all 0s and 1s, respectively. We can express, for each instance of the sampled network,

$$\alpha := Y(\mathbf{0}), \quad \alpha + \phi := Y(\mathbf{0}) + [Y(\mathbf{1}) - Y(\mathbf{0})] = Y(\mathbf{1}). \quad (2.1)$$

We decompose these vectors $\alpha = h_\alpha + \varepsilon_\alpha$, and $\phi = h_\phi + \varepsilon_\phi$, where h_α, h_ϕ are homophilous components, capturing smooth variation of the potential outcome coefficients with the graph

structure. We formalize this smoothness via a quadratic constraint, and define this formally in Definition 1. The $\varepsilon_\alpha, \varepsilon_\phi$ terms are heterogeneous variation, capturing components of the outcomes not explained by homophily and interference, formalized by moment constraints. These are nothing but the residuals or model misspecifications, terms more commonly seen in other literature, if we model the true generative (potential) outcomes by just interference and homophily.

Remark 1. It is equivalent to write $\alpha = \bar{\alpha} + h_\alpha + \varepsilon_\alpha$, and $\phi = \bar{\phi} + h_\phi + \varepsilon_\phi$, where $h_\alpha, h_\phi, \varepsilon_\alpha, \varepsilon_\phi$ are mean-zero, and $\bar{\alpha}, \bar{\phi}$ are constant vectors. We note that the decompositions into $h_\alpha + \varepsilon_\alpha$ and $h_\phi + \varepsilon_\phi$ are not unique (see also Remark 3). \diamond

2.1 Homophily

We formalize the definition of homophily we consider. To our knowledge, the only other work that has used a similar definition is [Ugander and Yin \[2023\]](#). Informally, homophily captures the extent to which similar nodes are strongly connected and dissimilar nodes are weakly connected. The quantity $\sum_{(i,j) \in E} W_{ij}(g_i - g_j)^2$ encapsulates this idea by aggregating the dissimilarities in potential outcomes coefficients g_i across edges. In a connected graph that is well-clusterable, high levels of homophily could result in clusters of nodes that are very similar while being significantly dissimilar across clusters. Large dissimilarities across clusters would result in a large value of $\sum_{(i,j) \in E} W_{ij}(g_i - g_j)^2$.

Definition 1 (η -homophily). We say that the vector g satisfies η -homophily, or is η -homophilous, if $g^T L g \leq \eta$, where $L := D - W$ is the graph Laplacian. That is, $\sum_{(i,j) \in E} W_{ij}(g_i - g_j)^2 \leq \eta$.

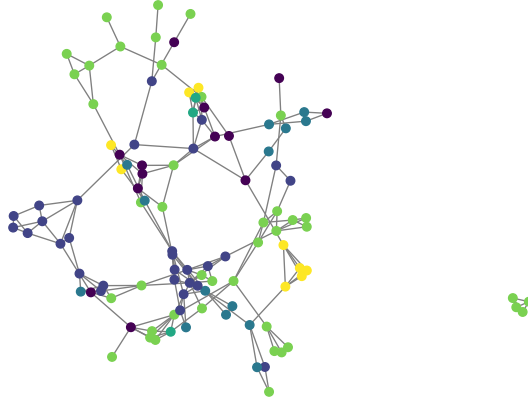


Figure 2.1: Network of home visits between members of a village (no.6) with different node colors representing different castes of village members.

In such a setting, one natural design might be to have a spread out treatment assignment, to diversify treatment samples across the natural clusters. In Section 4, we demonstrate

how this formalization leads to a design that distributes treatment assignments across the underlying graph clusters, aligning with intuition.

Remark 2. Throughout the paper, unless specified otherwise, we use η -homophily to refer to homophily with respect to the graph Laplacian L . There are settings where other kernels may be more appropriate. For example, if we wish to define homophily with respect to similarity in node degrees d_i , a natural approach is to use the symmetric normalized Laplacian $L_{\text{sym}} := I - D^{-1/2}WD^{-1/2}$, and consider the quadratic form $g^T L_{\text{sym}} g \leq \eta$. Here, we say that the vector g is (η, L_{sym}) -homophilous. This formulation incorporates an appropriate normalization of the edge weights by the square roots of the degrees of the corresponding nodes. Explicitly, $g^T L_{\text{sym}} g = \sum_{(i,j) \in E} W_{ij} \left(\frac{g_i}{\sqrt{d_i}} - \frac{g_j}{\sqrt{d_j}} \right)^2 \leq \eta$ captures the smoothness of g when degree similarity is taken into account. \diamond

Remark 3. Our mathematical notion of homophily can be tailored to conform to the known idea of homophily explaining cluster formation in social networks [McPherson et al., 2001, Currarini et al., 2009, Jackson et al., 2023, Jackson, 2025]. In our setting, this is well-approximated by the Rayleigh quotient of the graph Laplacian $g^T L g / \|g\|^2$, the ratio η'/κ' of the homophily and heterogeneity of a centered vector g . When this ratio is small, the potential outcomes g have little discrepancy between neighbors in the graph compared to the variation of the vector. Equivalently, the variations in g are primarily inter-cluster rather than intra-cluster, and this can be characterized spectrally as g lying predominantly in the span of the eigenvectors associated with the smallest eigenvalues of the graph Laplacian. This is most insightful in our decomposition of α and ϕ into homophilous and heterogeneous components h_f and ε_f , where $f \in \{\alpha, \phi\}$, respectively. As will become apparent in bounds such as Theorem 2, this decomposition will be particularly effective numerically when h_f is selected so that the corresponding ratio η'/κ' is minimal, and vice versa for ε_f , $f \in \{\alpha, \phi\}$, thus aligning these two notions of homophily. \diamond

Remark 4. We use the term “homophily” in a broad sense. Although it technically refers to similarity in social ties, we adopt it here to encompass similarities that may arise in contexts beyond social networks. If the practitioner, for instance, were to include some other likeness measure such as spatial positioning or geography, then a different similarity kernel, rather than or in addition to the Laplacian L , can be used. For example, under a similarity kernel \mathcal{K} , we can write our homophily formulation as $g^T \mathcal{K} g \leq \eta$. That is, g is (η, \mathcal{K}) -homophilous. We write the generalized characterization in Appendix F.1. \diamond

2.2 Robustness to heterogeneous variation

Our model accounts for heterogeneous variation via the ε components, which we only constrain by certain moment conditions. In its simplest form, this corresponds to an ℓ_2 constraint on ε which leads to an operator norm as previously realized in Harshaw et al. [2024]. Indeed, let $X = \mathbb{E}[xx^T]$, $x = 2z - 1$, then $\sup_{\|\varepsilon_f\|^2 \leq \kappa} \text{Tr}(\varepsilon_f^T X \varepsilon_f) = \|X\|_{\text{op}} \kappa$, for $f = \alpha, \phi$.

Our framework encompasses heterogeneous variation arising both from unobserved subject co-

variates and from unobserved dependence between units independent of treatment assignment. In works such as [Li et al. \[2021\]](#), the setting of interference under noisy network observations has previously been considered, resulting in stochasticity of the potential outcome model. The observed network is a sample from a super-population of possible dependencies between the finite population of experimental units. In Example 3, we discuss how this noisy interference is encapsulated by our generalized notion of network interference. Our notion of robustness in the current section addresses the resulting correlation in the baseline α and treatment effect ϕ in addition to that induced by unobserved subject covariates and homophily with respect to the observed network. In particular, we allow for ε_f , $f = \alpha, \phi$, to act as a random effect, drawing particular inspiration from the spatial statistics literature [[Gaetan et al., 2010](#)]. In our potential outcomes framework, we place constraints on $\Sigma_f := \mathbb{E}[\varepsilon_f \varepsilon_f^T]$, and we discuss how different penalties relate to inter-unit dependencies. This encompasses relationships between the outcomes that are not restricted to the observed network encoded by homophily. We employ duality to relate this back to the treatment design.

Example 1. A prominent example of stochastic heterogeneous variation is through the lens of noisy network observations. Consider the setting where α (and similarly ϕ) is a fixed function of the units in our finite population that is η -homophilous with respect to the graph G with Laplacian L . Thus, we can express $\alpha = L^{\dagger/2}\beta$ for a coefficient vector β with length $\sqrt{\eta}$. Now consider the observed network G_{obs} with corresponding Laplacian L_{obs} (see, for example, Figure C.2). We can decompose $\alpha = L^{\dagger/2}\beta = h + \varepsilon$, $h := L_{\text{obs}}^{\dagger/2}\beta$, and $\varepsilon := (L^{\dagger/2} - L_{\text{obs}}^{\dagger/2})\beta$. In this decomposition, h is η -homophilous with respect to the observed graph, and ε is a function of the randomly observed graph structure. Imposing conditions on $\Sigma := \mathbb{E}[\varepsilon \varepsilon^T]$ imposes minimal moment constraints on the extent of heterogeneous variation. \diamond

We can characterize worst-case bounds in terms of Schatten norms, $\sup_{\|\Sigma_f\|_{q^*} \leq \kappa} \text{Tr}(X \Sigma_f) = \|X\|_q \kappa$. We write this out formally in Section 4. When $q^* = 1$, $q = \infty$, we recover the previous operator-norm bound. When $q^* = q = 2$, we get a bound in terms of the Frobenius norm of the covariance matrix, $\kappa \|X\|_F$. This leads to a novel connection to [Viviano et al. \[2023\]](#).

Concretely, these are realized as penalizations that encourage randomization in our designs, with the extreme case being unit-level Bernoulli randomization. Randomization results in robust designs [[Rubin, 1978](#)] that ensure a controlled worst-case MSE under minimal moment assumptions. This underscores the interpolation of the two extremes of randomization and determinism. In principle, we uniformly independently randomize when we have no information and assumptions at all. Conversely, if we had all the necessary information, i.e., all potential outcomes were encoded through our notions of homophily and interference, then we can deterministically solve for an optimal design.

3 Potential Outcomes Model and Network Interference

Let $z \in \{0, 1\}^n$ denote the binary treatment assignment vector. We consider the following potential outcome model

$$Y_i(z) = \alpha_i + \phi_i z_i + s_i(z), \quad (3.1)$$

with $z_i \in \{0, 1\}$, for all $i \in [n]$. The term $s(z)$ denotes interference that vanishes when $z \in \{\mathbf{1}, \mathbf{0}\}$, with α denoting the baseline, and ϕ the treatment effect (see Equation (2.1)).

Definition 2 (γ -interference). We say that $s(z)$ satisfies γ -interference, or is γ -interferent, if $s(z)^T L^\dagger s(z) \leq \gamma$ for all $z \in \{0, 1\}^n$, where L^\dagger is the pseudo-inverse graph Laplacian.

Remark 5. Similar to our definition of homophily (see Remark 2), unless specified otherwise, we use γ -interference to refer to interference with respect to L . For a similar level of interference with respect to a different kernel \mathcal{K} , we say that $s(z)$ is (γ, \mathcal{K}) -interferent. \diamond

Example 2 (Neighborhood Interference). A form of $s(z)$ that is commonly studied in the literature, such as in [Chin \[2019\]](#), [Eckles et al. \[2017\]](#), [Harshaw et al. \[2023\]](#), [Yu et al. \[2022\]](#), is the linear neighborhood interference term, i.e., $s(z) \propto D^{-1} L z$. This corresponds to a neighborhood interference setting, where a unit's outcome depends only on its own and its neighbors' treatment assignments, not on assignments beyond its neighborhood. A simple outcome model with such a (γ, \tilde{L}) -interferent $s(z)$ component with a \sqrt{n} -scaling reminiscent of the local asymptotic framework [[Viviano et al., 2023](#), [Hirano and Porter, 2009](#)], is $Y_i = \alpha_i + \beta_i Z_i + \frac{\gamma}{\sqrt{n}} \sum_j \frac{W_{ij}}{\sum_j W_{ij}} z_j$. Indeed, the equation above can be rewritten as $Y_i = \alpha_i + \phi_i z_i - \frac{\gamma}{\sqrt{n}} e_i^T (I - D^{-1} W) z$, where $\phi_i := \beta_i + \gamma / \sqrt{n}$, $D = \text{diag}(d)$ for the vector $d \in \mathbb{R}^n$ of degrees of the nodes $d_i = \sum_{j \in N(i)} W_{ij}$, $W \in \mathbb{R}^{n \times n}$ is the matrix of the edge weights $\{W_{ij}\}_{i,j}$, and α, ϕ are vectors with entries α_i, ϕ_i , respectively, for $i = 1, 2, \dots, n$. Let the normalized graph Laplacian $\tilde{L} := I - D^{-1} W$, i.e., $\tilde{L} = D^{-1} L$, and \tilde{L}^\dagger to be the pseudo-inverse of the normalized Laplacian. Then, in matrix-vector form, the previous expression can be written as $Y = \alpha + \text{diag}(\phi) z - \frac{\gamma}{\sqrt{n}} \tilde{L} z$. Here, $s(z) = -\frac{\gamma}{\sqrt{n}} \tilde{L} z$, which is (γ, \tilde{L}) -interferent. Additionally, the normalized Laplacian term appropriately vanishes when the full population is treated or controlled. \diamond

To capture settings with stochastically misspecified interference, we cannot use the approach from Example 1, since the resulting misspecification would be correlated with treatment assignment, complicating our later analysis. Instead, we rely on the intrinsic robustness of our constraint, which allows generalization beyond neighborhood interference models.

Example 3 (Full Network Interference). Our interference characterization allows for “perturbations” of the interference structure. Let \tilde{L} be the graph Laplacian of the perturbed network, and let L be the graph Laplacian underlying a neighborhood interference structure satisfying γ -interference. If both the perturbed and unperturbed networks are connected, then the column and row spaces of L and \tilde{L} are equal, and hence $\tilde{L}^{\dagger/2} L^{1/2} L^{\dagger/2} = \tilde{L}^{\dagger/2}$, and $L^{\dagger/2} L^{1/2} \tilde{L}^{\dagger/2} = \tilde{L}^{\dagger/2}$. Thus, if $\|\tilde{L}^\dagger L\|_{\text{op}} \leq c$, and both the perturbed and unperturbed networks are connected, we

can write $s(z)^T \tilde{L}^\dagger s(z) = s(z)^T (\tilde{L}^{\dagger/2} L^{1/2}) L^\dagger (L^{1/2} \tilde{L}^{\dagger/2}) s(z) \leq c s(z)^T L^\dagger s(z) \leq c\gamma$. In other words, if L and \tilde{L} are close in spectrum, i.e., $\|\tilde{L}^\dagger L\|_{\text{op}} \leq c$, then $s(z)$ being (γ, L) -interferent implies that $s(z)$ is $(c\gamma, \tilde{L})$ -interferent. For instance, if \tilde{L} encapsulates a full-interference structure with decaying interference (for example, [Leung \[2022a\]](#)) across nodes with longer distances such that \tilde{L} is well approximated by the neighborhood interference Laplacian L , we can write $c = 1 + O(\psi)$ for some $\psi \ll 1$. We describe this in more detail in Example 5. \diamond

4 Worst-case MSE Bounds and Trade-offs

4.1 GATE Estimation

Definition 3 (Global Average Treatment Effect (GATE)). The Global Average Treatment Effect (GATE) is defined to be

$$\tau = \frac{1}{n} \langle \mathbf{1}, Y(\mathbf{1}) - Y(\mathbf{0}) \rangle = \frac{1}{n} \langle \mathbf{1}, \phi \rangle.$$

Our primary focus is on the Horvitz-Thompson estimator with uniform treatment probability p across nodes, $p = \mathbb{P}(z_i = 1) = \mathbb{P}(z_j = 1)$ for all $i, j \in [n]$:

$$\hat{\tau} = \left\langle Y, \frac{z}{pn} - \frac{\mathbf{1} - z}{(1-p)n} \right\rangle.$$

We note here that the particular Horvitz-Thompson estimator we focus on throughout the paper is the vanilla one. In the literature on interference and cluster randomized designs, it is common to pair Horvitz-Thompson estimators with neighborhood exposure mappings [[Aronow and Samii, 2017](#), [Ugander et al., 2013](#), [Leung, 2022b](#), [Thiyageswaran et al., 2024](#), [Eichhorn et al., 2024](#)]. Under a correctly specified exposure mapping under network interference, the Horvitz-Thompson estimator remains unbiased, albeit with high variance. In contrast, the vanilla Horvitz-Thompson estimator is biased in the presence of interference, though it typically exhibits lower variance.

We focus on the vanilla estimator because it is much simpler, and our primary goal is to study the tradeoffs that occur under varying levels of interference, homophily and heterogeneous variation, for various designs. This includes settings without interference, where using a Horvitz-Thompson estimator paired with a neighborhood exposure mapping would introduce unnecessary variance. Moreover, applying exposure mappings requires specifying them correctly, and under more general forms of interference, beyond neighborhood interference, characterizing the correct exposure mapping (and the imprecision that arises from a misspecified exposure mapping) becomes much more complicated. In Appendix I we consider our framework with respect to the difference-in-means estimator. In fact, our framework applies to more general estimators of the form $\hat{\tau} = \langle Y, w \rangle$, with general weights w .

The measure of precision of the estimator we focus on is the worst-case mean

squared error (MSE) with respect to the potential outcomes within the class $\chi(\eta, \gamma, \kappa) = \chi_{q^*}(\eta, \gamma, \kappa) = \{h_f, \varepsilon_f, s(z) : \|L^{1/2}h_f\|^2 \leq \eta, \|\Sigma_f\|_{q^*} \leq \kappa, \|L^{\dagger/2}s(z)\|^2 \leq \gamma, \text{ for } f = \alpha, \phi\}$, $\sup_{h_f, \Sigma_f, s(z) \in \chi(\eta, \gamma, \kappa)} \mathbb{E}[(\hat{\tau} - \tau)^2]$. When τ and $\hat{\tau}$ incorporate stochastic network misspecification, this expectation is understood to be the iterated expectation $\mathbb{E}[\mathbb{E}[(\hat{\tau} - \tau)^2 \mid \varepsilon_f]]$, $f = \alpha, \phi$, over the network misspecification residual and the design, respectively.

Remark 6. The decomposition of the outcomes into these components may not be unique (see Remark 1). We focus on the decompositions that are meaningful. If the outcomes associated with all the units in the population are highly heterogeneous and not driven by the underlying network structure, then a larger share of the variation in the outcomes can be attributed to ε (and hence κ) rather than h (and hence η). See also Remark 3. \diamond

For the sake of clarity, we focus on deriving the worst-case MSE bound in the symmetric setting, i.e., when the probability of treatment assignment is equal to the probability of control assignment. The general setting is presented in Appendix B.

Theorem 2 (MSE bound). *Let $p := \mathbb{P}(z_i = 1) = 1/2$ for all $i \in [n]$, $a = \langle \alpha, \mathbf{1}/n \rangle$, and $b = \langle \phi, \mathbf{1}/n \rangle$. Let $|\langle s(z), \mathbf{1}/n \rangle| \leq \sqrt{\delta}$. Let also $x \in \{-1, 1\}^n$ by defining $x := 2z - 1$. Define $X := \mathbb{E}[xx^T]$ and $\Delta := (a + b/2)^2 + \delta$. Then, for $q \geq 1$,*

$$\sup_{\chi(\eta, \gamma, \kappa)} \mathbb{E}[(\hat{\tau} - \tau)^2] \leq \frac{28}{n^2} \{ \Delta \text{Tr}(\mathbf{1}\mathbf{1}^T X) + \frac{5\eta}{4} \text{Tr}(L^{\dagger}X) + \frac{5\kappa}{4} \|X\|_q + \gamma \text{Tr}(LX) \}. \quad (4.1)$$

Thus, to control the worst-case MSE it suffices to minimize the right-hand side in Equation (4.1) over the covariance matrix X . The proof of Theorem 2 is in Appendix J.2. We assume that the interference term is bounded in its center, i.e., $\langle s(z), \mathbf{1}/n \rangle \leq \sqrt{\delta}$, and this is implicitly adopted in later MSE bounds.

In Appendix G, we discuss an alternative where we constrain the quadratic form $s(z)^T(\delta\mathbf{1}\mathbf{1}^T + L)^{-1}s(z)$. If instead we were to constrain the quadratic form $s(z)^T(\lambda I + L)^{-1}s(z)$, we would arrive at the same bound up to a constant additive factor without necessitating this assumption. There are many alternatives that lead to fundamentally equivalent optimization problems, with another alternative provided in Example 11.

Trade-off parameters

Our design flexibly navigates homophily, robustness, and interference trade-offs parameterized by $\eta, \kappa, \gamma \in \mathbb{R}$:

1. $h_{\alpha}^T L h_{\alpha} \leq \eta$, and $h_{\phi}^T L h_{\phi} \leq \eta$ (see also Remark 2 for a measure of homophily including degree similarity)
2. $\|\Sigma_{\alpha}\|_q \leq \kappa$, and $\|\Sigma_{\phi}\|_q \leq \kappa$
3. $s(z)^T L^{\dagger} s(z) \leq \gamma$ for all $z \in \{0, 1\}^n$

As is typical in conducting power analyses, our method depends on baseline and treatment effect size, encapsulated by Δ . We dissect the three components in the trade-offs above.

4.2 Cut Minimization

If we fix the treatment vector x , then $X = xx^T$. In this setting, the term $\text{Tr}(LX) = x^T Lx$ in the theorem statement above is the same as the objective function in the cut minimization problem. Indeed, for $L = D - W$, and $x \in \{-1, 1\}^n$, $\frac{1}{4}x^T Lx = \sum_{i \in S, j \in S^c} W_{ij}$, where S and S^c make up the cut partition. Thus, this $x^T Lx$ term alone encourages a more “clustered” design. The term $\sum_{i \in S, j \in S^c} W_{ij}$ has previously appeared in [Brennan et al. \[2022\]](#), [Viviano et al. \[2023\]](#).

4.3 Effective Resistance

Once again, if we fix the treatment vector x , then $X = xx^T$. The term $\text{Tr}(L^\dagger X) = x^T L^\dagger x$ can be expressed in terms of the effective resistances. Let R be the matrix of effective resistances across edges, so that the (i, j) -th entry is the effective resistance R_{ij} across edge (i, j) . Then, for $x \in \{-1, 1\}^n$, $x^T L^\dagger x = -\frac{1}{2}x^T \Pi^T R \Pi x$, where Π is the projection matrix to the subspace orthogonal to $\mathbf{1}$ (see [Fontan and Altafini \[2021\]](#)). In the graph sparsification literature, [Spielman and Srivastava \[2008\]](#) use effective resistances to sample network edges. Selecting a cut to minimize $x^T L^\dagger x$ corresponds to the selection of a treatment design “spread-out” in the graph. We see in our MSE bounds that this provides a counterbalance to the $x^T Lx$ term above that incentivizes clustered designs, and thus improves our estimation procedure in the presence of homophilous outcomes.

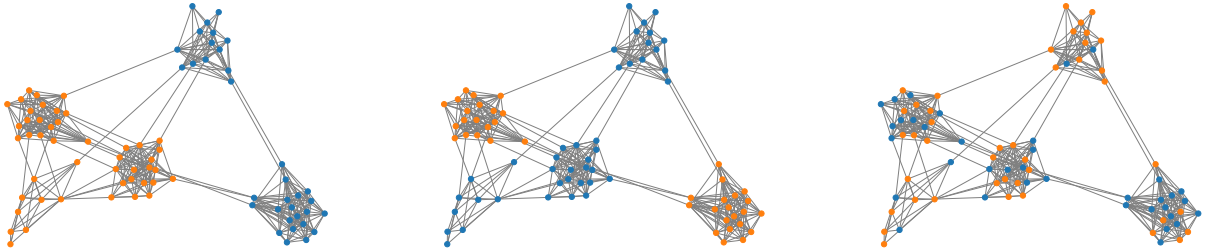


Figure 4.1: Optimized treatment assignments under homophily-robustness tradeoffs on a synthetic network as heterogeneous variation levels increase from left to right. See [Appendix A](#) for more details.

4.4 Randomization

We use [Proposition 3](#) to bound the contribution of the heterogeneous variation ε_f to the MSE of our estimator. We note that for deterministic $\varepsilon_\alpha, \varepsilon_\phi$, $\Sigma_f = \varepsilon_f \varepsilon_f^T$, and $\|\Sigma_f\|_q = \|\varepsilon_f\|^2$, $f = \alpha, \phi$.

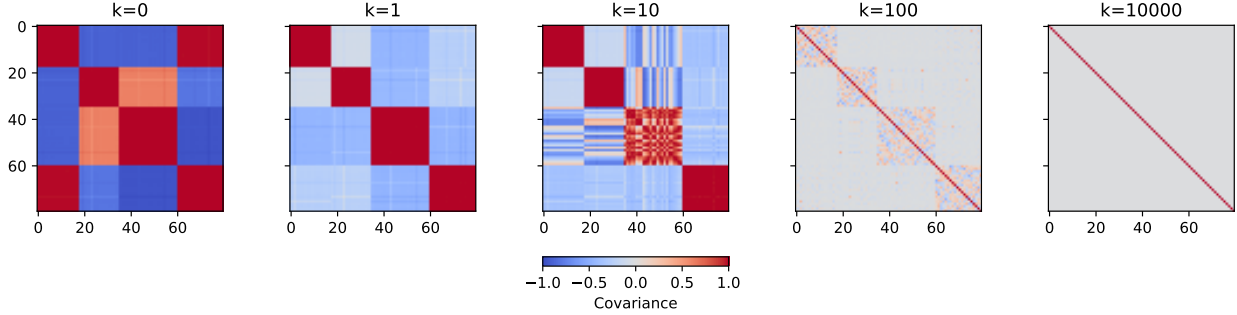


Figure 4.2: Optimal design covariance matrices under interference-robustness tradeoffs as heterogeneous variation levels increase from left to right. See Appendix A for more details.

Proposition 3 (Worst-case bound over deterministic heterogeneous variation). *For PSD matrices $X \in \mathbb{R}^{n \times n}$, $\Sigma = \varepsilon_f \varepsilon_f^T \in \mathbb{R}^{n \times n}$, $f = \alpha, \phi$ and $\kappa \in \mathbb{R}$,*

$$\sup_{\|\varepsilon_f\|_{\ell_2}^2 \leq \kappa} \text{Tr}(X\Sigma) = \sup_{\|\varepsilon_f\|_{\ell_2}^2 \leq \kappa} \varepsilon_f^T X \varepsilon_f = \lambda_{\max}(X)\kappa.$$

This recovers the operator-norm bound that is used as a robustness measure in [Harshaw et al. \[2024\]](#). We can generalize this further for the (uncentered) covariance matrix of the stochastic network misspecification.

Proposition 4 ([Bhatia, 2013](#), Exercise IV.2.12). *Let $\|\cdot\|_q$ denote the Schatten q -norm of a matrix. For symmetric positive semidefinite (PSD) matrices $X \in \mathbb{R}^{n \times n}$ and $\Sigma \in \mathbb{R}^{n \times n}$, and $1/q^* + 1/q = 1$, $\sup_{\|\Sigma\|_{q^*} \leq \kappa} \text{Tr}(X\Sigma) = \|X\|_q \kappa$.*

Particular choices of q^* relate to existing trade-offs in the literature.

Corollary 5 (Worst-case bound over the marginal variances). *For PSD matrices $X \in \mathbb{R}^{n \times n}$ and $\Sigma \in \mathbb{R}^{n \times n}$, $q^* = 1$, $q = \infty$, and $\kappa \in \mathbb{R}$, $\sup_{\|\Sigma\|_1 \leq \kappa} \text{Tr}(X\Sigma) = \lambda_{\max}(X)\kappa$.*

As a practical consideration, it is worth noting that the above supremization places little constraint on the off-diagonal of Σ . Indeed, the supremum is realized by a dense Σ , and as Σ is PSD, the Schatten-1 norm corresponds to the trace, hence the marginal variances of ε are directly constrained. However, in many circumstances, one may expect the coordinates of ε to be somewhat independent, making $q^* = 1$ an unrealistic modeling assumption.

In the other extreme Σ could be a diagonal matrix corresponding to independent heterogeneous variation, with the off-diagonal entries being completely nullified. Such a Σ is achieved if we were to instead supremize over the constraint $\|\Sigma\|_\infty \leq \kappa$, and the resulting error would be $\kappa \text{Tr}(X) = \kappa n$, which is constant. In other words, if the (edge) misspecification was, for example, i.i.d. across the nodes, then additional randomization to account for network misspecification would be unnecessary, as this value κn is constant, independent of the chosen design. As a reasonable compromise between these two extremes, we highlight the Frobenius

norm, $q^* = 2$.

Corollary 6 (Worst-case bound over the covariance structure). *For PSD matrices $X \in \mathbb{R}^{n \times n}$ and $\Sigma \in \mathbb{R}^{n \times n}$, $q^* = q = 2$, $\sup_{\|\Sigma\|_2 \leq \kappa} \text{Tr}(X\Sigma) = \kappa \|X\|_2 = \kappa \sqrt{\text{Tr}(X^2)} = \kappa \sqrt{\sum_{i=1}^n \lambda_i^2(X)}$. Additionally, $\sup_{\|\Sigma\|_2 \leq \kappa \|X\|_2} \text{Tr}(X\Sigma) = \kappa \text{Tr}(X^2) = \kappa \sum_{i=1}^n \lambda_i^2(X)$.*

In the bounds in Corollary 6, the total covariance structure of $(\varepsilon_i)_{i=1}^n$ is constrained, rather than just the marginal variances. By constraining the Frobenius norm, we bound the sum of the squared entries of all of the elements of Σ , putting equal importance on on and off-diagonal elements. The distinction between the two bounds in Corollary 6 is that the latter allows the norm of Σ to grow with X (and therefore n).

Under a cluster-level Bernoulli randomization design, the second part of Corollary 6 corresponds to the dominant term in the variance presented in Viviano et al. [2023]. Indeed, consider X such that $X_{ij} = 1$ if nodes i, j are in the same cluster, and 0 otherwise. This matrix X is the assignment covariance matrix for cluster-level Bernoulli randomization, where each cluster is independently assigned a treatment with probability p . The eigenvalues of this matrix are given by the sizes of the clusters, $|\mathcal{C}_i|$, hence $\text{Tr}(X^2) = \sum_i |\mathcal{C}_i|^2$. This is exactly the dominating term in the variance observed in Viviano et al. [2023, Theorem 3.2], hence the squared Frobenius norm generalizes this variance to generic designs. Further, as it appears as a convex penalty in our objective, it allows for easy computation. As unit-level clustering results in the smallest value of the Schatten q penalty, increases to the penalization parameter κ will force the solution towards this covariance structure.

Proposition 7. *Let $r \in \{-1, 1\}^n$ denote the treatment assignment under a Bernoulli randomization design. Then, for fixed $p = \mathbb{P}(r_i = 1)$ for all $i \in [n]$, and $q > 1$, $\arg \min_{\substack{X \succeq 0; \\ X_{ii}=1}} \|X\|_q = \text{Cov}(r)$.*

We note that the analogous result holds if $r \in \{-1, 1\}^n$ is the treatment assignment under a complete randomization design and $n_1 = n_0$, with the optimization constraint $X\mathbf{1} = \mathbf{0}$. We present this formally in Appendix J.

Thus, large κ permits a more robust design. Indeed, κ penalizes the Schatten norm of X , driving the design toward a Bernoulli randomization as $\kappa \rightarrow \infty$, as formalized in Proposition 7. We illustrate this behavior in Figures A.2 and 4.2, as the trade-off parameters in the SDP, described in Section 5.1, are varied.

Remark 7. We use the term randomization in a specific sense: by increased randomization, we refer to designs with denser covariance matrices, which lead to more robustness to heterogeneous variation. This stands in contrast to trivial randomizations, such as randomly flipping between fixed treatment and control assignment vectors, that preserve the covariance matrices and lie on level sets of the objective function. We do not refer to this latter scenario. \diamond

Additionally, Figure 1.2 illustrates the trade-offs of the minimum cut and minimum effective resistance components against each other. It depicts a “clustered” block structure in the

covariance matrices on the left-end of the spectrum when $\gamma > \eta$, and a more “diffusive” covariance structure on the right-end of the spectrum when $\gamma < \eta$. Figures 1.1 and 4.1 depict the trade-offs on a graph generated from an SBM with equal cluster membership probability across five clusters. Figure 4.1 isolates the trade-offs between clustering and randomization. In particular, as the ratio κ/γ increases, the designs interpolate from a clustered design to a design that resembles unit-level Bernoulli randomization. Figure 1.1 isolates the trade-offs between clustering and effective resistance minimization. In particular, as the ratio η/γ increases, the designs interpolate from a clustered design to a design that is maximally spread-out.

Remark 8. The term $\text{Tr}(\mathbf{1}\mathbf{1}^T X)$ in the bound encourages solutions that are orthogonal to $\mathbf{1}\mathbf{1}^T$ as $\Delta \rightarrow \infty$. Since the constant vector lies in the kernel of both the graph Laplacian and its pseudo-inverse, this term encourages non-degenerate solutions. \diamond

5 Experimental Design

We describe the two design approaches we propose. To keep ideas simple and clear, in the following, we write down only the general Schatten norms for the robustness trade-off term.

5.1 MSE-minimizing SDP relaxation and Gaussian Rounding

Let $\Delta = (a + b/2)^2 + \delta$. Reparameterizing the right-hand side of Theorem 2 with $\tilde{\gamma}, \tilde{\eta}$, and $\tilde{\kappa}$, so that $\tilde{\gamma} := \frac{\gamma}{\Delta}$, $\tilde{\eta} := \frac{5\eta}{4\Delta}$, and $\tilde{\kappa} := \frac{5\kappa}{4\Delta}$, we can write an SDP more explicitly in terms of the new trade-off parameters:

$$\begin{aligned} \min_{X \in \mathbb{R}^{n \times n}} \quad & \tilde{\eta} \text{Tr}(L^\dagger X) + \tilde{\gamma} \text{Tr}(LX) + \tilde{\kappa} \|X\|_q + \text{Tr}(\mathbf{1}\mathbf{1}^T X) \\ \text{s.t.} \quad & X \succeq 0 \\ & \text{diag}(X) = \mathbf{1} \end{aligned} \tag{5.1}$$

We generate our treatment assignment vector ζ using Algorithm 1, drawing ideas from [Goemans and Williamson \[1995\]](#).

5.2 Adapted Gram-Schmidt Walk algorithm

As a second approach, we adapt the Gram-Schmidt Walk algorithm [[Harshaw et al., 2024](#)], a vector-balancing procedure, to our problem. By specializing the robustness hyperparameter, we provide an alternative algorithm that yields a guarantee for the worst-case MSE.

Considering only the homophily term $x^T L^\dagger x$ in our MSE expression, we can write $x^T L^\dagger x = x^T A^T A x$, for A such as the Cholesky factor of L^\dagger scaled by $\sqrt{\eta}$, $A = \sqrt{\eta} L^{\dagger/2}$, or $A = \sqrt{\eta} \Lambda^{1/2} V$, where Λ is the matrix of eigenvalues of L^\dagger , V is the matrix of the corresponding eigenvectors. We then use the Gram-Schmidt Walk algorithm [[Harshaw et al., 2024](#)] on the augmented

Algorithm 1 GAUSSIANROUNDING

Require: Parameters: $q, \tilde{\gamma}, \tilde{\eta}, \tilde{\kappa}$, and marginal assignment probability $p \triangleright \mathbb{P}(x_i = 1) = p$ for all $i \in [n]$

- 1: Solve the SDP in Equation (5.1) with parameters $q, \tilde{\gamma}, \tilde{\eta}$, and $\tilde{\kappa}$; let the solution be X^*
- 2: Sample $\xi \sim \mathcal{N}(0, X^*)$ \triangleright Multivariate Gaussian with covariance matrix X^*
- 3: **for** each $i \in [n]$ **do**
- 4: $x'_i \leftarrow \text{sgn}(\xi_i)$
- 5: **if** $x'_i = 1$ **then**
- 6: Draw $\zeta_i \sim \text{Rademacher}(2p)$ $\triangleright \mathbb{P}(\zeta_i = 1 \mid x'_i = 1) = 2p$
- 7: $\mathbb{P}(\zeta_i = -1 \mid x'_i = 1) = 1 - 2p$
- 8: **else**
- 9: $\zeta_i \leftarrow -1$
- 10: **end if**
- 11: **end for**
- 12: **return** x^*

covariate matrix B with columns B_i corresponding to $[e_i \ A_i]^T$ where e_i are standard basis vectors, and randomization parameter $\lambda = \frac{\sqrt{\kappa n^{1/q}}}{\sqrt{\xi^2 n} + \sqrt{\kappa n^{1/q}}}$ in Algorithm 2.

5.3 Comparing the two approaches

Both proposed methods extend to more general kernels, since the final optimization objective function retains the same form after replacing the Laplacian (see Appendix F.1).

In the adapted Gram-Schmidt Walk algorithm, the bounds grow with n (see also discussion after Theorem 11), since this procedure is tailored to the minimization of the operator norm. By contrast, we can directly optimize the Schatten- q norm penalties, via an SDP for common choices of q (e.g. $q \in \{1, 2, \infty\}$), or via convex optimization more broadly, leading to finer control. However, the computational efficiency of the SDP significantly drops for larger n , making vector balancing a practical alternative. We incorporate our trade-off formulation into the Gram-Schmidt Walk algorithm [Harshaw et al., 2024] in Algorithm 2, line 1.

Our application of the Gram-Schmidt Walk algorithm reduces to the control of $\text{Tr}(A^T A X)$ with $A := (\tilde{\eta}L^\dagger + \tilde{\gamma}L + \mathbf{1}\mathbf{1}^T)^{1/2}$ (or $A^T := [\tilde{\eta}^{1/2}L^{\dagger/2} \ \tilde{\gamma}^{1/2}L^{1/2} \ \mathbf{1}\mathbf{1}^{T^{1/2}}]$) and $\tilde{\kappa}\|X\|_q$, directly relating MSE control to covariate balancing, with covariates given by a factor of A . This framing would allow one to think about “clustering” as part of the covariate-balancing problem, the original focus of Harshaw et al. [2024]. Our “covariates” will resemble $A^{1/2}$.

The SDP followed by Gaussian rounding described in Section 5.1 is specialized to uniform treatment probabilities, whereas the Gram-Schmidt Walk approach allows direct specification of non-uniform treatment probabilities: let $\mathbf{p} = (p_1, p_2, \dots, p_n)$ denote the vector of treatment probabilities, and set the initial vector $z_1 \leftarrow 2\mathbf{p} - 1$ in Algorithm 2, line 6. On the other hand, the SDP formulation makes it straightforward to add additional convex constraints

(see also Appendix I).

6 Theoretical guarantees

Theorem 9 and its corollary provide worst-case MSE bounds for the SDP solution paired with the Gaussian Rounding procedure. In Proposition 29, we provide worst-case MSE bounds for the Gram-Schmidt Walk algorithm by applying results from Harshaw et al. [2024].

6.1 SDP followed by Gaussian Rounding

Our proof of Theorem 9 utilizes the seminal ideas underlying the approximation bound for MAXCUT, as introduced in Goemans and Williamson [1995] (see Appendix K.1 for more details). Our problem is similar in flavour, except we look at the minimization problem instead of maximization, and as such we would like an inequality in the opposite direction for a meaningful approximation bound.

We describe the geometric identities associated with our Gaussian rounding Algorithm 1. When $p := \mathbb{P}(\zeta_i = 1) = 1/2$, we have Grothendieck's identity, as derived in Goemans and Williamson [1995], $\mathbb{E}[\zeta_i \zeta_j] = \frac{2}{\pi} \arcsin \langle v_i, v_j \rangle$, where v_i is the i -th column vector of $X^{1/2}$, where X is the solution to the SDP in Section 5.1. As described in Algorithm 1, when $p = 1/2$, it is equivalent to setting $\zeta_i = 1$, whenever $\langle \xi, v_i \rangle > 0$, $i \in [n]$. This is because $\mathbb{P}(\langle v_i, \xi \rangle > 0) = 1/2$. We derive the geometric identity more generally for the non-symmetric case. The symmetric setting $p = 1/2$ is a special case of this.

Lemma 8. *Let $p := \mathbb{P}(x_i = 1)$, and X be the SDP solution to B.1. Let also v_i , $i = 1, 2, \dots, n$ be the column vectors of $X^{1/2}$. Denote the vector returned by Algorithm 1 by ζ . Then,*

$$\text{Cov}(\zeta_i, \zeta_j) = \frac{8p^2}{\pi} \arcsin \langle v_i, v_j \rangle, \text{ for } i \neq j.$$

Figure K.1 displays this relationship for various treatment assignment probabilities p .

Theorem 9 (Approximation bound). *Let $\Xi := \text{Cov}(\zeta)$ be the covariance matrix of the associated Rademacher random variables. Let X be the SDP solution. We assume that X is non-degenerate, i.e., $X \succeq \delta_\kappa I$, $\delta_\kappa > 0$. For $c = \left(\frac{8p^2}{\pi} + \frac{8p^2 \psi_\kappa}{\pi \delta_\kappa} + \frac{4p(1-p)-8p^2/\pi}{\delta_\kappa} \right)$, $\psi_\kappa = n \alpha_\kappa^3$, where α_κ is the maximum off-diagonal entry of X , in absolute value, $\Xi \preceq c_\kappa X$.*

In the proof, presented in Appendix K, we make use of the Taylor expansion of $\arcsin(X)$, following Nesterov [1997] in the MAXCUT problem. The resulting bounds depend on the tradeoff parameter κ : as $\kappa \rightarrow \infty$, the factor $\psi_\kappa \rightarrow 0$ while $\delta_\kappa \rightarrow 1$. To encourage non-degeneracy of X , the design parameters must be appropriately balanced. In particular, for clusterable graphs, the small Laplacian eigenvalues can lead to heavy penalization of the corresponding inverse Laplacian eigenvectors.

Corollary 10. *Let $\Xi := \text{Cov}(\zeta)$ be the covariance matrix of the associated rademacher random variables. Let X^* be the optimal achievable covariance matrix of the design in Theorem 12. Let also X_{SDP} denote the SDP solution matrix. We assume that X_{SDP} is non-degenerate, i.e., $X_{SDP} \succeq \delta_\kappa I$, $\delta_\kappa > 0$. For $c_\kappa = \frac{1}{4p(1-p)} \left(\frac{8p^2}{\pi} + \frac{8p^2\psi_\kappa}{\pi\delta_\kappa} + \frac{4p(1-p)-8p^2/\pi}{\delta_\kappa} \right)$, $\psi_\kappa = n\alpha_\kappa^3$, where α_κ is the maximum off-diagonal entry of X_{SDP} , in absolute value, $\text{Tr}(L\Xi) + \text{Tr}(L^\dagger\Xi) + \|\Xi\|_q + \text{Tr}(\mathbf{1}\mathbf{1}^T\Xi) \leq c_\kappa \left(\text{Tr}(LX^*) + \text{Tr}(L^\dagger X^*) + \|X^*\|_q + \text{Tr}(\mathbf{1}\mathbf{1}^T X^*) \right)$.*

The proof is given in Appendix K. When κ is large, the rounding procedure closely approximates the optimal design covariance; in the limiting Bernoulli randomized design, $\alpha_\kappa = 0$. For a complete randomized design, $\alpha_\kappa = 1/(n-1)$. Our results allow for $\alpha_\kappa = \Theta(1/n^{1/3})$, far more correlation than Bernoulli or complete randomizations, while maintaining a constant level of error. In contrast, when κ is very small, we can optimally solve the problem deterministically.

6.2 Adapted Gram-Schmidt Walk algorithm

We leverage Harshaw et al. [2024, Theorem 6.4] (see also Proposition 29) and its proof. In particular, we use the fact that the Gram-Schmidt Walk algorithm yields treatment assignments x that satisfy (1) $\text{Cov}(x) \preceq \lambda^{-1}I$, and (2) $\text{Cov}(Ax) \preceq \xi^2(1-\lambda)^{-1}I$. To allow for non-symmetric designs ($p \neq 1/2$) we introduce β_1, β_2 as defined in Theorem 12.

Theorem 11. *Let $A := (\tilde{\eta}L^\dagger + \tilde{\gamma}L + \Delta\mathbf{1}\mathbf{1}^T)^{1/2}$, where $\tilde{\eta} = \eta[\beta_1^2 + \beta_2^2]$, $\tilde{\gamma} = \gamma\beta_1^2$, $\tilde{\kappa} = \kappa[\beta_1^2 + \beta_2^2]$, and $\Delta = (\alpha\beta_1 + b\beta_2)^2$. The Gram-Schmidt Walk algorithm, with randomization parameter λ , returns an assignment x such that $\|\text{Cov}(Ax)\|_{p'} \leq \xi^2/(1-\lambda)\|I\|_{p'}$, and $\|\text{Cov}(x)\|_q \leq \|I\|_q/\lambda = n^{1/q}/\lambda$, for $\xi := \max_{i \in n} \|A_i\|$, A_i the column i of the matrix A . Thus, for $q \geq 1$,*

$$\sup_{\chi(\eta, \gamma, \kappa)} \mathbb{E}[(\tau - \hat{\tau})^2] \leq 7 \left[\mathbb{E}[\|A(x - \mu)\|^2] + \tilde{\kappa}\|X\|_q \right] \leq 7 \left[\frac{\xi^2 n}{1 - \lambda} + \tilde{\kappa} \frac{n^{1/q}}{\lambda} \right],$$

where $\mu_i = \mathbb{E}[x_i]$, for all $i \in [n]$. This is minimized for $\lambda = \frac{\sqrt{\tilde{\kappa}n^{1/q}}}{\sqrt{\xi^2 n} + \sqrt{\tilde{\kappa}n^{1/q}}}$.

The proof is in Appendix K.1. The asymptotic results in Harshaw et al. [2024] require the trade-off parameter $\lambda \rightarrow 1$. That is, their asymptotic results require that $\kappa/\eta, \kappa/\gamma, \kappa/\Delta \rightarrow \infty$, mirroring the improvement in the approximation error bounds in Theorem 9.

The results in Corollary 10 and Theorem 11 are notably different. In Theorem 9 and Corollary 10, we prove that rounding yields comparable MSE control to the optimal SDP solution. In contrast, in Theorem 11 we directly bound the worst-case MSE resulting from the adapted Gram-Schmidt Walk design. See also Section 5.3 where we discuss how the design from the Gram-Schmidt Walk algorithm compares to the design from the SDP followed by Gaussian rounding. In theory, we expect the bounds from the Gram-Schmidt Walk algorithm to be loose when n is larger, and q is smaller.

7 Discussion

We develop a novel framework to understand the three-way trade-off between homophily, network interference, and robustness to heterogeneous variation, recovering existing designs in extreme cases within the trade-off. Along the way, we generalize several existing results and designs in related literature. We demonstrated the complementary behaviors of our two proposed approaches, solving an SDP followed by Gaussian Rounding, and the adapted Gram-Schmidt Walk algorithm. In proving approximation guarantees via the SDP approach, we leveraged and generalized ideas utilized in proving approximation guarantees for the MAXCUT problem. This generalization may be of independent interest.

While we focus on the Horvitz–Thompson estimator for GATE estimation, our framework naturally extends to more general estimators and estimands, which we leave for future work. In this paper, we study optimal designs under known bounds η , κ , and γ . Such bounds may be informed by domain expertise or learned from prior experiments and historical network data, and our approach makes explicit how this information can be incorporated. An important direction for future work is extending the framework to online settings, where treatments are assigned sequentially and the parameters η , κ , and γ are learned adaptively. Finally, for large-scale graphs, problem-specific algorithms could be used to accelerate the SDP, though this lies beyond the scope of the present work.

8 Acknowledgements

We thank Thomas Rothvoss for insightful discussions and for pointing us to [Raghavendra and Tan \[2012\]](#), Arun Chandrasekhar for pointing us to the village network dataset, and Davide Viviano for sharing the causal clustering code for verification purposes.

References

Peter M Aronow and Cyrus Samii. Estimating average causal effects under general interference, with application to a social network experiment. 2017.

Avanti Athreya, Donniell E Fishkind, Minh Tang, Carey E Priebe, Youngser Park, Joshua T Vogelstein, Keith Levin, Vince Lyzinski, Yichen Qin, and Daniel L Sussman. Statistical inference on random dot product graphs: a survey. *Journal of Machine Learning Research*, 18(226):1–92, 2018.

Sarah Baird, J Aislinn Bohren, Craig McIntosh, and Berk Özler. Optimal design of experiments in the presence of interference. *Review of Economics and Statistics*, 100(5):844–860, 2018.

Abhijit Banerjee, Arun G. Chandrasekhar, Esther Duflo, and Matthew O. Jackson. The Diffusion of Microfinance, 2013a. URL <https://doi.org/10.7910/DVN/U3BIHX>.

Abhijit Banerjee, Arun G Chandrasekhar, Esther Duflo, and Matthew O Jackson. The diffusion of microfinance. *Science*, 341(6144):1236498, 2013b.

Guillaume W Basse and Edoardo M Airoldi. Model-assisted design of experiments in the presence of network-correlated outcomes. *Biometrika*, 105(4):849–858, 2018.

Best Neighborhoods, n.d. <https://bestneighborhood.org/race-in-chicago-il/>, accessed August, 2025.

Rajendra Bhatia. *Matrix analysis*, volume 169. Springer Science & Business Media, 2013.

Jennifer Brennan, Vahab Mirrokni, and Jean Pouget-Abadie. Cluster randomized designs for one-sided bipartite experiments. *Advances in Neural Information Processing Systems*, 35: 37962–37974, 2022.

Qianyi Chen, Bo Li, Lu Deng, and Yong Wang. Optimized covariance design for ab test on social network under interference. *Advances in Neural Information Processing Systems*, 36, 2024.

Alex Chin. Regression adjustments for estimating the global treatment effect in experiments with interference. *Journal of Causal Inference*, 7(2):20180026, 2019.

Mayleen Cortez-Rodriguez, Matthew Eichhorn, and Christina Lee Yu. Analysis of two-stage rollout designs with clustering for causal inference under network interference. *arXiv preprint arXiv:2405.05119*, 2024.

Sergio Curranini, Matthew O Jackson, and Paolo Pin. An economic model of friendship: Homophily, minorities, and segregation. *Econometrica*, 77(4):1003–1045, 2009.

Nick Doudchenko, Khashayar Khosravi, Jean Pouget-Abadie, Sebastien Lahaie, Miles Lubin, Vahab Mirrokni, Jann Spiess, et al. Synthetic design: An optimization approach to experimental design with synthetic controls. *Advances in Neural Information Processing Systems*, 34:8691–8701, 2021.

Dean Eckles, Brian Karrer, and Johan Ugander. Design and analysis of experiments in networks: Reducing bias from interference. *Journal of Causal Inference*, 5(1):20150021, 2017.

Bradley Efron. Forcing a sequential experiment to be balanced. *Biometrika*, 58(3):403–417, 1971.

Matthew Eichhorn, Samir Khan, Johan Ugander, and Christina Lee Yu. Low-order outcomes and clustered designs: combining design and analysis for causal inference under network interference. *arXiv preprint arXiv:2405.07979*, 2024.

Zahra Fatemi and Elena Zheleva. Minimizing interference and selection bias in network experiment design. In *Proceedings of the International AAAI Conference on Web and Social Media*, volume 14, pages 176–186, 2020.

Zahra Fatemi and Elena Zheleva. Network experiment designs for inferring causal effects under interference. *Frontiers in big Data*, 6:1128649, 2023.

Angela Fontan and Claudio Altafini. On the properties of laplacian pseudoinverses. In *2021 60th IEEE Conference on Decision and Control (CDC)*, pages 5538–5543. IEEE, 2021.

Carlo Gaetan, Xavier Guyon, et al. *Spatial statistics and modeling*, volume 90. Springer, 2010.

David Gale and Lloyd S Shapley. College admissions and the stability of marriage. *The American mathematical monthly*, 69(1):9–15, 1962.

Michel X Goemans and David P Williamson. Improved approximation algorithms for maximum cut and satisfiability problems using semidefinite programming. *Journal of the ACM (JACM)*, 42(6):1115–1145, 1995.

Christopher Harshaw, Fredrik Sävje, David Eisenstat, Vahab Mirrokni, and Jean Pouget-Abadie. Design and analysis of bipartite experiments under a linear exposure-response model. *Electronic Journal of Statistics*, 17(1):464–518, 2023.

Christopher Harshaw, Fredrik Sävje, Daniel A Spielman, and Peng Zhang. Balancing covariates in randomized experiments with the gram–schmidt walk design. *Journal of the American Statistical Association*, 119(548):2934–2946, 2024.

Keisuke Hirano and Jack R Porter. Asymptotics for statistical treatment rules. *Econometrica*, 77(5):1683–1701, 2009.

Peter D Hoff, Adrian E Raftery, and Mark S Handcock. Latent space approaches to social network analysis. *Journal of the american Statistical association*, 97(460):1090–1098, 2002.

David Holtz, Felipe Lobel, Ruben Lobel, Inessa Liskovich, and Sinan Aral. Reducing interference bias in online marketplace experiments using cluster randomization: Evidence from a pricing meta-experiment on airbnb. *Management Science*, 71(1):390–406, 2025.

L. Isserlis. On a formula for the product-moment coefficient of any order of a normal frequency distribution in any number of variables. *Biometrika*, 12(1/2):134–139, 1918. ISSN 00063444, 14643510. URL <http://www.jstor.org/stable/2331932>.

Matthew O Jackson. Inequality’s economic and social roots: the role of social networks and homophily. *arXiv preprint arXiv:2506.13016*, 2025.

Matthew O Jackson, Stephen M Nei, Erik Snowberg, and Leeat Yariv. The dynamics of networks and homophily. Technical report, National Bureau of Economic Research, 2023.

Ravi Jagadeesan, Natesh S Pillai, and Alexander Volfovsky. Designs for estimating the treatment effect in networks with interference. 2020.

Nazgul Jenish and Ingmar R Prucha. Central limit theorems and uniform laws of large numbers for arrays of random fields. *Journal of econometrics*, 150(1):86–98, 2009.

Paul F Lazarsfeld, Robert K Merton, et al. Friendship as a social process: A substantive and methodological analysis. *Freedom and control in modern society*, 18(1):18–66, 1954.

Michael P Leung. Causal inference under approximate neighborhood interference. *Econometrica*, 90(1):267–293, 2022a.

Michael P Leung. Rate-optimal cluster-randomized designs for spatial interference. *The Annals of Statistics*, 50(5):3064–3087, 2022b.

Wenrui Li, Daniel L Sussman, and Eric D Kolaczyk. Causal inference under network interference with noise. *arXiv preprint arXiv:2105.04518*, 2021.

Xinran Li, Peng Ding, and Donald B Rubin. Asymptotic theory of rerandomization in treatment–control experiments. *Proceedings of the National Academy of Sciences*, 115(37):9157–9162, 2018.

Miller McPherson, Lynn Smith-Lovin, and James M Cook. Birds of a feather: Homophily in social networks. *Annual review of sociology*, 27(1):415–444, 2001.

Kari Lock Morgan and Donald B Rubin. Rerandomization to improve covariate balance in experiments. 2012.

Yurii Nesterov. Quality of semidefinite relaxation for nonconvex quadratic optimization. Technical report, Université catholique de Louvain, Center for Operations Research and . . ., 1997.

Jean Pouget-Abadie, Vahab Mirrokni, David C Parkes, and Edoardo M Airoldi. Optimizing cluster-based randomized experiments under monotonicity. In *Proceedings of the 24th ACM SIGKDD International Conference on Knowledge Discovery & Data Mining*, pages 2090–2099, 2018.

Prasad Raghavendra and Ning Tan. Approximating csp with global cardinality constraints using sdp hierarchies. In *Proceedings of the twenty-third annual ACM-SIAM symposium on Discrete Algorithms*, pages 373–387. SIAM, 2012.

Donald B Rubin. Bayesian inference for causal effects: The role of randomization. *The Annals of statistics*, pages 34–58, 1978.

Daniel A Spielman and Nikhil Srivastava. Graph sparsification by effective resistances. In *Proceedings of the fortieth annual ACM symposium on Theory of computing*, pages 563–568, 2008.

Vydhourie Thiyyageswaran, Tyler McCormick, and Jennifer Brennan. Data-adaptive exposure thresholds for the horvitz-thompson estimator of the average treatment effect in experiments with network interference. *arXiv preprint arXiv:2405.15887*, 2024.

Johan Ugander and Hao Yin. Randomized graph cluster randomization. *Journal of Causal Inference*, 11(1):20220014, 2023.

Johan Ugander, Brian Karrer, Lars Backstrom, and Jon Kleinberg. Network exposure to multiple universes. In *NIPS Workshop: Social network and social media analysis: Methods, models and applications, Lake Tahoe, NV*, 2012.

Johan Ugander, Brian Karrer, Lars Backstrom, and Jon Kleinberg. Graph cluster randomization: Network exposure to multiple universes. In *Proceedings of the 19th ACM SIGKDD international conference on Knowledge discovery and data mining*, pages 329–337, 2013.

Davide Viviano, Lihua Lei, Guido Imbens, Brian Karrer, Okke Schrijvers, and Liang Shi. Causal clustering: design of cluster experiments under network interference. *arXiv preprint arXiv:2310.14983*, 2023.

Christina Lee Yu, Edoardo M Airoldi, Christian Borgs, and Jennifer T Chayes. Estimating the total treatment effect in randomized experiments with unknown network structure. *Proceedings of the National Academy of Sciences*, 119(44):e2208975119, 2022.

APPENDIX

A More illustrations

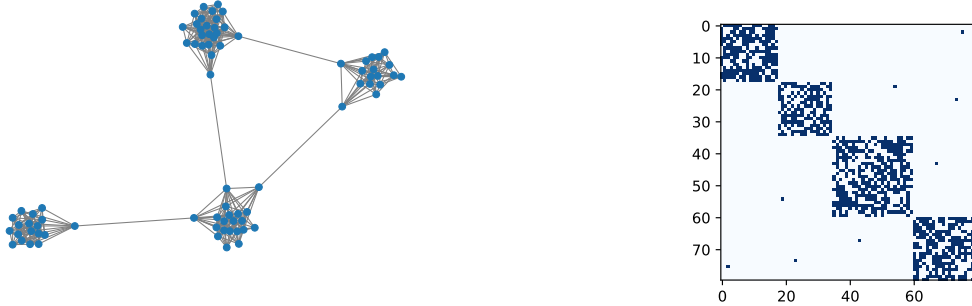


Figure A.1: An SBM graph with four underlying clusters, and its adjacency matrix (with dark blue representing the presence of an edge, and light blue representing absence of an edge).

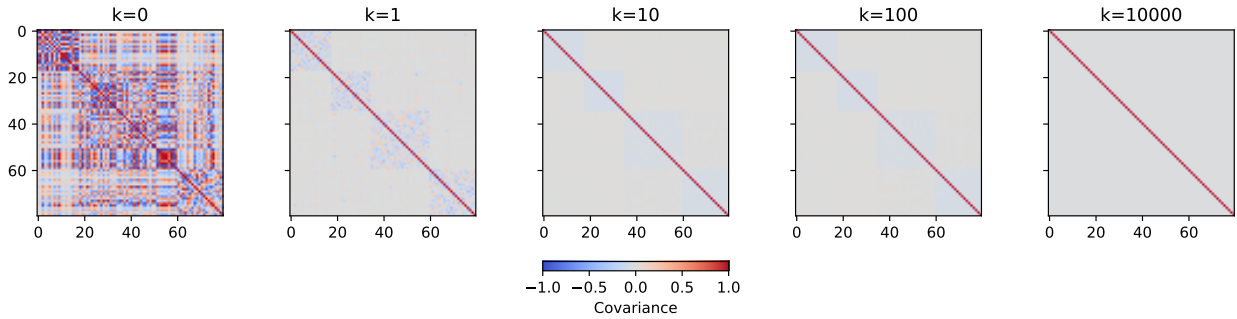


Figure A.2: Solutions of the SDPs described in Section 5.1 on the graph in fig. A.1 trading-off $10\text{Tr}(L^\dagger X) + k\|X\|_F + 10\text{Tr}(\mathbf{1}\mathbf{1}^T X)$. k ranges between $(0, 10^0, 10, 10^2, 10^4)$ from left to right.

In Figure 1.1, the treatment assignments are generated by Gaussian rounding. The panels vary the trade-off parameter ratio η/γ : Left: $\eta = 10, \gamma = 100, \kappa = 1, q = 2$; Center: $\eta = 1000, \gamma = 100, \kappa = 1, q = 2$; Right: $\eta = 10000, \gamma = 10, \kappa = 1, q = 2$.

Similarly, in Figure 4.1, the treatment assignments are generated by Gaussian rounding. The panels vary the trade-off parameter ratio κ/γ : Left: $\eta = 0, \gamma = 1000, \kappa = 1, q = 2$; Center: $\eta = 0, \gamma = 1, \kappa = 1, q = 2$; Right: $\eta = 0, \gamma = 1, \kappa = 1000, q = 2$.

In Figure 1.2, we display solutions of the SDPs described in Section 5.1 on the graph in Figure A.1 trading-off $10\text{Tr}(LX) + h\text{Tr}(L^\dagger X) + 10\text{Tr}(\mathbf{1}\mathbf{1}^T X)$. Here, h ranges between $(0, 10^0, 10, 10^2, 10^4)$ from left to right.

Similarly, we display solutions of the SDPs described in Section 5.1 on the graph in Figure A.1 trading-off $10 \text{Tr}(LX) + k\|X\|_F + 10 \text{Tr}(\mathbf{1}\mathbf{1}^T X)$. Here, k ranges between $(0, 10^0, 10, 10^2, 10^4)$ from left to right.

B Non-symmetric Case

We now consider the non-symmetric case, i.e., when $\mathbb{P}(z_i = 1) \neq \mathbb{P}(z_i = 0)$. We assume that the treatment probability p is uniform across nodes, i.e., $p = \mathbb{P}(z_i = 1) = \mathbb{P}(z_j = 1)$ for all $i, j \in [n]$. As before, our goal is to relax this problem to the minimization of a quadratic form $x^T Q x$ plus a penalization term to encourage randomization, which can then be optimized via an SDP or the adapted Gram-Schmidt Walk vector-balancing approach.

Theorem 12 (Non-symmetric MSE bound). *Let $p := \mathbb{P}(z_i = 1)$ for all $i \in [n]$, $\beta_1 := 1/(2np(1-p))$, $\beta_2 := 1/(2np)$, $a = \langle \alpha, \mathbf{1}/n \rangle$, $b = \langle \phi, \mathbf{1}/n \rangle$, and $\langle s(z), \mathbf{1}/n \rangle \leq \sqrt{\delta}$. Let also $x \in \{-1, 1\}^n$ by defining $x := 2z - 1$. Define $X := \text{Cov}(x)$. Then, for $q \geq 1$,*

$$\begin{aligned} \mathbb{E}[(\hat{\tau} - \tau)^2] &\leq \\ 7\{\text{Tr}((\gamma\beta_1^2 L + \eta[\beta_1^2 + \beta_2^2]L^\dagger)X) + \kappa[\beta_1^2 + \beta_2^2]\|X\|_q + &([a\beta_1 + b\beta_2]^2 + \beta_1^2\delta) \text{Tr}(\mathbf{1}\mathbf{1}^T X)\}. \end{aligned}$$

We display the proof in Appendix J.2.

Let $\Delta = (a\beta_1 + b\beta_2)^2 + \beta_1^2\delta$. Reparameterizing with $\tilde{\gamma}, \tilde{\eta}$, and $\tilde{\kappa}$ so that $\tilde{\gamma} := \frac{\gamma\beta_1^2}{\Delta}$, $\tilde{\eta} := \frac{\eta[\beta_1^2 + \beta_2^2]}{\Delta}$, and $\tilde{\kappa} := \frac{\kappa[\beta_1^2 + \beta_2^2]}{\Delta}$, we can write an SDP more explicitly in terms of the new trade-off parameters:

$$\begin{aligned} \min_{X \in \mathbb{R}^{n \times n}} \quad & \tilde{\eta} \text{Tr}(L^\dagger X) + \tilde{\gamma} \text{Tr}(LX) + \tilde{\kappa} \|X\|_q + \text{Tr}(\mathbf{1}\mathbf{1}^T X) \\ \text{s.t.} \quad & X \succeq 0 \\ & \text{diag}(X) = \mathbf{1} \end{aligned} \tag{B.1}$$

Figure D.2 presents the covariance matrices of the design across different treatment assignment probabilities p , generated from applying Algorithm 1 to the corresponding SDP solutions in Figure D.1.

In the adapted Gram-Schmidt Walk, we can take $A := (\tilde{\eta}L^\dagger + \tilde{\gamma}L + \mathbf{1}\mathbf{1}^T)^{1/2}$. Then, we can take the robustness parameter to be $\lambda = \frac{\sqrt{\tilde{\kappa}n^{1/q}}}{\sqrt{\xi^2 n} + \sqrt{\tilde{\kappa}n^{1/q}}}$, where $\xi := \max_{i \in n} \|A_i\|$. Alternatively, one could append the vectors so $A_i^T = [\tilde{\eta}^{1/2}L_i^{\dagger/2} \quad \tilde{\gamma}^{1/2}L_i^{1/2} \quad \mathbf{1}\mathbf{1}^T_i]^{1/2}$.

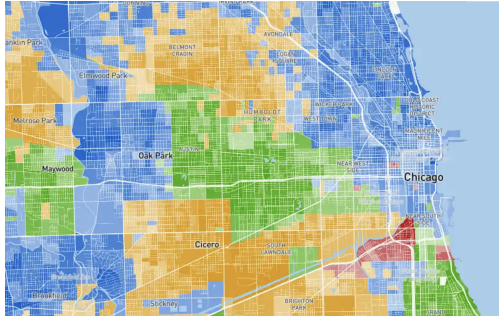


Figure C.1: A real example of homophily. The map from [Best Neighborhoods \[n.d.\]](#) depicts majority race by geographic area in the Chicago region, based on self-identification on the US census. Darker shades indicate a larger racial majority. This spatial map can be modeled as a network, where nodes represent geographic areas and edge weights are inversely proportional to the distance between them. This network exhibits a high level of homophily, as racial composition varies smoothly across neighboring areas in the graph.

C More examples

C.1 Homophily

Figure C.1 depicts a concrete real example of homophily.

Example 4. One natural interpretation of homophily is via the latent space framework [Athreya et al., 2018, Hoff et al., 2002], where we identify a homophilous vector h with a smooth function of common latent variables that determine the graph weights W_{ij} . As a concrete example, each node may be associated to a latent vector u_i , and for $U := [u_1, \dots, u_n]^T$, there is some $\beta \in \mathbb{R}^d$ such that $h = U\beta$, and $W_{ij} \propto \exp(-\|u_i - u_j\|^2)$. \diamond

Remark 9. The quadratic form $g^T L g = \langle g, Lg \rangle_{\ell_2}$ directly quantifies the smoothness of the function g with respect to the graph structure. Its continuous analogue, replacing the discrete graph with a manifold or a domain equipped with a measure μ , is the quadratic form $\langle g, \Delta_\mu g \rangle_{L^2(\mu)} = \int g \Delta_\mu g \, d\mu = \int \|\nabla g\|^2 \, d\mu$, where Δ_μ is the Laplacian operator with respect to μ , and ∇g is the gradient of a sufficiently smooth function g supported on μ . \diamond

C.2 Interference

Example 5 (Full Network Interference). Take for example an instance of the weak-dependence model [Leung, 2022a] adapting α -mixing spatial processes (see, for example, Jenish and Prucha [2009]) to path lengths ρ_n in the network, where $\sum_{m=2}^n M_m^\partial \tilde{\theta}_m = o(\psi_1)$, for some $\psi_1 \ll 1$, $M_m^\partial := \frac{1}{n} \sum_{i=1}^n |\mathcal{N}^\partial(i, m)|$, $\mathcal{N}^\partial(i, m) := \{j \in [n] : \rho_n(i, j) = m\}$, and correlation between outcomes $\tilde{\theta}_m \rightarrow 0$, as $m \rightarrow \infty$. That is, the correlation $\tilde{\theta}$ between outcomes of units decay over (path length) distances ρ_n . Here \tilde{L} can be taken to be the graph Laplacian of a complete graph, modeling a full interference structure, with edge weights $\tilde{\theta}$ corresponding to the correlation under path lengths in the original path length weak-dependence structure



Figure C.2: Example of noisy network observation. Left panel: True network, G . Right panel: Noisy observation G_{obs} of the network with grey edges preserved and newly added dark blue edges. The orange edges depict missing edges.

(see, for example, Figure C.3). Under the setting with such a $\tilde{\theta}$ decaying quickly, we have that the full degree matrix $\tilde{D} = D + \text{diag}(\delta)$, and full adjacency matrix $\tilde{W} = W + \epsilon$, where $\delta_i = \sum_{j \in [n]} \epsilon_{ij}$, for all $i = 1, 2, \dots, n$. Then, writing $L_{\text{res}} := \text{diag}(\delta) - \epsilon$, $\tilde{L} = L + L_{\text{res}}$. The spectrum of L_{res} are upper-bounded by some $\psi_2 \ll 1$, such that $\|\tilde{L}^\dagger L\|_{\text{op}} \leq 1 + O(\psi)$, for $\psi \ll 1$. Then, our worst-case MSE bound would consist of the perturbed bound, $\gamma(1 + O(\psi))$ instead of just γ . \diamond



Figure C.3: Full interference example. Left panel: First-order (neighborhood) interference, where outcomes depend only on treatments of immediate neighbors. Right panel: Full network interference induced by the same underlying graph, allowing interference to propagate along paths of increasing length, with strength decaying in path length. Darker edges indicate stronger (shorter-path) interference effects.

Example 6. We note the distinction between our model of interference and a generalized version of the previous example when the interference term $s(z)$ is $\frac{\boldsymbol{\gamma}}{\sqrt{n}} \tilde{L} z$, where $\boldsymbol{\gamma}_i, \boldsymbol{\gamma}_j$ are not necessarily equal for any (i, j) pair. A somewhat similar interference structure encapsulated by our model is one where $s(z) = L^{1/2} \text{diag}(\boldsymbol{\gamma} / \sqrt{2d_{\max} n}) L^{1/2} z$, where d_{\max} is the maximum degree of the nodes in the graph. Then, if $\|\boldsymbol{\gamma}\|_\infty^2 \leq \gamma$, indeed we have

$$\begin{aligned} s(z)^T L^\dagger s(z) &= z^T L^{1/2} \text{diag}(\boldsymbol{\gamma} / \sqrt{n}) L^{1/2} L^\dagger L^{1/2} \text{diag}(\boldsymbol{\gamma} / \sqrt{n}) L^{1/2} z \\ &= z^T L^{1/2} \text{diag}(\boldsymbol{\gamma} / \sqrt{2d_{\max} n}) \mathcal{P} \text{diag}(\boldsymbol{\gamma} / \sqrt{2d_{\max} n}) L^{1/2} z \\ &\leq \frac{z^T L z}{2d_{\max} n} \|\boldsymbol{\gamma}\|_\infty^2 \leq \gamma, \end{aligned}$$

where \mathcal{P} is the orthogonal projection matrix onto the column space of L . Thus, $s(z)$ is (γ, L) -interferent. \diamond

D More on the experimental designs

D.1 Gaussian Rounding on the SDP solutions

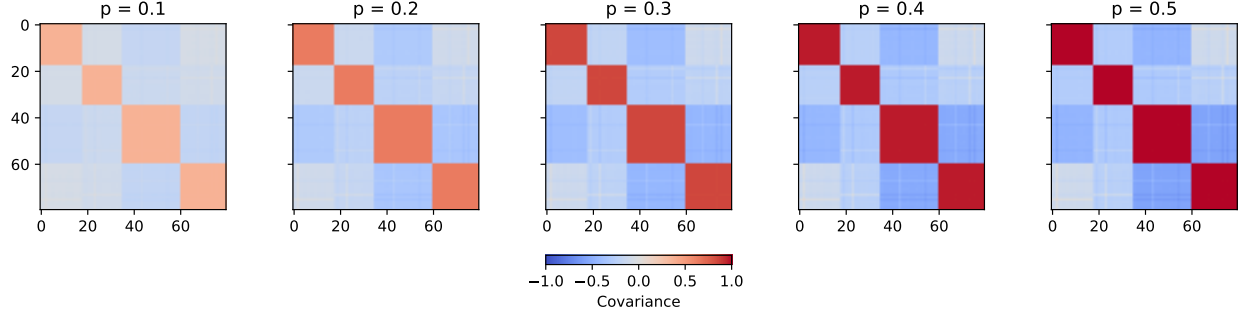


Figure D.1: SDP solutions on the graph from fig. A.1, with trade-off parameters $\gamma = 10$, $\eta = 1$, $\kappa = 1$, and $a = b = 1$, across varying treatment assignment probabilities p . Here p ranges between $(0.1, 0.2, 0.3, 0.4, 0.5)$ from left to right. The probabilities p scale each trade-off component of the SDP via β_1 and β_2 , and thus the SDP solutions exhibit only slight variation across values of p .

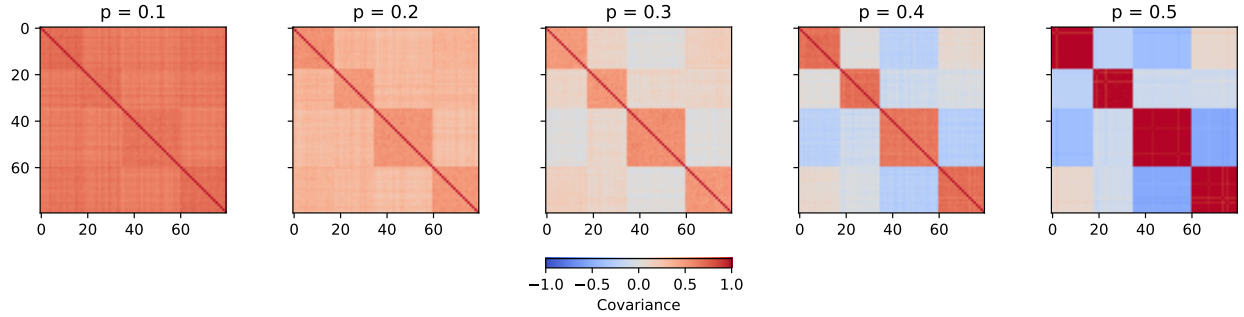


Figure D.2: Covariance matrices of our designs by applying Algorithm 1 to the SDP solutions in Figure D.1, across treatment assignment probabilities p ranging between $(0.1, 0.2, 0.3, 0.4, 0.5)$ from left to right.

D.2 Adapted Gram-Schmidt Walk algorithm

We include the Gram-Schmidt Walk algorithm adapted to our trade-off problem in Algorithm 2.

E Other related works

A common design approach with the goal of balancing covariates within a randomization scheme is re-randomization [Morgan and Rubin, 2012, Li et al., 2018]. While we do not directly compare our methods to re-randomization procedures, Harshaw et al. [2024] show superior

Algorithm 2 (Adapted) Gram-Schmidt Walk [Harshaw et al., 2024]

Require: q, η, γ, κ

- 1: Set $\lambda \leftarrow \frac{\kappa n^{1/q}}{\eta \xi^2 n + \kappa n^{1/q}}$
- 2: Define $\xi \leftarrow \max_{i \in [n]} \|A_i\|$
- 3: Define A_i as the i -th column of $\Lambda^{1/2}V$, where $V^\top \Lambda V = \tilde{\eta} L^\dagger + \tilde{\gamma} L + \mathbf{1}\mathbf{1}^\top$
(Alternatively, use the appended matrix A ; see discussion above)
- 4: Define $[B]_i \leftarrow \vec{b}_i \leftarrow \begin{bmatrix} \sqrt{\lambda} e_i \\ \xi^{-1} \sqrt{1 - \lambda} A_i \end{bmatrix}$
- 5: Initialize iteration counter $t \leftarrow 1$
- 6: Initialize assignment vector $\vec{z}_1 \leftarrow 2\mathbf{p} - 1$
- 7: Select pivot index $p \sim \text{Uniform}([n])$
- 8: **while** $\vec{z}_t \notin \{\pm 1\}^n$ **do**
- 9: Define active set $\mathcal{A} \leftarrow \{i \in [n] : |\vec{z}_t(i)| < 1\}$
- 10: **if** $p \notin \mathcal{A}$ **then**
- 11: Resample pivot $p \sim \text{Uniform}(\mathcal{A})$
- 12: **end if**
- 13: Compute step direction:
$$\vec{u}_t \leftarrow \underset{\vec{u} \in \mathbb{R}^n}{\operatorname{argmin}} \|\vec{B} \vec{u}\|^2 \quad \text{s.t.} \quad u(p) = 1, \quad u(i) = 0 \quad \forall i \notin \mathcal{A}$$
- 14: Define feasible step sizes:
$$\Delta \leftarrow \{\delta \in \mathbb{R} : \vec{z}_t + \delta \vec{u}_t \in [-1, 1]^n\}$$
- 15: Set $\delta^+ \leftarrow |\max \Delta|$, $\delta^- \leftarrow |\min \Delta|$
- 16: Randomly sample step size:
$$\delta_t \leftarrow \begin{cases} \delta^+ & \text{with probability } \frac{\delta^-}{\delta^+ + \delta^-} \\ -\delta^- & \text{with probability } \frac{\delta^+}{\delta^+ + \delta^-} \end{cases}$$
- 17: Update assignment: $\vec{z}_{t+1} \leftarrow \vec{z}_t + \delta_t \vec{u}_t$
- 18: Increment $t \leftarrow t + 1$
- 19: **end while**
- 20: **return** Final assignment vector $\vec{z}_t \in \{\pm 1\}^n$

trade-offs of their method, which ours resemble under reparameterization, in comparison to re-randomization. Basse and Airoldi [2018] study the re-randomization approach under homophily settings alone. Ugander and Yin [2023] introduce randomized graph cluster randomization (RGCR) to address exponentially small exposure probabilities arising in graph cluster randomization designs [Ugander et al., 2013]. They show that RGCR still exhibits large variance when the nodes in a ring graph are clustered into a small number of large randomization units under a potential outcomes model with a homophily drift, a phenomenon

also observed more generally in simulations. Related observations on the tension between homophily and cluster randomization appear in [Ugander et al. \[2012\]](#), [Cortez-Rodriguez et al. \[2024\]](#).

Another strategy is a matched-pair design, where randomization is restricted to pre-specified pairs of similar units. [Fatemi and Zheleva \[2020\]](#) propose CMatch, a two-stage procedure that clusters units via random walks on the graph and then matches clusters using a similarity measure to assign treatments. Our framework does not rely on local assumptions about inherent similarities between pairs of randomization units. We introduce a global optimization approach to address homophily, interference, and robustness simultaneously.

[Jagadeesan et al. \[2020\]](#) study estimation of direct effects by constructing treatment assignments that balance interference-related features between treated and control units. They introduce perfect quasi-colorings, which eliminate interference bias by matching units with identical treated and control neighborhood structure, and analyze the bias and variance of restricted randomization schemes that approximate such colorings when they do not exist. Their design can be viewed as stratified randomization based on node similarity, and they characterize the resulting MSE under various settings, including models with homophily and network interference, showing improvements over Bernoulli and complete randomization in some regimes.

Optimization-based designs in this setting include the approach of [Fatemi and Zheleva \[2023\]](#), where the authors formulate a mixed-integer program to identify maximally independent node sets for direct effect estimation. In a different application, [Doudchenko et al. \[2021\]](#) use a mixed-integer program to jointly optimize design and weights in synthetic control settings. Solving mixed-integer programs to optimality is not polynomial-time and does not scale; solving an SDP, as in our method, is polynomial-time and admits efficient solvers that can be sped up by exploiting problem structure.

Bipartite networks arising from preference-based matching processes, such as those studied by [Gale and Shapley \[1962\]](#), naturally induce homophily. Our framework therefore extends to bipartite settings, including marketplaces, generalizing existing bias-variance and graph-cut characterizations [[Brennan et al., 2022](#), [Holtz et al., 2025](#), [Pouget-Abadie et al., 2018](#), [Harshaw et al., 2023](#)].

F Generalizations and a special case

F.1 General Similarity Kernels and Stochastic Misspecification

Under a more general potential outcomes model,

$$Y = \sum_{i=1}^{N_\alpha} h_\alpha^i + \sum_{i=1}^{N'_\alpha} \varepsilon_\alpha^i + z \cdot \left(\sum_{i=1}^{N_\phi} \text{diag}(h_\phi^i) + \sum_{i=1}^{N'_\phi} \text{diag}(\varepsilon_\phi^i) \right) \quad (\text{F.1})$$

where h_f^i , $f \in \{\alpha, \phi\}$, satisfy quadratic constraints $h_f^{i^T} \mathcal{K}_f^i h_f^i \leq \eta_f^i$, \mathcal{K}_f^i a kernel/psd matrix (see Remark 4), and the misspecifications ε_f^i , $f \in \{\alpha, \phi\}$, satisfy Schatten-norm constraints $\|\Sigma_f^i\|_{q_f^i} := \|\mathbb{E}[\varepsilon_f^i \varepsilon_f^{i^T}]\|_{q_f^i} \leq \kappa_f^i$. Defining $\boldsymbol{\eta} := [\eta_\alpha, \eta_\phi]$, $\boldsymbol{\kappa} := [\kappa_\alpha, \kappa_\phi]$ for $\eta_f := (\eta_f^i)_{i=1}^{N_f}$, $\kappa_f := (\kappa_f^i)_{i=1}^{N'_f}$, where $f \in \{\alpha, \phi\}$, and $N := N_\alpha + N_\phi + N'_\alpha + N'_\phi$, this is summarized by the constraint set

$$\chi(\boldsymbol{\eta}, \boldsymbol{\kappa}) := \{h_f^i, \varepsilon_f^i : h_f^{i^T} \mathcal{K}_f^i h_f^i \leq \eta_f^i, \|\Sigma_f^i\|_{q_f^i} \leq \kappa_f^i\}.$$

This leads to the following bound.

Theorem 13. (General MSE) *Let $p := \mathbb{P}(z_i = 1)$ for all $i \in [n]$, $a = \langle \alpha, \mathbf{1}/n \rangle$, $b = \langle \phi, \mathbf{1}/n \rangle$, and $\beta_\alpha := 1/(2np(1-p))$, $\beta_\phi := 1/(2np)$. Let also $x \in \{-1, 1\}^n$ by defining $x := 2z - 1$, $X := \text{Cov}(x)$. Then, for $q_f^i \geq 1$, $i \in [N'_f]$,*

$$\sup_{\chi(\boldsymbol{\eta}, \boldsymbol{\gamma}, \boldsymbol{\kappa})} \mathbb{E}[(\hat{\tau} - \tau)^2] \leq (N+1)\{(a\beta_1 + b\beta_2)^2 \text{Tr}(\mathbf{1}\mathbf{1}^T X) + \sum_{f \in \{\alpha, \phi\}} \beta_f^2 \sum_{i=1}^{N_f} \eta_f^i \text{Tr}((\mathcal{K}_f^i)^\dagger X) + \sum_{i=1}^{N'_f} \kappa_f^i \|X\|_{q_f^i}\}.$$

Before exploring the utility of this framework, let's first see how this corresponds to the basic structure established previously in the paper.

Example 7. If we set $\mathcal{K}_\alpha^1 = \mathcal{K}_\phi^1 = L^\dagger$, $\mathcal{K}_\alpha^2 = L$, $\eta_\alpha = [\eta, \gamma]$, $\eta_\phi = \eta$, $q_\alpha = q_\phi = q$, and $\kappa_\alpha = \kappa_\phi = \kappa$, then we arrive at the constraint set $\chi(\eta, \gamma, \kappa)$. Indeed, this gives us a potential outcome model

$$Y = h_\alpha^1 + h_\alpha^2 + \varepsilon_\alpha^1 + z \cdot (h_\phi^1 + \varepsilon_\phi^1) = (h_\alpha^1 + \varepsilon_\alpha^1) + z \cdot (h_\phi^1 + \varepsilon_\phi^1) + h_\alpha^2 =: \alpha + z \cdot \phi + s(z).$$

We note that $s(z) = h_\alpha^2$ may or may not explicitly depend on the assignment z in this framework, as we only specify that it satisfies a quadratic constraint. Adversarially selecting this term to maximize the MSE bound results in a typical graph interference setting. \diamond

Our extended framework provides a convenient means to incorporate information from other sources besides the graph and correlation motivated objectives discussed earlier.

Example 8. Of key importance in practice is the incorporation of covariates into the potential outcome model beyond the graph adjacency. In its most basic form, this is a covariate balancing problem, where one would like to penalize the squared discrepancy $x^T C C^T x$, for C the design matrix/matrix of additional covariates. In our framework, this corresponds to a potential outcome component satisfying a quadratic constraint with respect to $(C C^T)^{-1}$, with the typical example being a linear model $C\beta$. More general potential outcomes can be captured by kernel gram matrices $\mathcal{K} := [k(c_i, c_j)]_{i,j=1}^n$, c_i, c_j the covariates of units i and j . This provides particular utility for designs on disconnected graphs, which we discuss in more detail in Appendix F.2. \diamond

Another point of theoretical importance is the disaggregation of the heterogeneous variation

components in the model.

Example 9. For the majority of the paper, we streamlined our presentation by presenting different heterogeneous variation, such as deterministic residuals and stochastic network effects, as mutually exclusive modeling choices made by the practitioner. This is of course unnecessary, as our general MSE demonstrates, as both of these terms can be separately included. This is particularly important for large graphs, as the Schatten- q , $q < \infty$, norm of X may grow rapidly with the sample size. Thus, it may be desirable to assume a constant level of deterministic residuals, only penalizing the operator norm of X , and a vanishing stochastic network misspecification. In other words, as the graph grows, we expect the homophily and interference terms to capture the majority of the correlation structure. \diamond

F.2 Disconnected Components in the Graph

We have assumed, so far, that the graph is connected. In the following, we consider the worst-case bounds if the graph had T connected components instead.

Let Π be the projection to the null-space of the Laplacian matrix.

Theorem 14 (Disconnected MSE bound). *Let $p := \mathbb{P}(z_i = 1)$ for all $i \in [n]$, $\beta_1 := 1/(2np(1-p))$, $\beta_2 := 1/(2np)$. Let also $x \in \{-1, 1\}^n$ by defining $x := 2z - 1$, and $X := \text{Cov}(X)$. Then,*

$$\mathbb{E}[(\hat{\tau} - \tau)^2] \leq 6\{\text{Tr}((\gamma\beta_1^2 L + \eta[\beta_1^2 + \beta_2^2]L^\dagger)X) + \kappa[\beta_1^2 + \beta_2^2]\|X\|_q + \|\Pi(\beta_1\alpha + \beta_2\phi)\|^2\text{Tr}(\Pi X)\}.$$

Proof. We decompose $\alpha = \Pi\alpha + (I - \Pi)\alpha$, $\phi = \Pi\phi + (I - \Pi)\phi$. For the latter terms orthogonal to the kernel of L , the same analysis as applied to the mean 0 residuals in Theorem 12 is applicable, hence it suffices to bound the projected terms. Following the proof of Theorem 12, we compute

$$\begin{aligned} & \mathbb{E}[(\langle \Pi\alpha, z/(np) - (1 - z)/(n(1 - p)) \rangle + \langle \Pi\phi, z/(np) - \mathbf{1}/n \rangle)^2] \\ &= \text{Var}(\langle \Pi\alpha, z/(np) - (1 - z)/(n(1 - p)) \rangle + \langle \Pi\phi, z/(np) - \mathbf{1}/n \rangle) \\ &= \text{Var}(\langle \Pi\alpha, \beta_1(x - \mu) \rangle + \langle \Pi\phi, \beta_2(x - \mu) \rangle) \\ &= \text{Tr}(\Pi(\beta_1\alpha + \beta_2\phi)(\beta_1\alpha + \beta_2\phi)^T\Pi X) \\ &\leq \|\Pi(\beta_1\alpha + \beta_2\phi)\|^2\text{Tr}(\Pi X). \end{aligned}$$

\square

F.3 Quadratic Penalization of X

So far in this paper, we have restricted our MSE optimization to first order terms linear in the design covariance matrix X , either via a trace inner-product $\text{Tr}(AX)$ or norm penalties. However, there are many natural examples where higher-order dependence is a more appropriate model.

Example 10. A simple and practical model for the interference is $s(z) = Lz$. We can easily compute

$$(Lz)^T L^\dagger (Lz) = z^T Lz,$$

thus Lz is $z^T Lz$ -interferent. In the MSE, this results in an objective $\propto (x^T Lx)^2$ for the Rademacher assignment variables x . This quadratic dependence on the cut is exactly because both the level of interference and the extent to which interference impedes the quality of our estimator are both linear $x^T Lx$. \diamond

Thus, assuming $x^T Lx$ interference requires optimization of $\mathbb{E}[(x^T Lx)^2]$, and this may similarly be of interest for other kernels \mathcal{K} . One strategy to deal with this is to uniformly upper-bound $x^T Lx$, reducing this to a linear optimization. However, this is quite loose, and fails to capture the desired behavior of the assumed outcome model.

Within the framework of Gaussian Rounding, Algorithm 1, we relax the Rademacher assignment vectors x to a multivariate Gaussian distribution. This allows us to apply Isserlis's theorem (also commonly known as Wick's probability theorem) [Isserlis, 1918], to yield

$$\mathbb{E}[(x^T Lx)^2] = \text{Tr}(LX)^2 + 2 \text{Tr}([LX]^2) = \text{Tr}(LX)^2 + 2\|L^{1/2}XL^{1/2}\|_F^2.$$

This is convex in X , and thus amenable to our optimization routine.

Example 11. Quadratic dependencies also naturally appear when considering alternative models for the interference. As a simple example, we may consider a typical setting where $s_i(z)$ is linear in the exposure fraction of treated neighbors adjacent to the vertex i (see, for example, Thiyageswaran et al. [2024]; see also Example 2). In other words, $s(\mathbf{1}) - s(z) = LD^{-1}W[\mathbf{1} - z] = L/2W[x] + L/2\mathbf{1}$ where D is the degree matrix and W is the graph adjacency. When considering the treatment effect, we may decompose

$$\begin{aligned} \langle \mathbf{1}/n, s(\mathbf{1}) \rangle - \langle z/np - (\mathbf{1} - z)/np, s(z) \rangle = \\ \langle \mathbf{1}/n - [z/np - (\mathbf{1} - z)/np], s(\mathbf{1}) \rangle - \langle z/np - (\mathbf{1} - z)/np, s(z) - s(\mathbf{1}) \rangle, \end{aligned}$$

so that the first term can be bounded by our typical error analysis, with some moment restrictions placed on the vector $s(\mathbf{1})$. For the remaining term, its contribution can be bounded by

$$\langle z/np - (\mathbf{1} - z)/np, s(z) - s(\mathbf{1}) \rangle = L/2\beta_1 x^T D^{-1} W x + L/2x^T \mathbf{1} + L/2c_1 n.$$

In other words, in general settings, we can evaluate the quantity

$$\begin{aligned} \langle z/np - (\mathbf{1} - z)/np, s(z) - s(\mathbf{1}) \rangle &= \langle \beta_1 x + c_1 \mathbf{1}, s(z) - s(\mathbf{1}) \rangle \\ &= 2\beta_1 \langle z - \mathbf{1}, s(z) - s(\mathbf{1}) \rangle + (c_1 - \beta_1) \langle \mathbf{1}, s(z) - s(\mathbf{1}) \rangle \end{aligned}$$

and similar control of the MSE is achieved if we assume a quadratic domination $|\langle z - \mathbf{1}, s(z) - s(\mathbf{1}) \rangle| \leq (z - \mathbf{1})^T A(z - \mathbf{1})$, as well as a linear bound $\langle \mathbf{1}, s(z) - s(\mathbf{1}) \rangle \leq |v^T(\mathbf{1} - z)|$, for some

matrix A and vector v . A similar analysis reduces the baseline $s(\mathbf{0})$ into suitable terms for our SDP, falling within the framework of Theorem 13. \diamond

G An alternative approach to the interference term

Instead of using the bound $\|\langle s_z, \mathbf{1} \rangle\| \leq \sqrt{\delta}$, one could also treat the interference term in the following manner. Suppose that $s(z)$ is $(\gamma, L + \delta \mathbf{1} \mathbf{1}^T)$ -interferent, where $\delta > 0$. Then,

$$\begin{aligned} \sup_{\langle s(z), (L + \delta \mathbf{1} \mathbf{1}^T)^\dagger s(z) \rangle \leq \gamma} \langle x, s(z) \rangle &= \sup_{\langle s(z), (L + \delta \mathbf{1} \mathbf{1}^T)^\dagger s(z) \rangle \leq \gamma} \langle x, (L + \delta \mathbf{1} \mathbf{1}^T)^{1/2} (L + \delta \mathbf{1} \mathbf{1}^T)^\dagger s(z) \rangle \\ &= \sup_{\langle s(z), (L + \delta \mathbf{1} \mathbf{1}^T)^\dagger s(z) \rangle \leq \gamma} \langle (L + \delta \mathbf{1} \mathbf{1}^T)^{1/2} x, (L + \delta \mathbf{1} \mathbf{1}^T)^\dagger s(z) \rangle. \end{aligned}$$

Therefore, by Cauchy-Schwarz,

$$\sup_{\langle s(z), (L + \delta \mathbf{1} \mathbf{1}^T)^\dagger s(z) \rangle \leq \gamma} \mathbb{E}[\langle x, s(z) \rangle^2] = \gamma \text{Tr}((L + \delta \mathbf{1} \mathbf{1}^T)X),$$

and the results follow.

H A practical consideration on trade-off parameters

Our framework allows practitioners with domain expertise on the experimental units and the complex mechanisms governing their interactions to navigate the trade-offs between homophily η , robustness κ , and spillover effects γ , in addition to Δ , in order to identify Pareto-optimal experimental designs.

Much like in traditional power calculations, historical data from similar experiments or pilot studies can provide reasonable approximations for Δ , which encompasses the baseline means as well as the expected effect sizes.

Beyond Δ , historical data can also inform γ , quantifying the “effective spillover”. This is done by comparing outcomes under different treatment saturation levels. For instance, in [Baird et al., 2018], the authors examine the difference in responses for treated units under varying neighborhood exposure levels, i.e., $Y(1, p) - Y(1, 0)$, where p represents the fraction of treated neighbors. Similarly, spillover effects on control units are assessed via $Y(0, p) - Y(0, 0)$. Similar hyperparameter estimation is also described in [Viviano et al., 2023].

For the robustness parameter κ , historical data can again prove useful. Specifically, one can compute the sample covariance matrix from outcomes from prior experiments within, and across, treatment saturation levels and covariate groups. This involves aggregating products of residuals across various experimental conditions, and then computing the appropriate Schatten norm.

A natural starting point for estimating the homophily parameter η is to use pre-experiment baseline measurements b . We can compute the average of the baselines \hat{b} across units with similar covariates which are believed to be predictive of the outcomes, so that the number of unique elements in \hat{b} is equal to the number of distinct covariate groups. Then, an initial estimate of η is $\hat{b}^T L \hat{b}$. In fact, we could refine this further by the use a linear combination of these individual η s with coefficients learned through, for instance, a linear regression of outcomes from previous experiments on covariates. For example, regressing on gender, ethnicity, and age, one would obtain three coefficients $\beta_1, \beta_2, \beta_3$ with which we can estimate η to be $\beta_1 \hat{\eta}_{\text{gender}} + \beta_2 \hat{\eta}_{\text{ethnicity}} + \beta_3 \hat{\eta}_{\text{age}}$. This gives us an estimate of η in the baselines. To estimate η in ϕ , one could do the same with a sample restricted to nodes that are treated and for which all of their neighbors are treated, as well as nodes that are controlled and for which all of their neighbors are controlled, from a previous experiment. For our final η , we can simply take the maximum of these two values. To generalize this heuristic, we can frame the estimation procedure in regression terms. Taking V to be the covariate matrix, and x to be the treatment assignment vector, regressing historical outcomes

$$y = V\beta + x\beta' + D^{-1}Wx\beta'' + \varepsilon,$$

we define $\eta = \hat{\beta}^T V^T L V \hat{\beta}$, $\kappa = \|S_\varepsilon\|_q$, where S_ε is the sample covariance matrix of the ε residuals. In particular, a simple and general approach is to specify candidate potential outcome models, such as those linear in some covariates, for example. Then, one could try different hyperparameter configurations and select the ones that minimize a prespecified loss.

The regression approach is now reminiscent of the covariate-balancing formalization in [Harshaw et al., 2024]. We also point the reader to the discussion in [Basse and Airoldi, 2018] addressing the specification of a similar parameter in their framework.

Ultimately, the strength of our framework lies in its adaptability. Much like the Gram-Schmidt Walk algorithm in Harshaw et al. [2024], our approach does not prescribe a rigid estimation protocol. Instead, it provides a structured yet flexible methodology that practitioners can tailor to their specific experimental context, whether by refining parameter estimates through machine learning, incorporating alternative homophily metrics, or integrating auxiliary data sources. This adaptability ensures that domain experts can efficiently explore trade-offs and arrive at designs that balance interference, homophily, and robustness in a principled manner.

I Difference-in-Means estimator with Fixed Treatment Groups Sizes

In this section, we consider our proposed framework applied to the difference-in-means estimator. Let $n_1 := \sum_{i=1}^n z_i$, and $n_0 := n - n_1$, i.e., the number of treated and control units

respectively. Then,

$$\begin{aligned}
\hat{\tau}_{\text{DiM}} &= \frac{1}{n_1} \langle z, Y \rangle - \frac{1}{n_0} \langle 1 - z, Y \rangle \\
&= \frac{1}{n_1} \langle z, \alpha + \text{diag}(\phi)z - s(z) \rangle - \frac{1}{n_0} \langle 1 - z, \alpha + \text{diag}(\phi)z - s(z) \rangle \\
&= \left\langle \frac{z}{n_1} - \frac{1-z}{n_0}, \alpha - s(z) \right\rangle + \left\langle \frac{z}{n_1}, \phi \right\rangle.
\end{aligned}$$

Therefore,

$$\hat{\tau}_{\text{DiM}} - \tau = \left\langle \frac{z}{n_1} - \frac{1-z}{n_0}, \alpha - s(z) \right\rangle + \left\langle \frac{z}{n_1} - \frac{\mathbf{1}}{n}, \phi \right\rangle.$$

Theorem 15 (MSE bound). *Let $x \in \{-1, 1\}^n$ by defining $x := 2z - 1$. Define $X := \mathbb{E}[xx^T]$. Let $\mathbf{1}^T X \mathbf{1} - \mathbf{1}^T \mu \mu^T \mathbf{1} = 0$, where $\mu = \frac{n_1 - n_0}{n} \mathbf{1}$, and let $\beta_1 := n/(2n_1 n_0)$, and $\beta_2 := 1/(2n_1)$. Then, for $q \geq 1$,*

$$\mathbf{E}[(\hat{\tau}_{\text{DiM}} - \tau)^2] \leq 7\{\text{Tr}((\gamma\beta_1^2 L + \eta[\beta_1^2 + \beta_2^2]L^\dagger)X) + \kappa[\beta_1^2 + \beta_2^2]\|X\|_q\}.$$

The proof is in Appendix [J.4](#).

Corollary 16 (MSE bound (Symmetric case)). *For the symmetric case, i.e., when $n_1 = n_0 = n/2$, let $x \in \{-1, 1\}^n$ by defining $x := 2z - 1$. Let $\mathbf{1}^T X \mathbf{1} = 0$. Define $X := \mathbb{E}[xx^T]$. Then, for $q \geq 1$,*

$$\mathbf{E}[(\hat{\tau}_{\text{DiM}} - \tau)^2] \leq \frac{5}{n^2} \{\text{Tr}((4\gamma L + 5\eta L^\dagger)X) + 5\kappa\|X\|_q\}.$$

Let $\mu = \frac{n_1 - n_0}{n} \mathbf{1}$. Reparameterizing with $\tilde{\gamma}$ and $\tilde{\eta}$ so that

$$\tilde{\gamma} := \frac{\gamma\beta_1^2}{\kappa[\beta_1^2 + \beta_2^2]} \text{ and } \tilde{\eta} := \frac{\eta}{\kappa},$$

we can write an SDP more explicitly in terms of the new trade-off parameters:

$$\begin{aligned}
\min_{X \in \mathbb{R}^{n \times n}} \quad & \tilde{\eta} \text{Tr}(L^\dagger X) + \tilde{\gamma} \text{Tr}(LX) + \|X\|_q \\
\text{s.t.} \quad & X \succeq 0 \\
& \text{diag}(X) = 1 \\
& \mathbf{1}^T X \mathbf{1} = \mathbf{1}^T \mu \mu^T \mathbf{1}
\end{aligned} \tag{I.1}$$

Let X^* be the solution to the SDP above. Finally, we generate our treatment assignment

vector x^* by running Algorithm 1 on X^* .

Remark 10. When $\kappa = 0$, we can proceed with a matrix lifting and a SDP relaxation as previously demonstrated, or solve the problem more exactly with a mixed-integer program as described below. We note however that solving an SDP is polynomial-time with efficient solvers that can be sped up by exploiting problem structure. This is not true for the mixed-integer programs. From the calculations in the proof of Theorem 15, when $\kappa = 0$, and $\tilde{\gamma} := \frac{\gamma\beta_1^2}{[\beta_1^2 + \beta_2^2]}$ and $\tilde{\eta} := \eta[\beta_1^2 + \beta_2^2]$, we have the following Mixed Integer Programming (MIP) problem:

$$\min_{x \in \mathbb{R}^n} \tilde{\eta}x^T L^\dagger x + \tilde{\gamma}x^T Lx \quad (\text{I.2})$$

$$\text{s.t. } x_i = \pm 1 \quad \forall i \quad (\text{I.3})$$

$$x^T \mathbf{1} = \mathbf{1}^T \mu \quad (\text{I.4})$$

◇

I.1 Gaussian Rounding

One approach to proving theoretical guarantees of this approximation procedure is by leveraging and adapting results from [Raghavendra and Tan, 2012] who provide approximation guarantees to the min-bisection problem. For convenience, we restate the min-bisection problem followed by the main result of [Raghavendra and Tan, 2012].

Recall that the min-bisection problem is:

$$\begin{aligned} & \underset{x \in \mathbb{R}^n}{\text{minimize}} \quad \frac{1}{2} \sum_{i < j} w_{ij}(1 - x_i \cdot x_j) \\ & \text{s.t.: } x_i \in \{-1, 1\} \quad \forall i \\ & \quad \sum_i x_i = 0 \end{aligned}$$

The SDP relaxation is given by,

$$\begin{aligned} & \underset{\mathbb{E}}{\text{minimize}} \quad \mathbb{E} \left[\sum_{i < j} w_{ij}(v_i - v_j)^2 \right] \\ & \text{s.t.: } \|v_i\|^2 = 1 \quad \forall i \in V \\ & \quad \sum_i v_i = 0 \end{aligned}$$

or

$$\begin{aligned} & \underset{X \in \mathbb{R}^{n \times n}}{\text{minimize}} \quad \text{Tr}(LX) \\ & \text{s.t.: } X_{ii} = 1 \quad \forall i \in V \end{aligned}$$

$$\begin{aligned}\mathbf{1}^T X \mathbf{1} &= 0 \\ X &\succeq 0\end{aligned}$$

For this min-bisection problem, [Raghavendra and Tan \[2012\]](#) propose an algorithm and provide a corresponding approximation error bound.

Theorem 17 ([Raghavendra and Tan, 2012](#), Theorem 1.2). *For every $\delta > 0$, there exists an algorithm, which given a graph with a bisection cutting ϵ -fraction of the edges, finds a bisection cutting at most $\mathcal{O}(\sqrt{\epsilon}) + \delta$ -fraction of edges with high probability.*

Their algorithm comprises of two parts. First, they lift the problem through the Lasserre hierarchy and iteratively solve by conditioning on assignments of a subset of nodes, until a pre-specified α -level of independence is achieved between the solutions across the nodes. The second part of their approach, given this α -independence solution, is a rounding procedure reminiscent of [\[Goemans and Williamson, 1995\]](#). Finally, to meet the cardinality constraints, they flip the assignments of the nodes with the smallest degrees on the larger side of the cut.

In proving their guarantees from this rounding, they leverage the α -independence conditioning. While their α -conditioning in the first-part of their procedure does not apply to our setting, one could adapt their ideas to proving guarantees in our setting under a α_κ -independence level, dependent on the randomization tuning parameter κ as per [Proposition 7](#). To adapt their final “flipping” procedure to achieve cardinality constraints to our settings, we propose targeting the nodes with the smallest a_i with a_i corresponding to the columns vectors of the matrix A , instead of the nodes of the smallest degrees. Then, one could prove analogous results for this difference-in-means setting.

I.2 Adapted Gram Schmidt Walk algorithm

As a heuristic, one could use the use the adapted Gram Schmidt Walk algorithm as in the Horvitz-Thompson section, followed by the assignment “flipping” procedure targeting the nodes, on the larger side of the cut, with the smallest Q_{ii} corresponding to columns vectors in the matrix Q . We also refer to [\[Harshaw et al., 2024, S8.4\]](#). In particular, the authors describe how appending a constant vector to the covariate matrix helps make the treatment group sizes, n_1, n_0 closer to equal. A variant proposed by [Harshaw et al. \[2024, S8.4\]](#) is by adding a cardinality constraint within the Gram-Schmidt Walk algorithm. This variant, however, does not inherit the theoretical results from the Bernoulli rounding procedures in [\[Harshaw et al., 2024\]](#) due to violation of orthogonality of updates between pivot phases in the algorithm.

J Proofs to trade-off results

J.1 Proof to Proposition 7

We restate [Proposition 7](#) and prove it below.

Proposition 18. Let $r \in \{-1, 1\}^n$ denote the treatment assignment under a Bernoulli randomization design. Then, for fixed $p = \mathbb{P}(r_i = 1)$ for all $i \in [n]$, and $q > 1$

$$\arg \min_{\substack{X \succeq 0; \\ X_{ii}=1}} \|X\|_q = \frac{1}{4p(1-p)} \text{Cov}(r).$$

Proof. Let $X^* := I$. Then, X^* has n non-zero eigenvalues which are all equal to 1. We first show that X^* is the unique minimizer of $\|X\|_q^q$ over $X \in \mathcal{C} := \{X : X \succeq 0, X_{ii} = 1\}$, and then we show that $X^* = \frac{1}{4p(1-p)} \text{Cov}(r)$. It is easy to see that $X^* \in \mathcal{C}$. For $p > 1$, and any $X \in \mathcal{C}$, with eigenvalues λ_i ,

$$\|X\|_q^q = (n) \times \frac{1}{n} \sum_{i=1}^n \lambda_i^q \geq (n) \times \left(\frac{1}{n} \sum_{i=1}^n \lambda_i \right)^q = (n) \times 1 = \|X^*\|_q^q,$$

as $f : x \rightarrow x^q$ is convex on $x \geq 0$, and $\sum_i \lambda_i = \sum_i X_{ii} = n$. That X^* is the unique minimizer follows from the strict convexity of $\|\cdot\|_q^q$ on \mathcal{C} for $q > 1$. Indeed, if we express $\|X\|_q^q = g(\lambda_1, \dots, \lambda_n) = \sum_{i=1}^n \lambda_i^q$, then

$$\nabla^2 g = p(p-1) \begin{bmatrix} \lambda_1^{q-2} & 0 & \dots & 0 \\ 0 & \lambda_2^{q-2} & \dots & 0 \\ \vdots & \vdots & \ddots & \vdots \\ 0 & 0 & \dots & \lambda_n^{q-2} \end{bmatrix},$$

which is positive definite at X^* with its n eigenvalues $\lambda_i = 1$ for $i = 1, 2, \dots, n-1$.

It is now sufficient to show that this matrix X^* is equivalent to the $\frac{1}{4p(1-p)} \text{Cov}(r)$ under Bernoulli randomization with uniform treatment assignment probability. We begin by observing that $\text{Cov}(r) = \mathbb{E}[rr^T] - \mathbb{E}[r]\mathbb{E}[r]^T$. Therefore, since $r \in \{-1, 1\}$ with $\mathbb{P}(r_i = 1) = p$ for all i , we have that $\text{Cov}(r)_{ii} = 4p(1-p)$. Recall that unit-level Bernoulli randomization is a randomization scheme where each unit is independently assigned to treatment or control. Therefore, $\text{Cov}(r)_{ij} = 0$ for all $j \neq i$. \square

We state below the analogous result for complete randomization.

Proposition 19. Let $r \in \{-1, 1\}^n$ denote the treatment assignment under a complete randomization design. Then, for fixed $n_1 = n_0$, i.e., $r^T \mathbf{1} = 0$, and $q > 1$

$$\arg \min_{\substack{X \mathbf{1} = \mathbf{0}; \\ X \succeq 0; \\ X_{ii}=1}} \|X\|_q = \text{Cov}(r).$$

Proof. Let $X^* := (1 + \frac{1}{n-1})I - \frac{1}{n-1}\mathbf{1}\mathbf{1}^T = \frac{n}{n-1}I - \frac{n}{n-1}(\mathbf{1}/\sqrt{n})(\mathbf{1}/\sqrt{n})^T$. Then, X^* has $n-1$ non-zero eigenvalues which are all equal to $\frac{n}{n-1}$, and one zero eigenvalue. Indeed, the first term has n eigenvalues that are equal to $\frac{n}{n-1}$, while the second term has one eigenvalue that is equal to $\frac{n}{n-1}$, and $n-1$ eigenvalues that are equal to 0, and as they share the same

eigenvectors, their difference has the desired property. We first show that X^* is the unique minimizer of $\|X\|_p^p$ over $X \in \mathcal{C} := \{X : X\mathbf{1} = \mathbf{0}, X \succeq 0, X_{ii} = 1\}$, and then we show that $X^* = \text{Cov}(r)$. It is easy to see that $X^* \in \mathcal{C}$. For $q > 1$, and any $X \in \mathcal{C}$, with eigenvalues λ_i ,

$$\|X\|_q^q = (n-1) \times \frac{1}{n-1} \sum_{i=1}^n \lambda_i^q \geq (n-1) \times \left(\frac{1}{n-1} \sum_{i=1}^n \lambda_i \right)^q = (n-1) \times \left(\frac{n}{n-1} \right)^q = \|X^*\|_q^q,$$

as $f : x \rightarrow x^q$ is convex on $x \geq 0$, and $\sum_i \lambda_i = \sum_i X_{ii} = n$. That X^* is the unique minimizer follows from the strict convexity of $\|\cdot\|_q^q$ on \mathcal{C} for $q > 1$. Indeed, if we express $\|X\|_q^q = g(\lambda_1, \dots, \lambda_{n-1}) = \sum_{i=1}^{n-1} \lambda_i^q$, then

$$\nabla^2 g = p(p-1) \begin{bmatrix} \lambda_1^{q-2} & 0 & \dots & 0 \\ 0 & \lambda_2^{q-2} & \dots & 0 \\ \vdots & \vdots & \ddots & \vdots \\ 0 & 0 & \dots & \lambda_{n-1}^{q-2} \end{bmatrix},$$

which is positive definite at X^* with its first $n-1$ eigenvalues $\lambda_i = \frac{n}{n-1}$ for $i = 1, 2, \dots, n-1$.

It is now sufficient to show that this matrix X^* is equivalent to the $\text{Cov}(r)$ under complete randomization, with equal number of treated and control units, i.e., $r^T \mathbf{1} = 0$. We begin by observing that $\text{Cov}(r) = \mathbb{E}[rr^T]$, and that $\text{Cov}(r)\mathbf{1} = \mathbb{E}[rr^T\mathbf{1}] = 0$. Therefore, since $r \in \{-1, 1\}$ with equal probability, we have that $\text{Cov}(r)_{ii} = 1$, and that the row sums of $\text{Cov}(r) = 0$. This must imply that $\sum_{j \neq i} \text{Cov}(r)_{ij} = -1$, for all $i \in [n]$. Recall that unit-level complete randomization is a uniform randomization process. Therefore, $\text{Cov}(r)_{ij} = \text{Cov}(r)_{ik}$ for all $j \neq k \neq i$. Therefore, this together with $\sum_{j \neq i} \text{Cov}(r)_{ij} = -1$ imply that $\text{Cov}(r)_{ij} = -\frac{1}{n-1}$ for all $j \neq i$, for every i . \square

J.2 Proof to Theorem 12

We first state and proof lemmas we use to proof Theorem 12.

Lemma 20. *Suppose that h is η -homophilous, $\langle h, \mathbf{1} \rangle = 0$, and $X := \mathbb{E}[xx^T]$, then*

$$\mathbb{E}[\langle x, h \rangle^2] \leq \eta \text{Tr}(L^\dagger X).$$

Proof. Observe, as h is orthogonal to the kernel of L , and L is PSD,

$$\sup_{\langle h, Lh \rangle \leq \eta} \langle x, h \rangle = \sup_{\langle h, Lh \rangle \leq \eta} \langle x, L^{\dagger/2} L^{1/2} h \rangle = \sup_{\langle h, Lh \rangle \leq \eta} \langle L^{\dagger/2} x, L^{1/2} h \rangle.$$

Therefore, by Cauchy-Schwarz,

$$\sup_{\langle h, Lh \rangle \leq \eta} \mathbb{E}[\langle x, h \rangle^2] = \eta \text{Tr}(L^\dagger X).$$

□

Lemma 21. Suppose that $s(z)$ is γ -interferent, $\langle s(z), \mathbf{1}/n \rangle = 0$, and $X := \mathbb{E}[xx^T]$, then

$$\mathbb{E}[\langle x, s(z) \rangle^2] \leq \gamma \operatorname{Tr}(LX).$$

Proof. Observe, as $s(z)$ is orthogonal to the kernel of L , and L is PSD,

$$\sup_{\langle s(z), L^\dagger s(z) \rangle \leq \gamma} \langle x, s(z) \rangle = \sup_{\langle s(z), L^\dagger s(z) \rangle \leq \gamma} \langle x, L^{1/2} L^{\dagger/2} s(z) \rangle = \sup_{\langle s(z), L^\dagger s(z) \rangle \leq \gamma} \langle L^{1/2} x, L^{\dagger/2} s(z) \rangle.$$

Therefore, by Cauchy-Schwarz,

$$\sup_{\langle s(z), L^\dagger s(z) \rangle \leq \gamma} \mathbb{E}[\langle x, s(z) \rangle^2] = \gamma \operatorname{Tr}(LX).$$

□

Lemma 22. Suppose that ε is independent of x and $\Sigma := \mathbb{E}[\varepsilon \varepsilon^T]$ is such that $\|\Sigma\|_q \leq \kappa$, $1/q^* + 1/q = 1$. Let $X := \mathbb{E}[xx^T]$. Then,

$$\mathbb{E}[\langle x, \varepsilon \rangle^2] \leq \kappa \|X\|_q.$$

Proof. We begin by writing

$$\mathbb{E}[\langle x, \varepsilon \rangle^2] = \operatorname{Tr}(\mathbb{E}[\varepsilon \varepsilon^T] \mathbb{E}[xx^T]) = \operatorname{Tr}(\Sigma X).$$

Then, the proof follows from Proposition 4. □

In fact, the results in Lemma 20 can be tightened. We write this formally in the following lemma.

Lemma 23. Suppose that h is η -homophilous, $\langle h, \mathbf{1} \rangle = 0$, and $X := \mathbb{E}[xx^T]$, then

$$\mathbb{E}[\langle x, h \rangle^2] \leq \eta \lambda_{\max}(L^{\dagger/2} X L^{\dagger/2}).$$

Proof. Observe, as h is orthogonal to the kernel of L , and L is PSD,

$$\begin{aligned} \sup_{\langle h, Lh \rangle \leq \eta} \mathbb{E}[\langle x, h \rangle^2] &= \sup_{\langle h, Lh \rangle \leq \eta} h^T X h = \sup_{\|L^{1/2} h\| \leq \eta^{1/2}} h^T L^{1/2} L^{\dagger/2} X L^{\dagger/2} L^{1/2} h \\ &= \sup_{\|w\| \leq 1} \eta w^T L^{\dagger/2} X L^{\dagger/2} w \\ &= \eta \|L^{\dagger/2} X L^{\dagger/2}\|_{\text{op}}. \end{aligned}$$

□

We restate Theorem 12 below.

Theorem 24 ((General) MSE bound). *Let $p := \mathbb{P}(z_i = 1)$ for all $i \in [n]$, $\beta_1 := 1/(2np(1-p))$, $\beta_2 := 1/(2np)$, $a = \langle \alpha, \mathbf{1}/n \rangle$, $b = \langle \phi, \mathbf{1}/n \rangle$, and $\langle s(z), \mathbf{1}/n \rangle \leq \sqrt{\delta}$. Let also $x \in \{-1, 1\}^n$ by defining $x := 2z - 1$. Define $X := \mathbb{E}[xx^T] - \mu\mu^T$, $\mu := \mathbb{E}[x]$. Then,*

$$\mathbb{E}[(\hat{\tau} - \tau)^2] \leq 7\{\text{Tr}((\gamma\beta_1^2 L + \eta[\beta_1^2 + \beta_2^2]L^\dagger)X) + \kappa[\beta_1^2 + \beta_2^2]\|X\|_q + ([a\beta_1 + b\beta_2]^2 + \beta_1^2\delta)\text{Tr}(\mathbf{1}\mathbf{1}^T X)\}.$$

Proof. The relevant quantities of interest are

$$\hat{\tau} = \frac{1}{n} \langle Y, z/p - (1-z)/(1-p) \rangle = \frac{1}{n} \langle \alpha + s(z), z/p - (1-z)/(1-p) \rangle + \frac{1}{n} \langle \phi, z/p \rangle, \quad (\text{J.1})$$

$$\tau = \langle \phi, \mathbf{1}/n \rangle, \quad (\text{J.2})$$

$$\hat{\tau} - \tau = \langle \alpha + s(z), z/(np) - (1-z)/(n(1-p)) \rangle + \langle \phi, z/(np) - \mathbf{1}/n \rangle. \quad (\text{J.3})$$

Notice that we can re-write

$$\begin{aligned} z/(np) - (1-z)/(n(1-p)) \\ = & \left[z/(np) - (1-z)/(n(1-p)) - \frac{1}{2}(1/(np) - 1/(n(1-p)))\mathbf{1} \right] + \frac{1}{2}(1/(np) - 1/(n(1-p)))\mathbf{1} \\ =: & \beta_1 x + c_1 \mathbf{1} \end{aligned}$$

where $c_1 := \frac{1}{2}(1/(np) - 1/(n(1-p)))$. Similarly,

$$z/(np) - \mathbf{1}/n = [z/(np) - \mathbf{1}/n - (1/(2np) - 1/n)\mathbf{1}] + (1/(2np) - 1/n)\mathbf{1} =: \beta_2 x + c_2 \mathbf{1}$$

where $c_2 := (1/(2np) - 1/n)$. Before proceeding, we first center α, ϕ , decomposing them as $\alpha = \bar{\alpha} + \alpha'$, $\phi = \bar{\phi} + \phi'$, $\bar{\alpha}, \bar{\phi}$ denoting the projection onto the constant vector for each term respectively. Similarly, we decompose $s(z) = \bar{s}(z) + \tilde{s}(z)$. Then, we can write,

$$\begin{aligned} \mathbb{E}[(\hat{\tau} - \tau)^2] &= \mathbb{E}[(\langle \alpha + s(z), z/(np) - (1-z)/(n(1-p)) \rangle + \langle \phi, z/(np) - \mathbf{1}/n \rangle)^2] \\ &= 7\mathbb{E}[(\langle \bar{\alpha}, z/(np) - (1-z)/(n(1-p)) \rangle + \langle \bar{\phi}, z/(np) - \mathbf{1}/n \rangle)^2 \\ &\quad + \langle \bar{s}(z), z/(np) - (1-z)/(n(1-p)) \rangle^2 \\ &\quad + \langle h_\alpha, \beta_1(x - \mu) \rangle^2 + \langle \tilde{s}(z), \beta_1(x - \mu) \rangle^2 + \langle \varepsilon_\alpha, \beta_1(x - \mu) \rangle^2 \\ &\quad + \langle h_\phi, \beta_2(x - \mu) \rangle^2 + \langle \varepsilon_\phi, \beta_2(x - \mu) \rangle^2], \end{aligned}$$

where the last two lines on the right-hand-side come from the mean-zero components of $\alpha, s(z)$, and ϕ . Indeed, as these are orthogonal to $\mathbf{1}$ we can drop the $c\mathbf{1}$ terms from the expression, and add the μ terms. Thus, we can write

$$\begin{aligned} &\langle \alpha' + \tilde{s}(z), z/(np) - (1-z)/(n(1-p)) \rangle + \langle \phi', z/(np) - \mathbf{1}/n \rangle \\ &= \langle h_\alpha, \beta_1(x - \mu) \rangle + \langle \tilde{s}(z), \beta_1(x - \mu) \rangle + \langle \varepsilon_\alpha, \beta_1(x - \mu) \rangle + \langle h_\phi, \beta_2(x - \mu) \rangle + \langle \varepsilon_\phi, \beta_2(x - \mu) \rangle. \end{aligned}$$

We can upper-bound the contribution of the terms in the first two lines, as we notice that by the definition of our marginal probabilities,

$$\mathbb{E}[\langle \bar{\alpha}, z/(np) - (1-z)/(n(1-p)) \rangle] = 0 = \mathbb{E}[\langle \bar{\phi}, z/(np) - \mathbf{1}/n \rangle],$$

hence,

$$\begin{aligned} & \mathbb{E}[(\langle \bar{\alpha}, z/(np) - (1-z)/(n(1-p)) \rangle + \langle \bar{\phi}, z/(np) - \mathbf{1}/n \rangle)^2] \\ &= \text{Var}(\langle \bar{\alpha}, z/(np) - (1-z)/(n(1-p)) \rangle + \langle \bar{\phi}, z/(np) - \mathbf{1}/n \rangle) \\ &= \text{Var}(\langle \bar{\alpha}, \beta_1(x-\mu) \rangle + \langle \bar{\phi}, \beta_2(x-\mu) \rangle) \\ &= \text{Var}([\beta_1 a + \beta_2 b] \langle \mathbf{1}, (x-\mu) \rangle) + \text{Var}(\langle \bar{s}(z), (x-\mu) \rangle) \\ &= (\beta_1 a + \beta_2 b)^2 \text{Tr}(\mathbf{1} \mathbf{1}^T X), \end{aligned}$$

for $X := \mathbb{E}[xx^T] - \mu\mu^T$, $\mu := \mathbb{E}[x]$, $a = \langle \alpha, \mathbf{1}/n \rangle$, $b = \langle \phi, \mathbf{1}/n \rangle$.

Similarly,

$$\begin{aligned} \mathbb{E}[\langle \bar{s}(z), z/(np) - (1-z)/(n(1-p)) \rangle^2] &\leq \delta \mathbb{E}[\langle \mathbf{1}, z/(np) - (1-z)/(n(1-p)) \rangle^2] \\ &= \delta \text{Var}(\langle \mathbf{1}, z/(np) - (1-z)/(n(1-p)) \rangle) \\ &= \delta \text{Var}(\langle \mathbf{1}, \beta_1(x-\mu) \rangle) \\ &\leq \beta_1^2 \delta \text{Tr}(\mathbf{1} \mathbf{1}^T X). \end{aligned}$$

Thus, by Lemmas 20 to 22, we get

$$\mathbb{E}[(\hat{\tau} - \tau)^2] \leq \text{Tr}((\gamma \beta_1^2 7L + \eta[\beta_1^2 + \beta_2^2] 7L^\dagger)X) + \kappa[\beta_1^2 + \beta_2^2] 7\|X\|_q + ([a\beta_1 + b\beta_2]^2 + \beta_1^2 \delta) 7 \text{Tr}(\mathbf{1} \mathbf{1}^T X).$$

□

J.3 Tighter bounds

In Theorem 12, we relied on the inequality from Lemma 20. If we, instead, used the tighter inequality from Lemma 23, we obtain the following worst-case bound.

Theorem 25 ((Tighter) MSE bound). *Let $p := \mathbb{P}(z_i = 1)$ for all $i \in [n]$, $\beta_1 := 1/(2np(1-p))$, $\beta_2 := 1/(2np)$, $a = \langle \alpha, \mathbf{1}/n \rangle$, $b = \langle \phi, \mathbf{1}/n \rangle$, and $\langle s(z), \mathbf{1}/n \rangle \leq \sqrt{\delta}$. Let also $x \in \{-1, 1\}^n$ by defining $x := 2z - 1$. Define $X := \mathbb{E}[xx^T] - \mu\mu^T$, $\mu := \mathbb{E}[x]$. Then, for $q \geq 1$,*

$$\begin{aligned} \mathbb{E}[(\hat{\tau} - \tau)^2] &\leq 7\{\gamma \beta_1^2 \text{Tr}(LX) + \eta[\beta_1^2 + \beta_2^2] \lambda_{\max}(L^{\dagger/2} X L^{\dagger/2}) + \kappa[\beta_1^2 + \beta_2^2] \|X\|_q \\ &\quad + ([a\beta_1 + b\beta_2]^2 + \beta_1^2 \delta) \text{Tr}(\mathbf{1} \mathbf{1}^T X)\}. \end{aligned}$$

However, writing this as an SDP introduces an additional PSD constraint, and the resulting optimization problem is much more computationally intensive.

J.4 Proof to Theorem 15

We restate Theorem 15 below.

Theorem 26 (MSE bound). *Let $x \in \{-1, 1\}^n$ by defining $x := 2z - 1$. Define $X := \mathbb{E}[xx^T]$. Let $\mathbf{1}^T X \mathbf{1} - \mathbf{1}^T \mu \mu^T \mathbf{1} = 0$, where $\mu = \frac{n_1 - n_0}{n} \mathbf{1}$, and let $\beta_1 := n/(2n_1 n_0)$, and $\beta_2 := 1/(2n_1)$. Then, for $q \geq 1$,*

$$\mathbb{E}[(\hat{\tau}_{DiM} - \tau)^2] \leq 7\{\text{Tr}((\gamma\beta_1^2 L + \eta[\beta_1^2 + \beta_2^2]L^\dagger)X) + \kappa[\beta_1^2 + \beta_2^2]\|X\|_q\}.$$

Proof. The relevant quantities of interest are

$$\hat{\tau}_{DiM} = \langle Y, z/n_1 - (1 - z)/n_0 \rangle = \langle \alpha + s(z), z/n_1 - (1 - z)/n_0 \rangle + \langle \phi, z/n_1 \rangle, \quad (\text{J.4})$$

$$\tau = \langle \phi, \mathbf{1}/n \rangle, \quad (\text{J.5})$$

$$\hat{\tau}_{DiM} - \tau = \langle \alpha + s(z), z/n_1 - (1 - z)/n_0 \rangle + \langle \phi, z/n_1 - \mathbf{1}/n \rangle. \quad (\text{J.6})$$

Notice that we can re-write

$$\begin{aligned} z/n_1 - (1 - z)/n_0 &= \left[z/n_1 - (1 - z)/n_0 - \frac{1}{2}(1/n_1 - 1/n_0)\mathbf{1} \right] + \frac{1}{2}(1/n_1 - 1/n_0)\mathbf{1} \\ &=: \beta_1 x + c_1 \mathbf{1} \end{aligned}$$

where $c_1 := \frac{1}{2}(1/n_1 - 1/n_0)$. Similarly,

$$z/n_1 - \mathbf{1}/n = [z/n_1 - \mathbf{1}/n - (1/(2n_1) - 1/n)\mathbf{1}] + (1/(2n_1) - 1/n)\mathbf{1} =: \beta_2 x + c_2 \mathbf{1}$$

where $c_2 := (1/(2n_1) - 1/n)$. Before proceeding, we first center α, ϕ , decomposing them as $\alpha = \bar{\alpha} + \alpha'$, $\phi = \bar{\phi} + \phi'$, $\bar{\alpha}, \bar{\phi}$ denoting the projection onto the constant vector for each term respectively. Similarly, we decompose $s(z) = \bar{s}(z) + \tilde{s}(z)$. Then, we can write

$$\begin{aligned} \mathbb{E}[(\tau - \hat{\tau}_{DiM})^2] &= 7\mathbb{E}[(\langle \bar{\alpha}, z/n_1 - (1 - z)/n_0 \rangle + \langle \bar{\phi}, z/n_1 - \mathbf{1}/n \rangle)^2 + \langle \bar{s}(z), z/n_1 - (1 - z)/n_0 \rangle^2 \\ &\quad + \langle h_\alpha, \beta_1 x \rangle^2 + \langle \tilde{s}(z), \beta_1 x \rangle^2 + \langle \varepsilon_\alpha, \beta_1 x \rangle^2 + \langle h_\phi, \beta_2 x \rangle^2 + \langle \varepsilon_\phi, \beta_2 x \rangle^2], \end{aligned}$$

where the terms in the second line of the right-hand-side come from the mean-zero components of $\alpha, s(z)$, and ϕ . Indeed, as these are orthogonal to $\mathbf{1}$ we can drop the $c\mathbf{1}$ terms from the expression. Thus, we can write

$$\begin{aligned} \langle \alpha' + \tilde{s}(z), z/n_1 - (1 - z)/n_0 \rangle + \langle \phi', z/n_1 - \mathbf{1}/n \rangle &= \langle h_\alpha, \beta_1 x \rangle + \langle \tilde{s}(z), \beta_1 x \rangle + \langle \varepsilon_\alpha, \beta_1 x \rangle \\ &\quad + \langle h_\phi, \beta_2 x \rangle + \langle \varepsilon_\phi, \beta_2 x \rangle. \end{aligned}$$

We can upper-bound the contribution of the terms in the first line, as we notice that by the

definition of our marginal probabilities,

$$\mathbb{E}[\langle \bar{\alpha}, z/n_1 - (1-z)/n_0 \rangle] = 0 = \mathbb{E}[\langle \bar{\phi}, z/n_1 - \mathbf{1}/n \rangle],$$

hence,

$$\begin{aligned} \mathbb{E}[(\langle \bar{\alpha}, z/n_1 - (1-z)/n_0 \rangle + \langle \bar{\phi}, z/n_1 - \mathbf{1}/n \rangle)^2] &= \text{Var}(\langle \bar{\alpha}, z/n_1 - (1-z)/n_0 \rangle + \langle \bar{\phi}, z/n_1 - \mathbf{1}/n \rangle) \\ &= \text{Var}(\langle \bar{\alpha}, \beta_1 x \rangle + \langle \bar{\phi}, z/n_1 - \mathbf{1}/n \rangle) \\ &= (\beta_1 a + \beta_2 b)^2 \text{Tr}(\mathbf{1}\mathbf{1}^T[X - \mu\mu^T]) \end{aligned}$$

for $X := \mathbb{E}[xx^T]$, $\mu := \mathbb{E}[x]$, $a = \langle \alpha, \mathbf{1}/n \rangle$, $b = \langle \phi, \mathbf{1}/n \rangle$.

By our constraints $\mathbf{1}^T X \mathbf{1} - \mathbf{1}^T \mu \mu^T \mathbf{1} = 0$,

$$\mathbb{E}[(\langle \bar{\alpha}, z/n_1 - (1-z)/n_0 \rangle + \langle \bar{\phi}, z/n_1 - \mathbf{1}/n \rangle)^2] = 0.$$

Similarly,

$$\begin{aligned} \mathbb{E}[\langle \bar{s}(z), z/n_1 - (1-z)/n_0 \rangle^2] &\leq \delta \mathbb{E}[\langle \mathbf{1}, z/n_1 - (1-z)/n_0 \rangle^2] \\ &= \delta \text{Var}(\langle \mathbf{1}, z/n_1 - (1-z)/n_0 \rangle) \\ &= \delta \text{Var}(\langle \mathbf{1}, \beta_1 x \rangle) \\ &= \beta_1^2 \delta \text{Tr}(\mathbf{1}\mathbf{1}^T[X - \mu\mu^T]), \end{aligned}$$

which is constrained to be zero by our constraints $\mathbf{1}^T X \mathbf{1} - \mathbf{1}^T \mu \mu^T \mathbf{1} = 0$.

Thus, by Lemmas 20 to 22, we get

$$\mathbb{E}[(\tau - \hat{\tau}_{\text{DiM}})^2] \leq \text{Tr}((\gamma\beta_1^2 7L + \eta[\beta_1^2 + \beta_2^2]7L^\dagger)X) + \kappa[\beta_1^2 + \beta_2^2]7\|X\|_q.$$

□

K Proofs to Theoretical Guarantees

Our proof of Theorem 9 utilizes the seminal ideas underlying the approximation bound for MAXCUT, as introduced in [Goemans and Williamson \[1995\]](#). For convenience, we reiterate the MAXCUT problem in the following subsection.

K.1 The MAXCUT problem

$$\begin{aligned} \underset{x \in \mathbb{R}^n}{\text{maximize}} \quad & \frac{1}{2} \sum_{i < j} w_{ij}(1 - x_i \cdot x_j) \\ \text{s.t.:} \quad & x_i \in \{-1, 1\} \quad \forall i \in V \end{aligned}$$

The SDP relaxation is given by

$$\begin{aligned} & \underset{X \in \mathbb{R}^{n \times n}}{\text{maximize}} \quad \text{Tr}(LX) \\ & \text{s.t.:} \quad X_{ii} = 1 \quad \forall i \in V \\ & \quad X \succeq 0 \end{aligned}$$

Let $\zeta = \text{sign}(\xi)$, $\xi \sim \mathcal{N}(0, X^*)$, where X^* is the solution to the SDP relaxation of MAXCUT above. [Goemans and Williamson \[1995\]](#) proved that

$$\mathbb{E}\zeta^T L \zeta \geq 0.878 \max_{x \in \{-1,1\}^n} x^T L x,$$

by leveraging Grothendieck's identity

$$\frac{\pi}{2} \mathbb{E}[\zeta_i \zeta_j] = \arcsin(X_{i,j}^*).$$

We now prove our results in [Lemma 8](#), restated below.

Lemma 27. *Let $p := \mathbb{P}(x_i = 1)$, and X be the SDP solution to [B.1](#). Let also v_i , $i = 1, 2, \dots, n$ be the column vectors of $X^{1/2}$. Denote the vector returned by [Algorithm 1](#) by ζ . Then,*

$$\text{Cov}(\zeta_i, \zeta_j) = \frac{8p^2}{\pi} \arcsin \langle v_i, v_j \rangle,$$

for $i \neq j$.

Proof. Write $p_\xi^i := \mathbb{P}(\zeta_i = 1 | \langle v_i, \xi \rangle > 0)$. Since $\mathbb{P}(\langle v_i, \xi \rangle > 0) = 0.5$, and since $\mathbb{P}(\zeta_i = 1 | \langle v_i, \xi \rangle \leq 0) = 0$, we know that

$$\begin{aligned} p &:= \mathbb{P}(\zeta_i = 1) = \mathbb{P}(\zeta_i = 1 | \langle v_i, \xi \rangle > 0) \mathbb{P}(\langle v_i, \xi \rangle > 0) + \mathbb{P}(\zeta_i = 1 | \langle v_i, \xi \rangle \leq 0) \mathbb{P}(\langle v_i, \xi \rangle \leq 0) \\ &= p_\xi^i / 2. \end{aligned}$$

Therefore, we have that $p_\xi^i = 2p$ for all i . Define θ to be the angle corresponding to the region of vectors $\{v_k, v_l\}$ such that $\langle v_k, \xi \rangle > 0$, and $\langle v_l, \xi \rangle > 0$, i.e., $\theta := \{\max_{u,v} \arccos \langle u, v \rangle : \langle u, \xi \rangle > 0, \langle v, \xi \rangle > 0, \xi \in \text{Unif}(S^{n-1})\}$, where S^{n-1} is the $(n-1)$ -dimensional sphere. Then, $\theta = \pi - \arccos \langle v_i, v_j \rangle$, and

$$\begin{aligned} \mathbb{P}(\zeta_i \neq \zeta_j) &= \frac{4p(\pi - \theta) + 4p(1 - 2p)\theta}{2\pi} \\ &= \frac{2p}{\pi} (\pi - \theta + (1 - 2p)\theta) \end{aligned}$$

$$= \frac{2p}{\pi} [\arccos \langle v_i, v_j \rangle + (1 - 2p)(\pi - \arccos \langle v_i, v_j \rangle)].$$

Thus,

$$\begin{aligned} \mathbb{E}[\zeta_i \zeta_j] &= 1 - 2\mathbb{P}(\zeta_i \neq \zeta_j) \\ &= 1 - \frac{4p}{\pi} [\arccos \langle v_i, v_j \rangle + (1 - 2p)(\pi - \arccos \langle v_i, v_j \rangle)] \\ &= \frac{\pi(1 - 4p(1 - 2p)) - 8p^2 \arccos \langle v_i, v_j \rangle}{\pi}. \end{aligned}$$

$$\begin{aligned} \text{Cov}(\zeta_i, \zeta_j) &= \frac{\pi(1 - 4p(1 - 2p)) - 8p^2 \arccos \langle v_i, v_j \rangle}{\pi} - (2p - 1)^2 \\ &= \frac{8p^2}{\pi} \arcsin \langle v_i, v_j \rangle. \end{aligned}$$

□

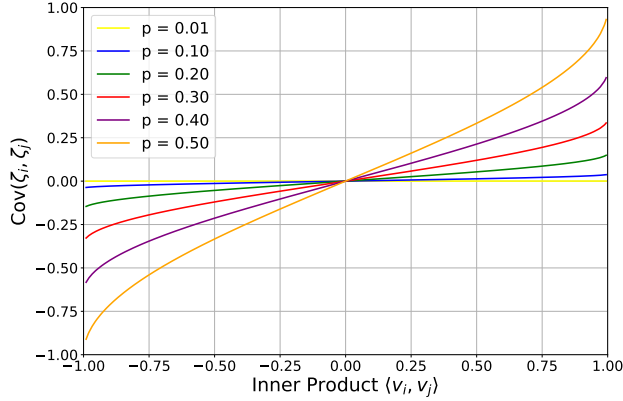


Figure K.1: The relationship between $\text{Cov}(\zeta_i, \zeta_j)$ and vector inner-products v_i, v_j in the SDP relaxation for various treatment assignment probabilities p .

We prove Theorem 9, restated below.

Theorem 28 (Approximation bound). *Let $\Xi = \text{Cov}(\zeta)$ be the covariance matrix of the associated Rademacher random variables. Let X be the SDP solution. We assume that X is non-degenerate, i.e., $X \succeq \delta I$, $\delta > 0$. For $c = \left(\frac{8p^2}{\pi} + \frac{8p^2\psi_\kappa}{\pi\delta} + \frac{4p(1-p)-8p^2/\pi}{\delta} \right)$ for $\psi_\kappa = n\alpha_\kappa^3$, where α_κ is the maximum off-diagonal entry of X ,*

$$\Xi \preceq c_\kappa X.$$

Proof. Recall that for Rademacher random variables $\zeta_i \in \{-1, 1\}$ with $\mathbb{P}(\zeta_i = 1) = 4p(1 - p)$. Therefore, we know that $\Xi_{ii} = 4p(1 - p)$, and what is left is to consider the

off-diagonals. From our derivation above for (i, j) pairs, we know that for the off-diagonals,

$$\Xi = \mathbb{E}[\zeta \zeta^T] - \mu \mu^T = \frac{8p^2}{\pi} \arcsin(X),$$

where $\arcsin(X)$ is written to be the entry-wise function on the matrix X , with Taylor expansion,

$$\arcsin(X) = X + \sum_{k=1}^{\infty} \frac{\binom{2k}{k}}{4^k(2k+1)} X^{\circ(2k+1)}.$$

Let α_κ be the maximum entry in the off-diagonals $X - I$. Here we note the dependence on κ ; by Proposition 7, as κ increases in the objective function relative to the other tradeoff parameters $\gamma, \eta, \alpha_\kappa$ decreases. Let also $f(X) := \sum_{k=1}^{\infty} \frac{\binom{2k}{k}}{4^k(2k+1)} X^{\circ(2k+1)}$, where $X^{\circ\beta}$ denotes all entries of X being raised to the power of β .

Denote the off-diagonal matrix of X by \tilde{R} . Therefore,

$$\begin{aligned} \Xi &= \frac{8p^2}{\pi} (\arcsin(X)) + 4p(1-2p)I \\ &= 4p^2 \left(\left(\frac{2}{\pi} \arcsin(X) - I \right) + I \right) + 4p(1-2p)I \\ &= \frac{8p^2}{\pi} (\tilde{R} + \mathcal{O}(\tilde{R}^{\circ 3})) + 4p(1-p)I, \\ &= \frac{8p^2}{\pi} X + \frac{8p^2}{\pi} \mathcal{O}(\tilde{R}^{\circ 3}) + (4p(1-p) - \frac{8p^2}{\pi})I. \end{aligned}$$

Let $\psi_\kappa = n\alpha_\kappa^3$, then $\|\mathcal{O}(\tilde{R}^{\circ 3})\|_{\text{op}} \leq \psi_\kappa$, and $\mathcal{O}(\tilde{R}^{\circ 3}) \preceq \frac{\psi_\kappa}{\delta} X$. That is, for κ large, $\alpha_\kappa = \mathcal{O}(n^{-1/3})$ and $\psi_\kappa = \mathcal{O}(1)$. It is easy to then see that

$$\left(\frac{8p^2}{\pi} + \frac{8p^2\psi_\kappa}{\pi\delta} + \frac{4p(1-p) - 8p^2/\pi}{\delta} \right) X \succeq \Xi.$$

□

We now prove Corollary 10. First, we restate it below.

Corollary 10. *Let $\Xi := \text{Cov}(\zeta)$ be the covariance matrix of the associated rademacher random variables. Let X^* be the optimal achievable covariance matrix of the design in Theorem 12. Let also X_{SDP} denote the SDP solution matrix. We assume that X_{SDP} is non-degenerate, i.e., $X_{SDP} \succeq \delta_\kappa I$, $\delta_\kappa > 0$. For $c_\kappa = \frac{1}{4p(1-p)} \left(\frac{8p^2}{\pi} + \frac{8p^2\psi_\kappa}{\pi\delta_\kappa} + \frac{4p(1-p) - 8p^2/\pi}{\delta_\kappa} \right)$ for $\psi_\kappa = n\alpha_\kappa^3$, where α_κ is the maximum off-diagonal entry of X_{SDP} , in absolute value,*

$$\text{Tr}(L\Xi) + \text{Tr}(L^\dagger\Xi) + \|\Xi\|_q + \text{Tr}(\mathbf{1}\mathbf{1}^T\Xi) \leq c_\kappa \left(\text{Tr}(LX^*) + \text{Tr}(L^\dagger X^*) + \|X^*\|_q + \text{Tr}(\mathbf{1}\mathbf{1}^T X^*) \right).$$

Proof. We see that $L, L^\dagger, \mathbf{1}\mathbf{1}^T$ are PSD. It is enough to notice that for PSD matrices A, B, C , with $B \succeq C$, $\text{Tr}(A(B - C)) \geq 0$. Finally, notice that for $X = 4p(1 - p)X_{\text{SDP}}$, where X_{SDP} is the SDP solution, and for X^* is the optimal achievable covariance matrix of a design, $\text{Tr}(LX) + \text{Tr}(L^\dagger X) + \|X\|_q + \text{Tr}(\mathbf{1}\mathbf{1}^T X) \leq \text{Tr}(LX^*) + \text{Tr}(L^\dagger X^*) + \|X^*\|_q + \text{Tr}(\mathbf{1}\mathbf{1}^T X^*)$. \square

Proposition 29 (Harshaw et al., 2024, Theorem 6.4). *The Gram-Schmidt Walk design with parameter $\lambda \in [0, 1]$ provides balance-robustness guarantee $\|\text{Cov}(Ax)\|_\infty \leq \frac{\max_{i \in [n]} \|x_i\|_2^2}{1 - \lambda}$ and $\|\text{Cov}(x)\|_\infty \leq \frac{1}{\lambda}$.*

Theorem 11. *Let $A := (\tilde{\eta}L^\dagger + \tilde{\gamma}L + \Delta\mathbf{1}\mathbf{1}^T)^{1/2}$, where $\tilde{\eta} = \eta[\beta_1^2 + \beta_2^2]$, $\tilde{\gamma} = \gamma\beta_1^2$, $\tilde{\kappa} = \kappa[\beta_1^2 + \beta_2^2]$, and $\Delta = (\alpha\beta_1 + b\beta_2)^2$. The Gram-Schmidt Walk algorithm, with randomization parameter λ , returns an assignment x such that $\|\text{Cov}(Ax)\|_{p'} \leq \xi^2/(1 - \lambda)\|I\|_{p'}$, and $\|\text{Cov}(x)\|_q \leq \|I\|_q/\lambda = n^{1/q}/\lambda$, for $\xi := \max_{i \in n} \|A_i\|$, A_i the column i of the matrix A . Thus, for $q \geq 1$,*

$$\sup_{\chi(\eta, \gamma, \kappa)} \mathbb{E}[(\tau - \hat{\tau})^2] \leq 7 \left[\mathbb{E}[\|A(x - \mu)\|^2] + \tilde{\kappa}\|X\|_q \right] \leq 7 \left[\frac{\xi^2 n}{1 - \lambda} + \tilde{\kappa} \frac{n^{1/q}}{\lambda} \right],$$

where $\mu_i = \mathbb{E}[x_i]$, for all $i \in [n]$. This is minimized for $\lambda = \frac{\sqrt{\tilde{\kappa}n^{1/q}}}{\sqrt{\xi^2 n} + \sqrt{\tilde{\kappa}n^{1/q}}}$.

Proof. From Theorem 12, we have

$$\sup_{\chi(\eta, \gamma, \kappa)} \mathbb{E}[(\tau - \hat{\tau})^2] \leq 7 \left[\text{Tr}(XAA^T) + \tilde{\kappa}\|X\|_q \right] = 7 \left[\mathbb{E}[\|A(x - \mu)\|^2] + \tilde{\kappa}\|X\|_q \right]$$

From the proof of Harshaw et al. [2024, Theorem 6.4], $\text{Cov}(x) \preceq \lambda^{-1}I$, and (2) $\text{Cov}(Ax) \preceq \xi^2(1 - \lambda)^{-1}I$. Thus, from (1) we have $\|X\|_q \leq \lambda^{-1}\|I\|_q = \lambda^{-1}n^{1/q}$. From (2), $\text{Tr}(XAA^T) \leq \xi^2(1 - \lambda)^{-1}I = \xi^2(1 - \lambda)^{-1}n$. Thererore,

$$7 \left[\text{Tr}(XAA^T) + \tilde{\kappa}\|X\|_q \right] \leq 7 \left[\frac{\xi^2 n}{(1 - \lambda)} + \tilde{\kappa} \frac{n^{1/q}}{\lambda} \right].$$

Next, to minimize the right-hand side above, we take the derivative with respect to λ and set it equal to zero. Let $m = \xi^2 n(1 - \lambda)^{-1} + \tilde{\kappa} n^{1/q} \lambda^{-1}$. Then,

$$\begin{aligned} \frac{dm}{d\lambda} &= \frac{\xi^2 n}{\lambda^2} - \frac{\tilde{\kappa} n^{1/q}}{\lambda^2} = 0 \\ \lambda &= \frac{\sqrt{\tilde{\kappa}n^{1/q}}}{\sqrt{\tilde{\kappa}n^{1/q}} \pm \sqrt{\xi^2 n}}. \end{aligned}$$

Since $\lambda \in [0, 1]$, $\lambda = \frac{\sqrt{\tilde{\kappa}n^{1/q}}}{\sqrt{\tilde{\kappa}n^{1/q}} + \sqrt{\xi^2 n}}$. Additionally, since $\xi^2 n(1 - \lambda)^{-1} + \tilde{\kappa} n^{1/q} \lambda^{-1}$ is convex in λ , $\lambda = \frac{\sqrt{\tilde{\kappa}n^{1/q}}}{\sqrt{\tilde{\kappa}n^{1/q}} + \sqrt{\xi^2 n}}$ is its minimizer, yielding the claim. \square

The result above also holds when $A^T := [\tilde{\eta}^{1/2}L^{\dagger/2} \quad \tilde{\gamma}^{1/2}L^{1/2} \quad \Delta^{1/2}\mathbf{1}\mathbf{1}^T]^{1/2}$.

L Simulations

L.1 Quantile rounding

One can also consider what we call “quantile rounding”, which is equivalent to Gaussian rounding when $p = 1/2$. Generally, quantile rounding for $p \leq 1/2$ is simply the procedure of selecting the threshold $t_q(i)$ for the rounding of $\xi \sim \mathcal{N}(0, X^*)$, $\xi \in \mathbb{R}^n$ to $\zeta \in \{-1, 1\}^n$ based on the quantiles of ξ_i . That is, we take $t_q(i) = \sqrt{X_{ii}^*} \cdot \Phi^{-1}(1 - p)$, and let $\zeta_i = 1$ if $\xi_i \geq t_q(i)$, and $\zeta_i = -1$ otherwise.

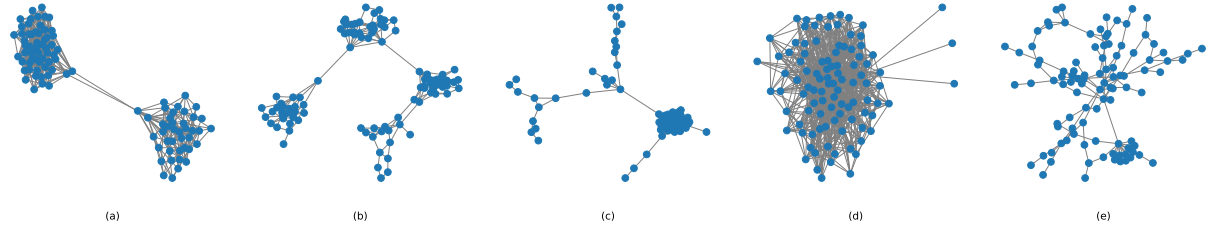


Figure L.1: From left to right: Graphs generated from (a): SBM (within cluster connection probability $20/n$, across connection probability $\frac{0.1}{n}$), with two clusters of equal membership assignment probability; (b): SBM (within cluster connection probability $20/n$, across connection probability $\frac{0.1}{n}$) with four clusters of equal membership assignment probability; (c): SBM (within cluster connection probability $20/n$, across connection probability $\frac{0.1}{n}$) with four clusters of membership assignment probabilities $0.7, 0.1, 0.1, 0.1$; (d): Barabasi-Albert (preferential-attachment) with initial $n/10$ ($=10$) nodes connected according to the Erdős-Rényi model with connection probability $10/n$; Graph 5: Erdős-Rényi with connection probability $2/n$.

L.2 Real Data

Figure 2.1 illustrates a single village network in rural Karnataka, South India [Banerjee et al., 2013b,a]. For context, Banerjee et al. [2013b] collected network data from 75 villages before the introduction of financial services in these villages by a microfinance institute. In particular, in 2006, six months before the the microfinance institute began their work, Banerjee et al. [2013b] conducted surveys on subsamples of villagers gathering demographic information. The survey included a portion on social network data along 12 dimensions. In Figure 2.1, we display Village No.6 which we had randomly selected. In this network, the nodes represent village members, and an edge between any pair of nodes is present if the corresponding villagers visit each other’s homes. In this figure, the nodes in the network are colored according to the castes of the corresponding villagers, illustrating homophily in the network, as members of the same caste are more connected.

Name	Description
SDP	SDP solution X^*
SDP + GaussRound	SDP followed by Gaussian rounding
SDP + QuantRound	SDP followed by quantile rounding (see Appendix L.1)
GSW	Adapted Gram-Schmidt Walk design [Harshaw et al., 2024]
GSW + covariates	Adapted Gram-Schmidt Walk design [Harshaw et al., 2024] using covariate-encoding directly instead of L^\dagger
Louvain	Cluster-randomization with default Python implementation of the Louvain clustering algorithm
ϵ -net	Cluster-randomization under ($\epsilon=1$)-net clustering [Ugander et al., 2013]
Spectral	Cluster-randomization under spectral clustering
Causal	Cluster-randomization under Causal clustering [Viviano et al., 2023] with a grid-search for optimal hyperparameters
Bernoulli	Uniform Bernoulli randomization

Table 1: Key of designs compared in this paper.

In Figure L.2, we illustrate treatment assignments under various cluster-randomized designs, depicting almost complete overlap with the underlying homophily structure. In the worst case where the distinct homophilous groups have heterogeneous treatment effects, such cluster-randomized designs can lead to imprecise estimates of the GATE. Generally, this imprecision worsens as the number of distinct homophilous groups increases for a fixed population size.

In the comparisons of the worst-case MSE bounds on this network data in Figures L.3 and L.5, we compare the bounds derived in Theorem 12 using covariance matrices from various designs. We describe the different designs we compare in Table 1. We note that the different cluster-randomized designs were also considered in [Viviano et al., 2023].

We also compare the MSEs by combining synthetic worst-case potential outcomes with the real network data together with the caste information. We generate the homophily components in the potential outcomes, h^α and h^ϕ from a random effects model across the castes. That is, we generate potential outcomes associated with each caste j

$$\nu_{jf} \sim \mathcal{N}(\mu_f, \sigma_f^2),$$

for some μ_f . Then, for each node i that belongs to caste j ,

$$h_{if} = \nu_{jf},$$

for all j , and $f = \alpha, \phi$. In our simulations, we take $\mu_\alpha = 2$, $\mu_\phi = 3$, and $\sigma_f^2 = 3$, $f = \alpha, \phi$. Then, we take $\eta = h_f^T L h_f$.

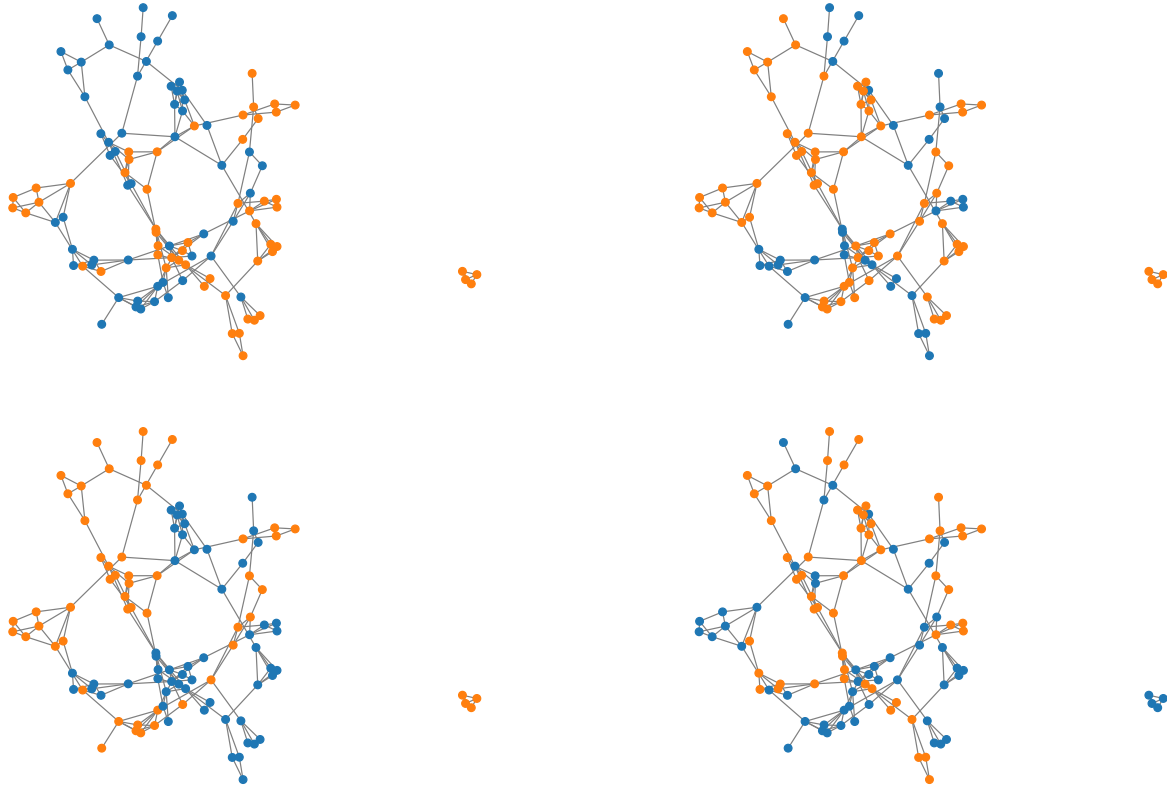


Figure L.2: Assignments under various cluster randomization designs. Top (left to right): $\epsilon = 1$ -net, causal cluster randomizations. Bottom (left to right): Louvain, and spectral cluster randomizations.

To generate the heterogeneous variation components ϵ_f , for $f = \alpha, \phi$, for $q^* = 2$, we take

$$\begin{aligned}\Sigma &\sim \mathcal{N}(0, 1)^{n \times n}, \\ X &= \Sigma / \|\Sigma\|_2, \\ z &\sim \mathcal{N}(0, I_n), \\ \epsilon_f &= \sqrt{\kappa} X^{1/2} z.\end{aligned}$$

If $q^* = \infty$ instead, we replace X with $X = vv^T$, where v is the leading eigenvector of Σ .

To generate the interference component for each treatment assignment vector $x = 2z - 1$ generated from X from the corresponding covariance matrix, we take

$$\begin{aligned}s(z) &= \frac{\sqrt{\gamma} L x}{\|x^T L^{1/2}\|_2}, \\ s(z) &= s(z) - \left\langle s(z), \frac{\mathbf{1}}{n} \right\rangle \mathbf{1}.\end{aligned}$$

We detail in Appendix L.4 why these generative models appropriately capture worst-case potential outcomes.

In Figure L.4, we compare the MSEs across various designs, under the generated worst-case potential outcomes, for various levels of γ and κ .

In Figure L.5, in addition to the comparisons with the adapted Gram-Schmidt Walk design using the worst-case bounds with $\eta = h_f^T L h_f$, we also compare with the adapted Gram-Schmidt Walk design directly using a one-hot encoding of caste information (see the plotted line labeled “GSW + covariates”), with potential outcomes generated according to the worst-case models described above. Specifically, let J be the number of different covariate groups. In our village data example, J is the number of castes. Given the random effects model above we can write the homophily component of the MSE as

$$\begin{aligned}\mathbb{E}[(h^T x)^2] &= \mathbb{E} \left[\left(\sum_{j=1}^J \left(\sum_{i:x_i=1} \mathbf{1}\{i \in \text{Caste}_j\} - \sum_{i:x_i=-1} \mathbf{1}\{i \in \text{Caste}_j\} \right) \nu_j \right)^2 \right] \\ &= \mathbb{E} \left[\left(\sum_{j=1}^J (n_{1j} - n_{0j}) \nu_j \right)^2 \right] \\ &= \sum_{j=1}^J (n_{1j} - n_{0j})^2 \text{Var}(\nu_j) = \sigma^2 \sum_{j=1}^J (n_{1j} - n_{0j})^2.\end{aligned}$$

Then, in this setting, we define $\eta = \sigma^2$, and take our pre-augmented covariate matrix

$A \in \mathbb{R}^{(J+2n) \times n}$ to be such that its i -th column,

$$A_i^T = [\tilde{\eta}^{1/2} \xi_i^j \quad \tilde{\gamma}^{1/2} L_i^{1/2} \quad (\mathbf{1}\mathbf{1}^T)_i^{1/2}]^T,$$

where ξ_i^j is column vector with entry 1 in row j if unit i belongs to caste j and zero otherwise, and the parameters $\tilde{\eta}, \tilde{\gamma}, \tilde{\kappa}$ defined as before. Then, the worst case MSE bound can be written in the previous form

$$\mathbb{E}[(\hat{\tau} - \tau)^2] \leq 7\Delta[\mathbb{E}[\|Ax\|_2^2] + \tilde{\kappa}\|X\|_q].$$

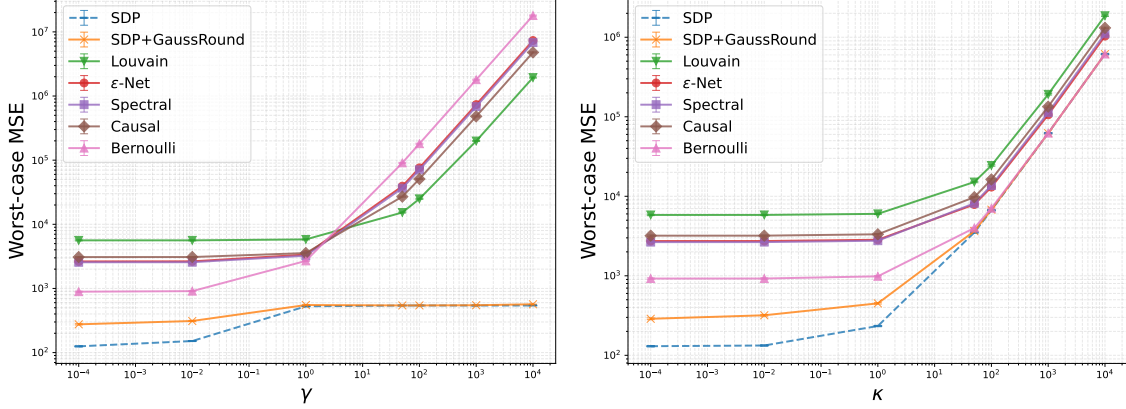


Figure L.3: Comparisons of the worst-case MSE bounds across various designs, for different levels of γ and κ , with the average (over 1000 trials) $\eta \approx 196$. Error bars represent the standard error.

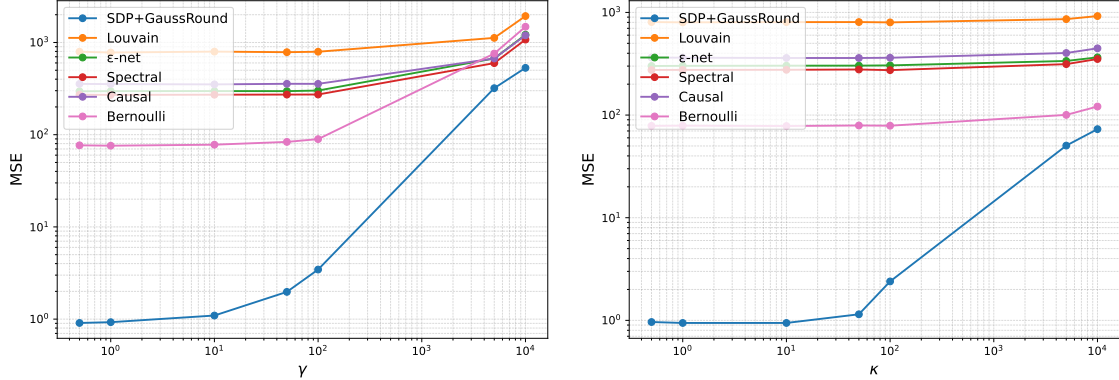


Figure L.4: Comparisons of the MSEs across various designs, for different levels of γ and κ , with the average (over 1000 trials) $\eta \approx 196$. Error bars represent the standard error.

L.3 Worst-case MSE bounds comparisons on simulated networks

Throughout this subsection and the next, we compare the performance of our designs against various designs from the literature. We describe the different designs we compare in Table 1.

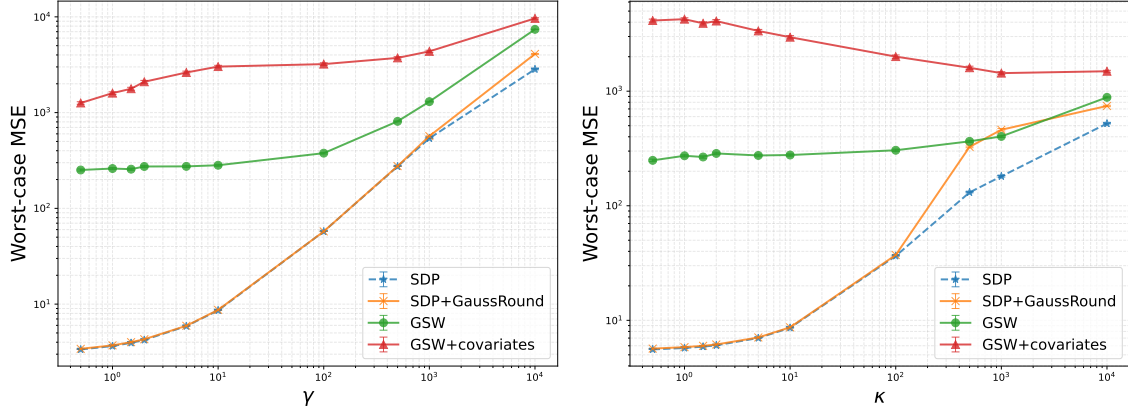


Figure L.5: Comparisons of the worst-case MSE bounds across various designs, with the average (over 1000 trials) $\eta \approx 196$. Error bars represent the standard error.

We note that the different cluster-randomized designs were also considered in [Viviano et al., 2023].

In Figures L.6 to L.10, we compare the worst case bounds by plugging into the bound in Theorem 12 the covariance matrices from various designs. We compare the worst-case MSE bounds for five different graph generation models, as described in Figure L.1, averaged across 1000 graph instances of each graph model. For procedures where we cannot directly compute the design covariance, we generate the sample covariance matrices of the designs over 1000 instances of the design vectors for each graph instance. We note that the gap between the optimal solution from solving the SDP and the other designs are due to unattainability of the optimal SDP solution given that the SDP formulation is a relaxation of the problem. In these settings, we set the fixed tradeoff parameters to be 1.

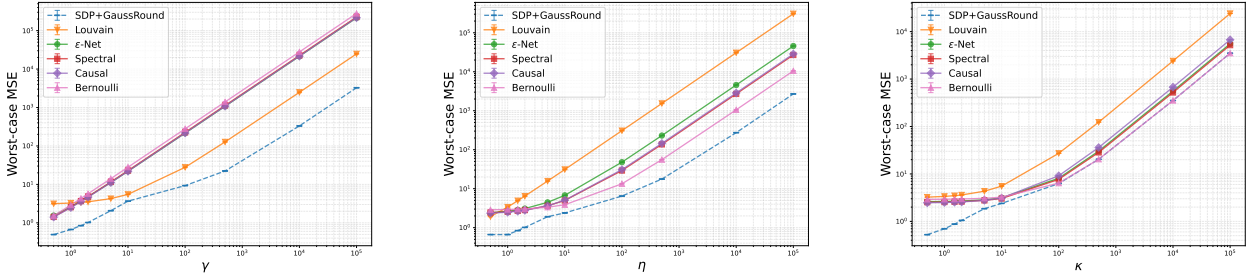


Figure L.6: Comparison of worst-case MSE bounds between our designs, cluster randomization designs (with various clusterings) and Bernoulli randomization averaged over graphs generated from an SBM (within cluster connection probability $20/n$, across connection probability $\frac{0.1}{n}$), with two clusters of equal membership assignment probability (see Graph 1 in Figure L.1). The other two trade-off parameters are set to one. Error bars represent the standard error.

Figures L.11 to L.15 compare worst-case MSE bounds using our SDP approach followed by Gaussian rounding, and our adapted Gram-Schmidt Walk approach, across various n . Here,

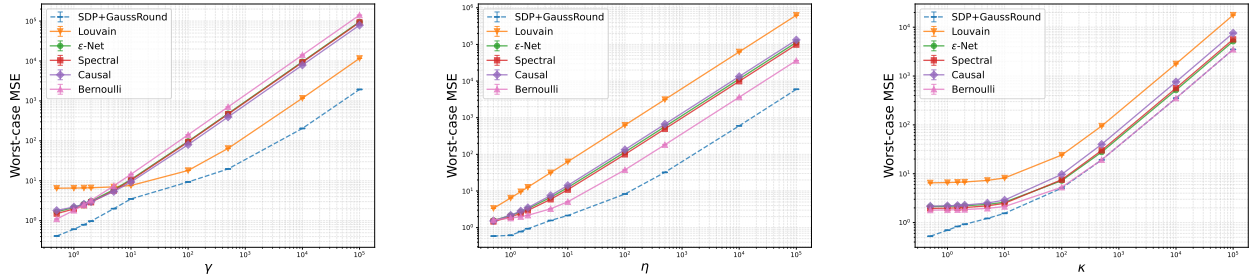


Figure L.7: Comparison of worst-case MSE bounds between our designs, cluster randomization designs (with various clusterings) and Bernoulli randomization averaged over graphs generated from an SBM (within cluster connection probability $20/n$, across connection probability $\frac{0.1}{n}$), with two clusters of equal membership assignment probability (see Graph 2 in fig. L.1). The other two trade-off parameters are set to one. Error bars represent the standard error.

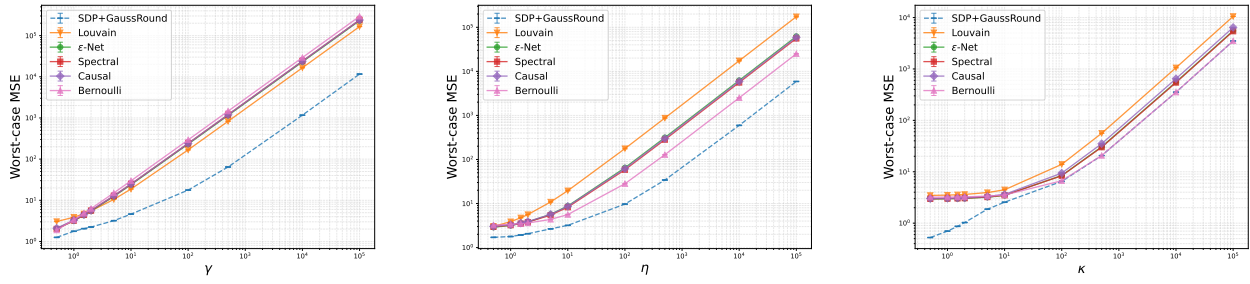


Figure L.8: Comparison of worst-case MSE bounds between our designs, cluster randomization designs (with various clusterings) and Bernoulli randomization averaged over graphs generated from an SBM (within cluster connection probability $20/n$, across connection probability $\frac{0.1}{n}$) with four clusters of membership assignment probability $(0.70, 0.1, 0.1, 0.1)$ (see Graph 3 in fig. L.1). The other two trade-off parameters are set to one. Error bars represent the standard error.

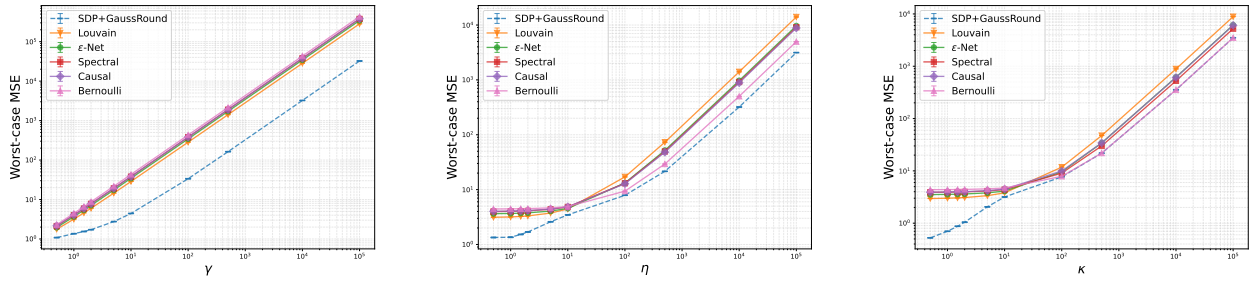


Figure L.9: Comparison of worst-case MSE bounds between our designs, cluster randomization designs (with various clusterings) and Bernoulli randomization averaged over graphs generated from a Barabasi-Albert (preferential-attachment) model with initial $n/10$ ($=10$) nodes connected according to the Erdős-Rényi model with connection probability $10/n$ (see Graph 4 in fig. L.1). The other two trade-off parameters are set to one. Error bars represent the standard error.

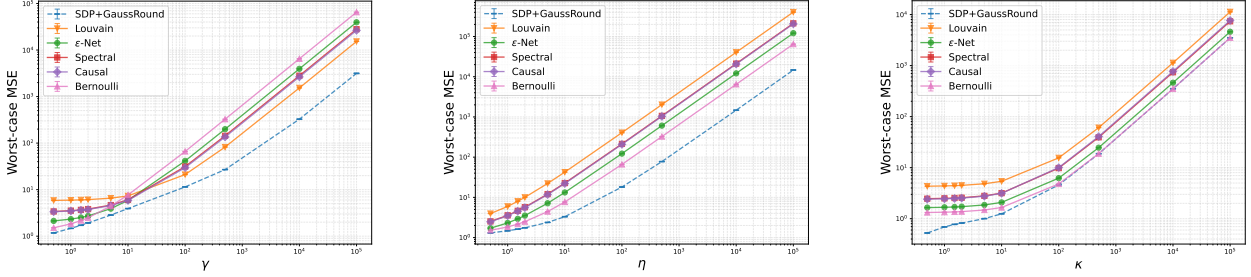


Figure L.10: Comparison of worst-case MSE bounds between our designs, cluster randomization designs (with various clusterings) and Bernoulli randomization averaged over graphs generated from an Erdős-Rényi model with connection probability $2/n$ (see Graph 5 in fig. L.1). The other two trade-off parameters are set to one. Error bars represent the standard error.

we set $\kappa = 100, \eta = 250, \gamma = 1000, q = 2$, and $\Delta = 0.01\gamma$. We observe that the adapted Gram-Schmidt Walk designs have comparable worst-case error bounds to the SDP solutions, for n ranging between 200 and 400. The SDP solutions followed by Gaussian rounding perform worse than the adapted Gram-Schmidt Walk designs for settings of types Graphs 2 – 5 in Figure L.1, while in settings of type Graph 1 in Figure L.1, the Gaussian rounding procedure almost perfectly approximates the SDP solution.

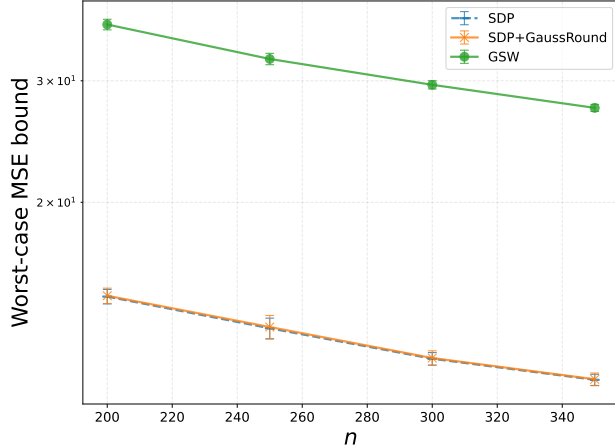


Figure L.11: Comparisons with adapted Gram-Schmidt algorithm averaged over graphs generated from an SBM (within cluster connection probability $20/n$, across connection probability $\frac{0.1}{n}$), with two clusters of equal membership assignment probability (see Graph 1 in fig. L.1), for different n . Error bars represent the standard error.

For completeness, we also compare the MSEs under simulated worst-case potential outcomes on various graphs. We present the results of these experiments in the next section.

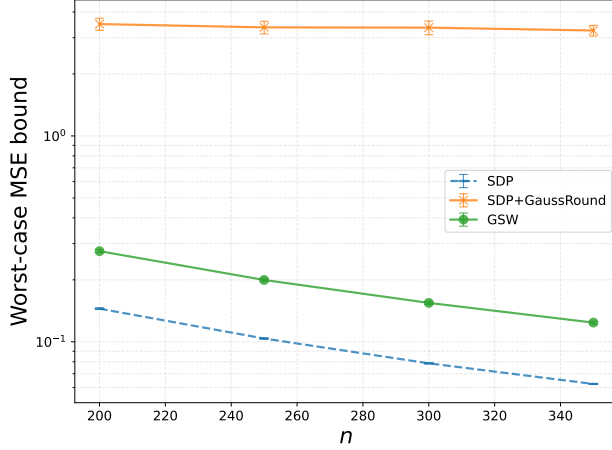


Figure L.12: Comparisons with adapted Gram-Schmidt algorithm averaged over graphs generated from an SBM (within cluster connection probability $20/n$, across connection probability $\frac{0.1}{n}$), with two clusters of equal membership assignment probability (see Graph 2 in fig. L.1), for different n . Error bars represent the standard error.

L.4 MSE comparisons under synthetic worst-case potential outcomes

In Figures L.16 to L.20, we display the MSE using simulated potential outcomes across various designs, namely our design, cluster-randomization under the default Python implementation of the Louvain clustering, ($\varepsilon = 1$)-net clustering [Ugander et al., 2013], Spectral clustering, Causal Clustering [Viviano et al., 2023], and Bernoulli Randomization. We compare the MSEs for five different graph generation models, averaged across 1000 graph instances of each graph model, as described in Figure L.1. In these settings, we set the fixed tradeoff parameters to be 1, and $a, b = 0.01\gamma$. We display the results in Figures L.16 to L.20.

The worst-case potential outcomes were generated according to the following model. For given $L, L^\dagger, \eta, \gamma, \kappa$, and randomly generated baselines α_0, ϕ_0 (and, thus, Δ), we compute the covariance matrices X corresponding to the different designs described above. Then, adversarially, for the worst-case, we compute the potential outcome components. We describe this in detail in the following: To generate the homophily components h_f , $f \in \{\alpha, \phi\}$,

$$\begin{aligned} v &= \max \text{eigenvector}(L^{\dagger/2} X L^{\dagger/2}), \\ h_f &= \sqrt{\eta} L^{\dagger/2} v, \\ h_f &= h_f - \left\langle h_f, \frac{\mathbf{1}}{n} \right\rangle \mathbf{1} \end{aligned}$$

In the above, we leverage the proof to the bounds in Lemma 23 to generate the worst-case homophily components. Indeed, let $w = L^{1/2} h_f / \sqrt{\eta}$, then, the h_f that achieves $\sup_{\|L^{1/2} h_f\|_2^2 \leq \eta} h_f^T L^{1/2} L^{\dagger/2} X L^{\dagger/2} L^{1/2} h_f$ is the same as the $\sqrt{\eta} L^{\dagger/2} w$ for the w that achieves

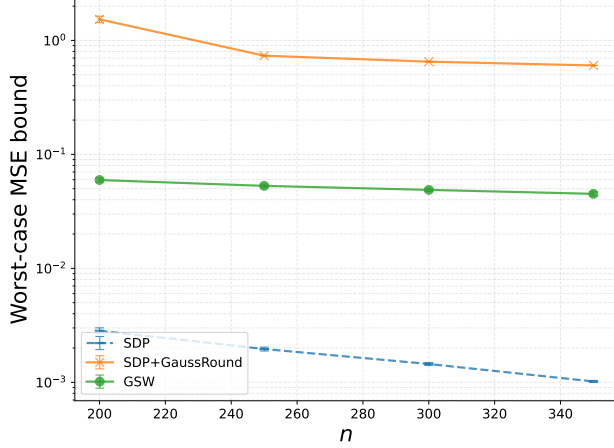


Figure L.13: Comparisons with adapted Gram-Schmidt algorithm averaged over graphs generated from an SBM (within cluster connection probability $20/n$, across connection probability $\frac{0.1}{n}$) with four clusters of membership assignment probability $(0.70, 0.1, 0.1, 0.1)$ (see Graph 3 in fig. L.1), for different n . Error bars represent the standard error.

$\sup_{\|w\|_2^2 \leq 1} w^T L^{\dagger/2} X L^{\dagger/2} w$, which is simply the maximum eigenvector of $L^{\dagger/2} X L^{\dagger/2}$.

To generate the heterogeneous variation components ϵ_f , $f \in \{\alpha, \phi\}$ $q^* = 2$, we take

$$\begin{aligned} \Sigma &= \kappa X / \|X\|_F, \\ z &\sim \mathcal{N}(0, I_n), \\ \epsilon_f &= \Sigma^{1/2} z. \end{aligned}$$

If $q^* = 1$ instead, we replace Σ above with $\Sigma = \kappa v v^T$, where v is the leading eigenvector of X . Indeed, it is not difficult to see that these are the ϵ_f that achieve the bounds in Lemma 22 and Proposition 4.

Finally, let $\tilde{\alpha} = h_\alpha + \epsilon_\alpha$, and $\tilde{\phi} = h_\phi + \epsilon_\phi$. Recall that here $a = \langle \alpha_0, \frac{1}{n} \rangle$, and $b = \langle \phi_0, \frac{1}{n} \rangle$. We take $\alpha = a\mathbf{1} + (\tilde{\alpha} - \langle \tilde{\alpha}, \frac{1}{n} \rangle \mathbf{1})$ and $\phi = b\mathbf{1} + (\tilde{\phi} - \langle \tilde{\phi}, \frac{1}{n} \rangle \mathbf{1})$.

To generate the interference component for each treatment assignment vector $x = 2z - 1$ generated from X from the corresponding covariance matrix, we take

$$\begin{aligned} s(z) &= \frac{\sqrt{\gamma} L x}{\|x^T L^{1/2}\|_2}, \\ s(z) &= s(z) - \left\langle s(z), \frac{\mathbf{1}}{n} \right\rangle \mathbf{1}. \end{aligned}$$

Indeed, through the proof the Cauchy-Schwarz inequality, it is not difficult to see that the $s(z)$ that achieves $\sup_{\|L^{\dagger/2} s(z)\|_2^2 \leq \gamma} \mathbb{E}[\langle x, s(z) \rangle^2]$, must satisfy $L^{\dagger/2} s(z) = \gamma^{1/2} L^{1/2} x / \|L^{1/2} x\|_2$.

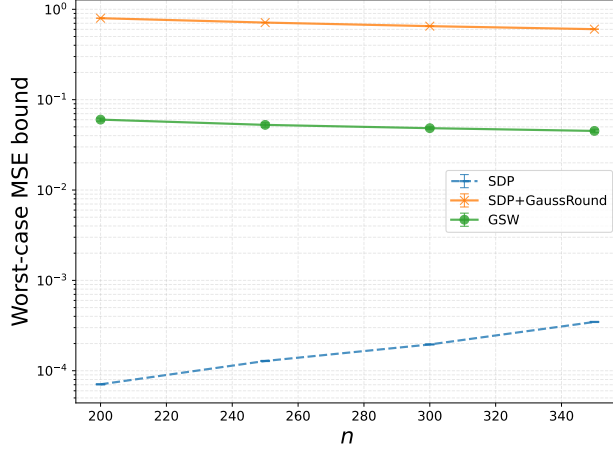


Figure L.14: Comparisons with adapted Gram-Schmidt algorithm averaged over graphs generated from a Barabasi-Albert (preferential-attachment) model with initial $n/10$ ($=10$) nodes connected according to the Erdős-Rényi model with connection probability $10/n$ (see Graph 4 in fig. L.1), for different n . Error bars represent the standard error.

L.5 Priors and Worst-Case

We take this opportunity to illustrate how our framework allows for the incorporation of priors in the bounds to improve the performance of the design otherwise tailored to the worst-case setting. Indeed, if the practitioner strongly believed that the homophily components of the potential outcomes followed a certain type of distribution, then we can refine the trade-off parameter bounds. In particular, if the practitioner believed that the homophily components followed a uniform distribution on a sphere, much like in the data generation procedure in the previous paragraph, we can replace the η parameter by η/n . Indeed, if $h \sim L^{\dagger 1/2} \text{Unif}(S_{n-1}^{\eta})$ where S_n^{η} is the $(n-1)$ -sphere of radius $\sqrt{\eta}$, i.e., the scaled normalized gaussians in the previous paragraph, then,

$$\begin{aligned}
\mathbb{E}[(h^T x)^2] &= \text{Tr}(X \mathbb{E}[L^{\dagger 1/2} v v^T L^{\dagger 1/2}]) \\
&= \text{Tr}(X L^{\dagger 1/2} \mathbb{E}[v v^T] L^{\dagger 1/2}) \\
&= \frac{\eta}{n} \text{Tr}(X L^{\dagger}).
\end{aligned}$$

Similarly, if the practitioner believed that the interference $s(z)$ followed a uniform distribution on the sphere, we can replace γ by γ/n . Indeed, if $s(z) \sim L^{1/2} \text{Unif}(S_{n-1}^{\gamma})$, where S_{n-1}^{γ} is the $(n-1)$ -sphere of radius $\sqrt{\gamma}$, then,

$$\begin{aligned}
\mathbb{E}[(s(z)^T x)^2] &= \text{Tr}(X \mathbb{E}[L^{1/2} v v^T L^{1/2}]) \\
&= \text{Tr}(X L^{1/2} \mathbb{E}[v v^T] L^{1/2})
\end{aligned}$$

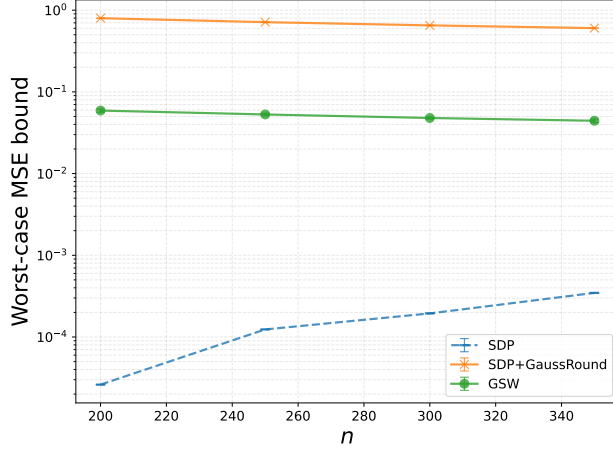


Figure L.15: Comparisons with adapted Gram-Schmidt algorithm averaged over graphs generated from an Erdős-Rényi model with connection probability $2/n$ (see Graph 5 in fig. L.1), for different n . Error bars represent the standard error.

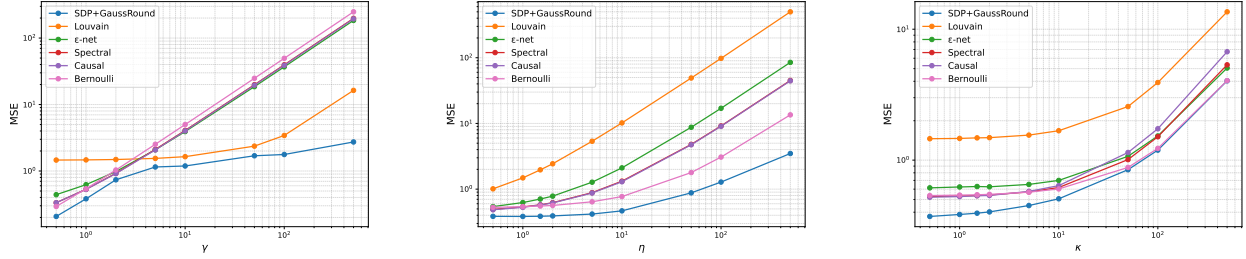


Figure L.16: Comparison of MSEs between our designs, cluster randomization designs (with various clusterings) and Bernoulli randomization averaged over graphs generated from an SBM (within cluster connection probability $20/n$, across connection probability $\frac{0.1}{n}$), with two clusters of equal membership assignment probability (see Graph 1 in Figure L.1). The other two trade-off parameters are set to one. Error bars represent the standard error.

$$= \frac{\gamma}{n} \text{Tr}(XL).$$

L.6 Comparisons between SDP and adapted Gram-Schmidt Walk designs

In Figures L.11 to L.15, we compare the worst-case bounds of the designs produced by the SDP and adapted Gram-Schmidt Walk algorithms for $n \in \{200, 250, 300, 350\}$. As expected, the SDP solutions yield uniformly smaller worst-case bounds, since the SDP directly optimizes the worst-case objective. However, over this range of n , we do not observe a clear trend in the gap between the SDP- and Gram-Schmidt-Walk-based bounds that would reflect the predicted looseness of the adapted Gram-Schmidt Walk bound at large n . This is likely because we only consider a limited range of n , as solving the SDP becomes computationally

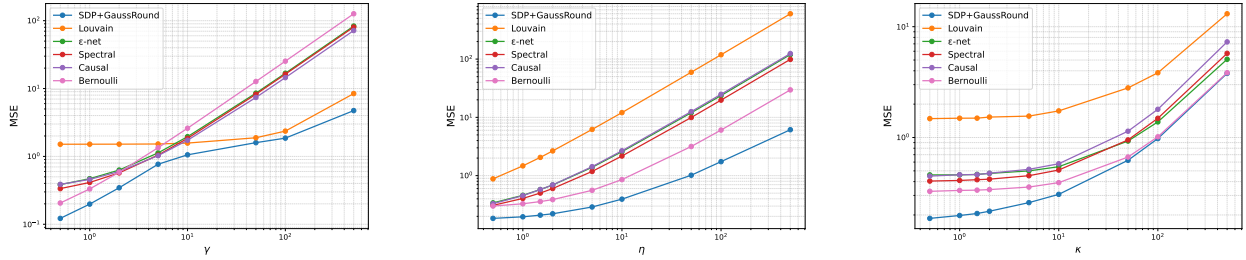


Figure L.17: Comparison of MSEs between our designs, cluster randomization designs (with various clusterings) and Bernoulli randomization averaged over graphs generated from an SBM (within cluster connection probability $20/n$, across connection probability $\frac{0.1}{n}$), with two clusters of equal membership assignment probability (see Graph 2 in Figure L.1). The other two trade-off parameters are set to one. Error bars represent the standard error.

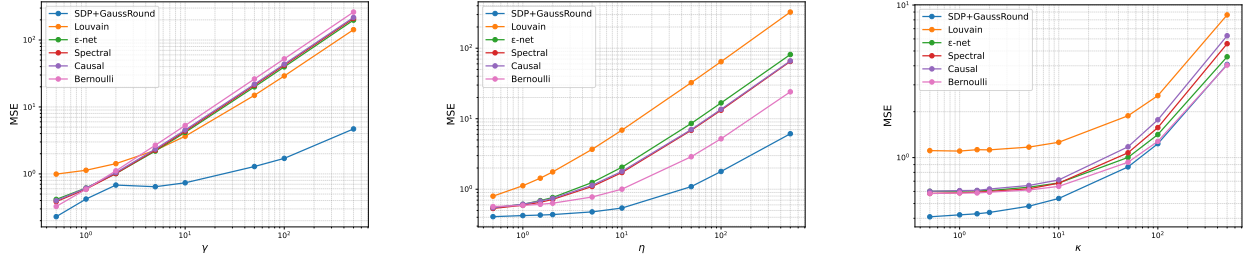


Figure L.18: Comparison of MSEs between our designs, cluster randomization designs (with various clusterings) and Bernoulli randomization averaged over graphs generated from an SBM (within cluster connection probability $20/n$, across connection probability $\frac{0.1}{n}$) with four clusters of membership assignment probability $(0.7, 0.1, 0.1, 0.1)$ (see Graph 3 in Figure L.1). The other two trade-off parameters are set to one. Error bars represent the standard error.

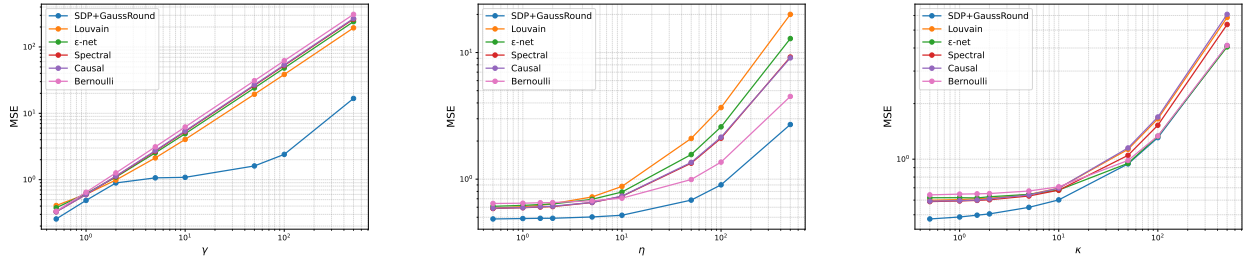


Figure L.19: Comparison of MSEs between our designs, cluster randomization designs (with various clusterings) and Bernoulli randomization averaged over graphs generated from a Barabasi-Albert (preferential-attachment) model with initial $n/10$ ($=10$) nodes connected according to the Erdös-Rényi model with connection probability $10/n$ (see Graph 4 in Figure L.1). The other two trade-off parameters are set to one. Error bars represent the standard error.

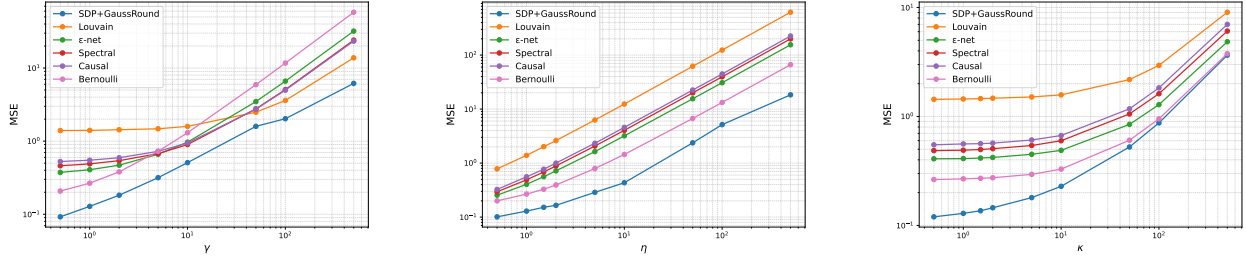


Figure L.20: Comparison of MSEs between our designs, cluster randomization designs (with various clusterings) and Bernoulli randomization averaged over graphs generated from an Erdős-Rényi model with connection probability $2/n$ (see Graph 5 in Figure L.1). The other two trade-off parameters are set to one. Error bars represent the standard error.

prohibitive for larger n . Finally, for all the simulated networks besides the SBM graphs with two equal-membership clusters, the adapted Gram–Schmidt Walk algorithm yields smaller bounds than Gaussian rounding applied to the SDP solutions.